



## In vivo analysis of actin and tropomyosin filament dynamics

**Author:**

Appaduray, Mark Ashwin

**Publication Date:**

2017

**DOI:**

<https://doi.org/10.26190/unsworks/20508>

**License:**

<https://creativecommons.org/licenses/by-nc-nd/3.0/au/>

Link to license to see what you are allowed to do with this resource.

Downloaded from <http://hdl.handle.net/1959.4/60153> in <https://unsworks.unsw.edu.au> on 2024-05-05

# ***In vivo* analysis of actin and tropomyosin filament dynamics**

**Mark Ashwin Appaduray**

*A thesis in fulfilment of the requirements for the degree of Doctor  
of Philosophy*



**School of Medical Sciences**

**Faculty of Medicine**

**August 2017**

**COPYRIGHT STATEMENT**

*'I hereby grant the University of New South Wales or its agents the right to archive and to make available my thesis or dissertation in whole or part in the University libraries in all forms of media, now or here after known, subject to the provisions of the Copyright Act 1968. I retain all proprietary rights, such as patent rights. I also retain the right to use in future works (such as articles or books) all or part of this thesis or dissertation.*

*I also authorise University Microfilms to use the 350 word abstract of my thesis in Dissertation Abstract International (this is applicable to doctoral theses only).*

*I have either used no substantial portions of copyright material in my thesis or I have obtained permission to use copyright material; where permission has not been granted I have applied/will apply for a partial restriction of the digital copy of my thesis or dissertation.'*

Signed .....

Date ..... 29/05/2018 .....

**AUTHENTICITY STATEMENT**

*'I certify that the Library deposit digital copy is a direct equivalent of the final officially approved version of my thesis. No emendation of content has occurred and if there are any minor variations in formatting, they are the result of the conversion to digital format.'*

Signed .....

Date ..... 29/05/2018 .....

PLEASE TYPE

THE UNIVERSITY OF NEW SOUTH WALES  
Thesis/Dissertation Sheet

Surname or Family name: **Appaduray**

First name: **Mark**

Other name/s: **Ashwin**

Abbreviation for degree as given in the University calendar: **PhD**

School: **Medical Sciences**

Faculty: **Medicine**

Title: *In vivo analysis of actin and tropomyosin filament dynamics*

Abstract 350 words maximum: (PLEASE TYPE)

The actin cytoskeleton is involved in virtually every biological process. Assembly of actin structures in cells is mediated by actin-associated proteins (AAPs) that collaborate to assemble and regulate actin filaments. Actin nucleators generate linear and branched actin filaments while the tropomyosins (Tpms), known as the master regulators of actin filaments, stabilise and confer specific functions to filaments by governing their interaction with other AAPs. The dynamics of actin assembly has been studied in *in vitro* and *ex vivo* systems; however, no studies have investigated the *de novo* assembly kinetics of functional actin structures *in vivo* in mammals. Furthermore, no study has thoroughly investigated the relationship between cytoskeletal Tpms and actin filaments in cells. This thesis employed cutting-edge subcellular intravital microscopy to investigate the recruitment kinetics of the linear and branched actin nucleators, formins mDia1, mDia2 and the Arp2/3 complex, respectively, Tpms 3.1 and 4.2, myosin IIA, and the crosslinker alpha-actinin 4 during *de novo* actin scaffold assembly that drives regulated secretory granule exocytosis in rodent salivary glands, as well as the relationship between Tpm3.1 and actin filaments. This was achieved by developing a novel mouse salivary gland gene delivery technique using both viral and non-viral vectors. The findings provide insights into Tpm regulation of actin filaments, suggesting that multiple functionally distinct actin populations exist and work in tandem. Actin scaffold assembly requires the collaborative effort between multiple actin nucleators that have unique recruitment kinetics and activities. Remarkably, actin scaffold-driven regulated secretory granule exocytosis *in vivo* was shown to occur in two distinct phases, which revealed novel functions and interdependence between the branched and linear actin networks.

Declaration relating to disposition of project thesis/dissertation

*I hereby grant to the University of New South Wales or its agents the right to archive and to make available my thesis or dissertation in whole or in part in the University libraries in all forms of media, now or here after known, subject to the provisions of the Copyright Act 1968. I retain all property rights, such as patent rights. I also retain the right to use in future works (such as articles or books) all or part of this thesis or dissertation.*

*I also authorise University Microfilms to use the 350 word abstract of my thesis in Dissertation Abstracts International (this is applicable to doctoral theses only).*

30/08/2017

.....  
Signature

.....  
Witness Signature

.....  
Date

*The University recognises that there may be exceptional circumstances requiring restrictions on copying or conditions on use. Requests for restriction for a period of up to 2 years must be made in writing. Requests for a longer period of restriction may be considered in exceptional circumstances and require the approval of the Dean of Graduate Research.*

FOR OFFICE USE ONLY

Date of completion of requirements for Award:

## ORIGINALITY STATEMENT

'I hereby declare that this submission is my own work and to the best of my knowledge it contains no materials previously published or written by another person, or substantial proportions of material which have been accepted for the award of any other degree or diploma at UNSW or any other educational institution, except where due acknowledgement is made in the thesis. Any contribution made to the research by others, with whom I have worked at UNSW or elsewhere, is explicitly acknowledged in the thesis. I also declare that the intellectual content of this thesis is the product of my own work, except to the extent that assistance from others in the project's design and conception or in style, presentation and linguistic expression is acknowledged.'

Signed .....

30/08/2017

Date .....

## Abstract

The actin cytoskeleton is involved in virtually every biological process. Assembly of actin structures in cells is mediated by actin-associated proteins (AAPs) that collaborate to assemble and regulate actin filaments. Actin nucleators generate linear and branched actin filaments while the tropomyosins (Tpms), known as the master regulators of actin filaments, stabilise and confer specific functions to filaments by governing their interaction with other AAPs. The dynamics of actin assembly has been studied in *in vitro* and *ex vivo* systems; however, no studies have investigated the *de novo* assembly kinetics of functional actin structures *in vivo* in mammals. Furthermore, no study has thoroughly investigated the relationship between cytoskeletal Tpms and actin filaments in cells. This thesis employed cutting-edge subcellular intravital microscopy to investigate the recruitment kinetics of the linear and branched actin nucleators, formins mDia1, mDia2 and the Arp2/3 complex, respectively, Tpms 3.1 and 4.2, myosin IIA, and the crosslinker alpha-actinin 4 during *de novo* actin scaffold assembly that drives regulated secretory granule exocytosis in rodent salivary glands, as well as the relationship between Tpm3.1 and actin filaments. This was achieved by developing a novel mouse salivary gland gene delivery technique using both viral and non-viral vectors. The findings provide insights into Tpm regulation of actin filaments, suggesting that multiple functionally distinct actin populations exist and work in tandem. Actin scaffold assembly requires the collaborative effort between multiple actin nucleators that have unique recruitment kinetics and activities. Remarkably, actin scaffold-driven regulated secretory granule exocytosis *in vivo* was shown to occur in two distinct phases, which revealed novel functions and interdependence between the branched and linear actin networks.

## Acknowledgements

My PhD journey has been without a doubt, the most enriching and flavourful experience I have had thus far. This is due in part to the amazing science which I was fortunate to be involved with and also to having the privilege of working with a group of exceptional individuals.

Firstly to Edna and Peter, my primary and co-supervisors. Thank you so much for giving me the opportunity to embark on this journey and for all the support you have given me throughout my project. I have certainly not encountered anyone else who can so effectively combine infinite enthusiasm with practical rigour and discipline. The lessons I have learned from the both of you has helped me develop not only technical skills and knowledge, but also maturity and self-awareness of character, the impact of which certainly extends far beyond the confines of the work environment. I cannot thank the both of you enough for this amazing experience.

To Anthony, Galina, Nicole, Christine, Thomas, Jeff Hook, Fabien, Sook, Lars, Yazi, Arne, Mate, Jeff Stear and Roberto Weigert. Thank you very much for all the bits of advice and help you have provided me throughout my project. Particularly Nicole, for doing an amazing job with the final edits my first paper through all those versions!

To my fellow student members of Team Intravital, Marco and Maria. It was awesome working with you guys! Thanks for the company and all the laughs we shared down in the scope room, when we subsequently escaped into sunlight, and during our various food-centered hangout sessions. To my fellow students in the CGMU, Joyce, Ashleigh, Simon, Anita, Alex from the Fath group and all the other students and staff on Level 2 East, particularly Rachael and Andrea, as well as Jorge from the Biro lab. Thanks so much for all the help and fellowship you gave me throughout all the ups and downs of lab life. I am glad all of you were there with me.

To the amazing team at the BMIF, Renee, Alex, Richard and Michael for providing technical imaging support throughout my project. In particular Michael, who was always available and enthusiastic about helping me with imaging and data analysis, in and out of hours. Thanks very much for your time and advice.

Finally, Andrius. You have been both an exceptional friend and mentor to me and I consider myself most fortunate to have worked with you, under your wing. You have the amazing ability to inspire, support and bring out the best in people which undoubtedly made you a rock of positive influence throughout my journey. I cannot thank you enough for all the help and advice you've given me. I will certainly look back fondly on our time of intravital adventures!

## Publications

Masedunskas A., **M. Appaduray**, E.C. Hardeman, and P.W. Gunning. 2014. What makes a model system great? A case for intravital microscopy for studying the actin cytoskeleton. *IntraVital* 2:3, e26287

Masedunskas, A., **M. Appaduray**, P.W. Gunning, and E.C. Hardeman. 2014. Lighting up microtubule cytoskeleton dynamics in skeletal muscle. *Intravital* 30;3(1):e29293

Bonello, T.T., M. Janco, J. Hook, A. Byun A, **M. Appaduray**, I. Dedova, S. Hitchcock-DeGregori, E.C. Hardeman, J.R Stehn, T. Böcking, and P.W. Gunning PW. 2016. . *Sci Rep.* 25;6:19816

**Appaduray, M.A.**, A. Masedunskas, N.S. Bryce, C.A. Lucas, S.C. Warren, P. Timpson, J.H. Stear, P.W. Gunning, and E.C. Hardeman. 2016. Recruitment Kinetics of Tropomyosin Tpm3. 1 to Actin Filament Bundles in the Cytoskeleton Is Independent of Actin Filament Kinetics. *PLOS ONE*. 11:e0168203

## Meeting abstracts

### **Intravital imaging at subcellular resolution reveals multiple actin filament populations involved in exocytosis of secretory granules**

Masedunskas A.<sup>1</sup>, **Appaduray M.**<sup>2</sup>, Hardeman E.<sup>2</sup> and Gunning P.<sup>1</sup>

<sup>1</sup>Oncology Research Unit, School of Medical Sciences, UNSW, Sydney, Australia.

<sup>2</sup>Neuromuscular and regenerative Medicine Unit, School of Medical Sciences, UNSW, Sydney, Australia. **ComBio2014/EMBL PhD Symposium 2014**

### **To tag or not to tag? Insights into the cellular properties of tagged Tropomyosin**

**Mark Appaduray**<sup>2</sup> Andrius Masedunskas<sup>1</sup>, Peter Gunning<sup>1</sup> and Edna Hardeman<sup>2</sup>

<sup>1</sup>Oncology Research Unit & <sup>2</sup>Neuromuscular and Regenerative Medicine Unit, School of Medical Sciences, University of New South Wales, Sydney, Australia. **ComBio 2014**

### **Sub-cellular intravital imaging reveals unique recruitment kinetics of actin nucleators and tropomyosins during the assembly of an actin coat**

**Mark A. Appaduray**<sup>1</sup>, Andrius Masedunskas<sup>2</sup>, Nicole S. Bryce<sup>2</sup>, Peter W. Gunning<sup>2</sup>, Edna C. Hardeman<sup>1</sup>

<sup>1</sup>Cellular and Genetic Medicine Unit, <sup>2</sup>Oncology Research Unit, School of Medical Sciences, UNSW Australia, Sydney, NSW 2052, Australia. **Actin in Action 2016**

## Abbreviations

$\alpha$ -actinin	Alpha-actinin 4 protein
AAP	Actin-associated protein
AAV9	Adeno-associated virus serotype 9
ADF/cofilin	Actin-depolymerising factor/cofilin
ADP	Adenosine diphosphate
AdV	Adenovirus serotype 5
APM	Apical membrane
Arp2/3	Actin-related protein 2 and 3
ATP	Adenosine triphosphate
CMDR	Cell mask deep red dye
CRISPR	Clustered regularly interspaced palindromic repeats
C-Tpm3.1	C-terminally tagged tropomyosin isoform 3.1
DID	Diaphanous-inhibitory domain
DNA	Deoxyribonucleic acid
ERM	Ezrin/radixin/moesin proteins
F-actin	Filamentous actin
FH1	Formin-homology 1
FH2	Formin-homology 2
FMNL	Formin-like protein
FRAP	Fluorescence recovery after photobleaching
G-actin	Globular actin
GBD	GTPase-binding domain
GFP	Green fluorescent protein
HMW	High molecular weight
Inf	Infusion
Inj	Injection

Lipo3k	Lipofectamine 3000
Lipo LTX	Lipofectamine LTX
LMW	Low molecular weight
LV	Lentivirus
MEF	Mouse embryonic fibroblasts
NA	Numerical aperture
N-Tpm3.1	N-terminally tagged tropomyosin isoform 3.1
NG	mNeonGreen fluorescent protein
PEI	Polyethylenimine
PIP2	Phosphatidylinositol(4,5)biphosphate
PM	Plasma membrane
RFP	Red fluorescent protein
RNAi	Ribonucleic acid interference
S.E.M	Standard error measurement
SG	Secretory granule
SV	Secretory vesicle
TIRF	Total internal reflection fluorescence
Tpm	Tropomyosin
VASP	Vasodilator-stimulated phosphoprotein
WAVE	Wiskott-Aldrich syndrome protein
YFP	Yellow fluorescent protein

## List of Figures

Figure 1.1 The structures of globular and filamentous actin.....	3
Figure 1.2 Specialised organisation of actin filaments in cells.....	5
Figure 1.3. Domain map of the diaphanous formin mDia1.....	10
Figure 1.4 F-actin interaction with Tpm.....	14
Figure 1.5 Overview of the <i>in vivo</i> granule exocytosis model.....	33
Figure 3.1 Ultrastructure of the rodent salivary gland and ductal system with potential gene delivery routes.....	50
Figure 3.2 Lentiviral transduction of mouse salivary glands.....	53
Figure 3.3 Adenoviral transduction of mouse salivary glands.....	56
Figure 3.4 Adeno-associated virus serotype 9 transduction of mouse salivary glands.....	60
Figure 3.5 Transfection of salivary glands in mTomato mice with polyethyleneimine (PEI).....	65
Figure 3.6 Transfection of salivary glands in mTomato mice with Lipofectamine.....	69
Figure 3.7 Exocytosis can be triggered in mouse acinar cells transfected with Lipofectamine 3000.....	72
Figure 4.1. N- and C-terminal tagged Tpm3.1 both localise to stress fibres in mouse embryo fibroblasts.....	80
Figure 4.2. N- and C-terminal tagged Tpm3.1 constructs have similar mobile fractions but dissimilar recovery rates.....	86
Figure 4.3 Spatial recovery of tagged Tpm3.1 is consistent with exchange rather than a diffusive transport process .....	87
Fig 4.4 Intracellular intravital imaging of the kinetics of N- and C-terminal tagged Tpm3.1 constructs transfected into rat salivary gland acinar cells .....	91
Figure 4.5. The majority of actin in stress fibres is stable.....	95

Figure 4.6. Tpm3.1 maintains constant and rapid cycling on stress fibres in the presence of jasplakinolide. ....	98
Figure 5.1 SG membrane is integrated into the APM by an actin population at the interior of the actin scaffold.....	108
Figure 5.2 Tpm3.1 is co-recruited with actin and is enriched on a subset of actin filaments ...	113
Figure 5.3 Tpm3.1 and Tpm4.2 are simultaneously recruited onto the actin scaffold.....	116
Figure 5.4 Myosin IIA is enriched at the later phase of SG exocytosis. ....	120
Figure 5.5 $\alpha$ -Actinin 4 is enriched on filaments both on the actin scaffold and at the scaffold interior driving membrane compression.....	124
Figure 5.6 mDia2 is recruited to SGs prior to actin and nucleates the initial actin filaments....	128
Figure 5.7 mDia1 is recruited at multiple phases during SG exocytosis.....	131
Figure 5.8 The Arp2/3 complex nucleates branched filaments which drive membrane compression at the scaffold interior.....	135
Figure 5.9 AAP recruitment timeline with SG and actin scaffold diameter kinetics during exocytosis.....	144
Figure 5.10 Proposed model for regulated SG exocytosis in rodent salivary glands.....	145

## List of tables

Table 3.1 Mouse salivary gland Lipofectamine transfection trials and outcomes.....	67
Table 3.2 Summary of results from various DNA delivery methods.....	74
Table 4.1. Half-times from double-exponential fits of N- and C-Tpm3.1 recovery in transfected MEFs.....	86
Table 4.2. Half-times from double-exponential fits of N- and C-Tpm3.1 recovery in transfected rat acinar cells.....	92
Table 4.3 Half-times from double-exponential fits of GFP-actin recovery in control and drug-treated conditions.....	96
Table 4.4 Half-times from double-exponential fits of Lifeact-RFP recovery in control and drug-treated conditions.....	96
Table 4.5 Half-times from double-exponential fits of C-Tpm3.1 recovery in control and drug-treated conditions.....	99

# Table of Contents

Originality statement .....	ii
Abstract .....	iii
Acknowledgements.....	iv
Publications.....	v
Meeting abstracts .....	vi
Abbreviations .....	vii
List of figures.....	ix
List of tables .....	xi
<b>Chapter 1. Introduction .....</b>	<b>1</b>
1.1. Actin: A versatile protein essential for life.....	1
Actin filament homeostasis by actin-associated proteins (AAPs).....	2
1.2 The two faces of cytoskeletal actin.....	4
Branched actin filaments and the Arp2/3 complex.....	4
Linear actin filaments and formins .....	8
1.3 Tropomyosins: Master regulators of the actin cytoskeleton.....	12
Mammalian actin filament functional diversity is matched by tropomyosin (Tpm) isoform diversity.....	12
Tpm structure, dynamics and regulation of AAP access.....	12
Tpm sorting and recruitment to branched and linear filaments .....	16
1.4 Branched and linear actin networks are independent entities that cooperate in cells .....	18
1.5 Interdependence of actin networks and nucleators.....	21
1.6 Assembly kinetics of actin networks in cells.....	24
1.7 Regulated exocytosis as a model to assess actin assembly kinetics.....	25
1.8 The rodent secretory granule exocytosis model .....	31
1.9 Thesis rationale and aims .....	35
<b>Chapter 2. Materials and Methods.....</b>	<b>37</b>
Preparation of plasmid DNA .....	37
List of plasmid DNA constructs .....	37
List of viral constructs .....	38

Immunohistochemistry.....	39
Cell culture, transfection and drug treatment.....	39
Live cell imaging and FRAP.....	40
Reporter mouse lines.....	43
Viral transduction of mouse salivary glands.....	41
Mouse salivary gland transfections.....	41
Rat salivary gland transfections.....	42
Staining and imaging of excised salivary glands.....	42
Western blotting.....	42
Intravital imaging and FRAP.....	43
Image and data processing.....	44
<b>Chapter 3. Gene delivery into mouse salivary glands.....</b>	<b>46</b>
Introduction.....	46
Results.....	51
Viral gene delivery into mouse salivary glands.....	51
LV does not efficiently transduce cells in mouse salivary glands and elicits an immune response.....	51
AdV efficiently transduces secretory acini in mouse salivary glands however without long lasting gene expression.....	55
AAV transduces secretory acini with high efficiency and long lasting gene expression without an immune response.....	58
Non-viral gene delivery into mouse salivary glands.....	62
Cationic polymer (PEI).....	63
Cationic lipid (Lipofectamine).....	67
Discussion.....	74
<b>Chapter 4. Recruitment kinetics of tropomyosin Tpm3.1 to actin filament bundles in the cytoskeleton is independent of actin filament kinetics.....</b>	<b>78</b>
Introduction.....	78
Results.....	79
Visual characterisation of N- and C-terminal tagged Tpm3.1 constructs.....	79
Tpm3.1 has a rapid rate of exchange on stress fibres.....	83
Intravital imaging and FRAP analysis of Tpm3.1 recruitment in transfected rat salivary glands.....	89
Impact of the actin-filament stabilising drug jasplakinolide on Tpm3.1 recruitment into stress fibres.....	93

4.3 Discussion.....	100
<b>Chapter 5. Recruitment kinetics of AAPs during <i>de novo</i> assembly of actin scaffolds that drives regulated SG exocytosis in rodent salivary glands.....</b>	<b>103</b>
Introduction .....	103
Results.....	105
Actin polymerisation at the scaffold interior drives membrane compression and cargo delivery into canaliculi prior to scaffold constriction and disassembly .....	105
Tpms are enriched on a subset of actin filaments indicating multiple actin filament populations cooperate to build a functioning actin scaffold .....	110
Myosin IIA is involved in the scaffold constriction and disassembly phase of exocytosis.....	118
Alpha-actinin 4 is recruited onto filaments both on the outer and inner parts of the actin scaffold .....	122
Formins nucleate the initial actin filaments during scaffold formation and have dissimilar recruitment kinetics.....	126
Arp2/3 complex is involved in driving membrane compression at the scaffold interior using pre-existing formin-generated filaments as nucleation templates .....	133
Discussion .....	137
Actin nucleators have unique dynamics and collaborate to drive regulated SG exocytosis <i>in vivo</i> .....	137
Tpm recruitment to distinct actin populations.....	140
A new model of <i>in vivo</i> exocytosis.....	142
<b>Chapter 6. General Discussion.....</b>	<b>147</b>
Overview of findings .....	147
Interdependence between linear and branched actin networks .....	148
Multiple linear actin populations co-exist in time and space and are functionally specified by Tpms .....	150
Specific actin populations can be targeted to manipulate biological processes .....	151
<b>References .....</b>	<b>153</b>

# Chapter 1. Introduction

## 1.1 Actin: A versatile protein essential for life

Actin is present in all living cells from bacteria to eukaryotes. In humans, 6 different actin genes are expressed either in muscle or non-muscle tissue. The 4 muscle actins,  $\alpha$ -cardiac,  $\alpha$ -skeletal,  $\alpha$ -smooth and  $\gamma$ -smooth, are specialised for muscle contraction while the non-muscle  $\gamma$ - and  $\beta$ -actin actins, also known as the cytoskeletal actins, are involved in virtually all cellular processes (Gunning et al., 2015a). Despite that muscle and non-muscle actins carry out distinct functions, these isoforms share at least 93% sequence identity with each other (Perrin and Ervasti, 2010). Actin is the most abundant protein in eukaryotic cells and exists either as free monomers or as polymers. Monomeric globular actin (G-actin) subunits are 42kD and consist of 375 amino acid residues organised into four subdomains and with an adenosine triphosphate (ATP) binding cleft in the middle (Figure 1 A, B). G-actin monomers can bind with each other to form filamentous actin (F-actin), a helical structure with a barbed end and a pointed end (Figure 1.1 C,D) (Dominguez and Holmes, 2011; Pollard, 2016). This process is known as actin polymerisation, which can occur spontaneously *in vitro* under physiological salt conditions and in the presence of ATP (Kuhn and Pollard, 2005; Pollard, 1986). As G-actin subunits are added and the polymer is built, the ATPase activity of actin converts ATP to adenosine diphosphate (ADP) and Pi, then finally to ADP-actin. This results in ATP-actin monomers being bound to the barbed end, ADP and phosphate-actin in the middle, with ADP-actin at the pointed end of the polymer (Bugyi and Carlier, 2010). The ATP-G-actin binding rate at the barbed end is much higher than the dissociation rate of ADP-G-actin at the pointed end, thus actin filaments elongate at their barbed ends and de-polymerise at their pointed ends (Kuhn and Pollard, 2005). This ability of actin to cycle between G- and F-actin forms allows for robust and versatile remodelling of actin filaments in the cytoskeleton for diverse cellular functions.

## **Actin filament homeostasis by actin-actin associated proteins (AAPs)**

Unlike bacterial actins that have evolved a '1-filament-1-function' system requiring multiple distinct actin pools, eukaryotic actin filaments are polymerised from a single, universal G-actin pool, thus precise regulation of actin homeostasis is required to modulate cellular functions (Gunning et al., 2015a). This is made possible through interactions with actin-associated proteins (AAPs), of which over 60 classes have been discovered (Pollard et al., 2000). An example of this is G-actin regulation by profilin, one of the first AAPs discovered (Carlsson et al., 1977). Although actin polymerisation can occur spontaneously *in vitro* (Kuhn and Pollard, 2005; Pollard, 1986), this process is energetically unfavourable in living cells due to the binding of profilin to G-actin, which prevents spontaneous polymerisation (Korn, 1982; Paavilainen et al., 2004; Pollard and Borisy, 2003). This regulation of G-actin is essential for cell survival because it allows AAPs to modulate the G- and F-actin pool. AAPs are thus employed by cells to assemble, regulate and specify actin filaments and networks into diverse structures to mediate biological processes (Figure 1.2) (Blanchoin et al., 2014).

An essential part of actin homeostasis is actin filament turnover or treadmilling, that contributes to the cycling of F-actin filaments to G-actin for downstream remodelling. Cells employ a class of AAPs known as actin depolymerising factors (ADF)/cofilin to sever and depolymerise actin filaments in a regulated manner. All eukaryotic cells express ADF/cofilin and three isoforms exist in mammalian cells: ADF, cofilin-1 and cofilin-2 (Maciver and Hussey 2002). Cofilins preferentially sever the ADP-actin portion of F-actin, the 'older' section of a filament (Suarez 2011). This occurs by cooperative binding of cofilins to filaments that induces a conformational change in filament structure, likely making filaments more amenable to severing (Bamburg 1999, Galkin 2011, McGough 1997). Cofilins therefore play an essential role in regulating actin homeostasis and localise to areas in cells with high actin turnover, such as lamellipodia and filopodia at the leading edge of cells as well as contractile rings in mitosis (Bravo-Cordero 2013, Bamburg 1999, Maciver and Hussey 2002, Vartiainen 2002).

***Figure has been removed due to copyright restrictions. Please refer to the original publication at <http://cshperspectives.cshlp.org/content/8/8/a018226.short>***

**Figure 1.1 The structures of globular and filamentous actin.** (A) Ribbon diagram of the actin monomer with space-filling ATP (protein data bank [PDB]: 1ATN). N, amino terminus; C, carboxyl terminus. Numbers 1, 2, 3, and 4 label the four subdomains. (B) Space-filling model of the actin monomer showing the nucleotide-binding cleft with ATP *in situ* and barbed-end groove. (C) Reconstruction of the actin filament from cryo-electron micrographs. The labels are single-letter abbreviations for selected amino acids. (D) Cartoon of the actin filament showing the position of the pointed and barbed ends. *Figure and legend adapted from* (Pollard, 2016).

## **1.2 The two faces of cytoskeletal actin**

### **Branched actin filaments and the Arp2/3 complex**

Actin filaments that constitute the actin cytoskeleton can be categorised into two broad classes - branched and linear actin filaments. Branched filaments are short and highly interconnected (Blanchoin et al., 2000) while the linear filaments are longer in comparison and devoid of branching (Blanchoin et al., 2014; Pollard and Borisy, 2003). The branched and linear filament networks form the basic architectural components of actin structures in cells which include lamellipodia, filopodia, and stress fibres (Figure 1.2) (Blanchoin et al., 2014; Krause and Gautreau, 2014) as well as actin coats or scaffolds in cultured cells (Miklavc et al., 2012), and in cells in tissues *ex vivo* (Tran et al., 2015) and *in vivo* (Masedunskas et al., 2011a).

*Figure has been removed due to copyright restrictions. Please refer to the original publication at <https://www.ncbi.nlm.nih.gov/pubmed/24382887>*

**Figure 1.2 Specialised organisation of actin filaments in cells.** Motile cells have distinct actin organisations in different locations in the cell that are specialised for precise functions. (i) The actin cortex is anchored to the plasma membrane through ezrin/radixin/moesin (ERM) proteins and is contractile via myosin activity. (ii) One category of contractile bundles, the stress fibres, span the cell body and are usually oriented parallel to the direction of movement. They are attached to focal adhesions

and involve a specific set of regulatory factors including formins, Ena/VASP,  $\alpha$ -actinin and myosin. (iii) Transverse arcs are specific antiparallel actin filament formations found at the back of the lamellipodium. They are contractile via myosin activity. (iv) The motor organelle, the lamellipodium, hosts rapid, massive, and localised polymerisation of branched actin networks. (A) The initiation of this dendritic network occurs via an activated Arp2/3 complex binding to the side of an actin filament 'primer' together with an interaction with members of the WAVE family of proteins. Elongation of the network occurs by addition of the profilin/actin complex (black arrows) to the barbed ends of actin filaments in close contact with the plasma membrane. (B) Ena/VASP proteins, the formin FMNL2 and capping proteins control the elongation of the network by modulating the dynamics at filament barbed ends (right zoom inset). Ena/VASP and FMNL2 favour barbed end elongation; whereas, capping protein blocks it. (v) The sensor organelles, filopodia, are filled with parallel actin bundles elongated by the actin polymerases, Ena/VASP and formins, and tightly packed by the bundling protein fascin. Another type of leading edge protrusion are blebs, initially formed as cytoskeleton-free membrane bulges driven by the internal pressure of the cell (brown arrows). *Figure and legend adapted from (Blanchoin et al., 2014).*

A class of AAPs known as the actin nucleators generate or nucleate actin filaments in cells. Branched actin is nucleated by the Arp2/3 complex of proteins, which was the first actin nucleator to be discovered (Machesky et al., 1997). One of the primary functions of the branched actin network is to generate pushing forces necessary to expand cell membranes through rapid polymerisation and assembly of a dense meshwork (Borisy and Svitkina, 2000). These are present in cellular protrusions such as the lamellipodia (Pollard and Borisy, 2003; Svitkina and Borisy, 1999). This occurs through recruitment and coupling of the Arp2/3 complex and branched filaments to the cell membrane interface, mediated by AAPs and membrane phospholipids (Goley and Welch, 2006; Takenawa and Suetsugu, 2007). Branched filaments potentially grow until capped by a subset of AAPs known as capping proteins which bind the barbed ends of filaments, according to the dendritic nucleation model (Mullins et al., 1998; Pollard and Borisy, 2003; Svitkina and Borisy, 1999). The classical Arp2/3 complex was described as containing 7 subunits: 2 actin related proteins (Arp2 and Arp3) stabilised by 5 other subunits (Machesky et al., 1997; Robinson et al., 2001; Welch et al., 1997). In its inactive form, the other subunits hold Arp2 and Arp3 apart (Robinson et al., 2001). However, when activated by nucleation-promoting factors, a subset of proteins that serve to activate and regulate actin nucleators (Machesky et al., 1999; Rohatgi et al., 1999; Rottner et al., 2010), Arp2 and Arp3 are brought closer together and reorganised into a dimer. The dimer binds to the side of a pre-existing 'mother' actin filament, thus providing a template for elongation of a new daughter filament (Rouiller et al., 2008). Daughter filaments elongate at the barbed ends at a 70° angle (Blanchoin et al., 2000; Mullins et al., 1998; Vinzenz et al., 2012) thus providing the architectural basis of the branched actin network.

For many years the general understanding in the field was that the classical seven subunit Arp2/3 complex exclusively nucleated branched actin in cells. This was called into question when a study in adult human skin cells demonstrated that the Arp2/3 complex formed a hybrid complex with vinculin (DeMali et al., 2002), an AAP involved in coupling the actin cytoskeleton to cell membranes in focal adhesions (Geiger et al., 1980). The formation of the complex was only transient in cultured cells; however, direct binding of Arp2/3 and vinculin was demonstrated *in vitro* (DeMali et al., 2002).

Nevertheless, this opened a new avenue of inquiry into the possibility that non-canonical hybrid Arp2/3 complexes exist. This was recently confirmed by mass-spectrometry analysis of purified Arp2/3 complexes from chicken gizzard smooth muscle, which demonstrated that the Arp2/3 can indeed form stable hybrid complexes with vinculin or with vinculin and  $\alpha$ -actinin (Chorev et al., 2014).  $\alpha$ -Actinin is an AAP from the cross-linker family of proteins that ubiquitously bundle and crosslink both linear and branched actin filaments, thus contributing to structural stability (Blanchoin et al., 2014; Choi et al., 2008; Courson and Rock, 2010; Lazarides, 1976). Thus multiple hybrid Arp2/3 complexes co-exist in cells and are sorted to or assembled at specific locations such as focal adhesions (Chorev et al., 2014). Recently, new mammalian Arp2/3 subunit isoforms were discovered (Abella et al., 2016), revealing that the mammalian Arp2/3 complex is a family of complexes that likely co-exist in cells (Pizarro-Cerda et al., 2017). Interestingly, using a vaccinia virus model in which virus motility is dependent on the generation of dynamic actin tails, Abella *et al.* (2016) demonstrated that Arp2/3 complex variants nucleate branched actin with different efficiencies and unexpectedly, disassembly of the respective filaments was also different. This suggests that each Arp2/3 complex variant has different properties. They also showed that Arp2/3 complex variants also interacted differently with cortactin, a nucleation promoting factor that activates Arp2/3 and assists in its targeting to filament branch points (Uruno et al., 2001; Weaver et al., 2001).

## **Linear actin filaments and formins**

The linear actin network is comprised of long unbranched filaments nucleated and elongated by a family of linear actin nucleators known as the formins (Goode and Eck, 2007). Formins nucleate and elongate higher tensile linear filaments (Fritzsche et al., 2016) that provide structural support for the assembly of a variety of cytoskeletal structures (Figure 1.2) in various cell types, including cytokinetic contractile rings and cables in yeast (Chang, 1999; Evangelista et al., 2002), actin stress fibres (Hotulainen and Lappalainen, 2006; Takeya et al., 2008; Tojkander et al., 2011), filopodia (Harris et al., 2010; Pellegrin and Mellor, 2005a; Schirenbeck et al., 2005; Yang et al., 2007), lamellipodia (Sarmiento et al., 2008; Yang et al., 2007), cytoplasmic actin networks

(Blanchoin et al., 2014; Pfender et al., 2011; Schuh, 2011), cortical actin networks (Fritzsche et al., 2016; Fritzsche et al., 2013) and in the axons of neurons (Ganguly et al., 2015). Formins also have the ability to bundle actin filaments and thus play a role in regulating actin structures in cells (Harris et al., 2010; Harris et al., 2006; Heimsath and Higgs, 2012; Jaiswal et al., 2013; Vaillant et al., 2008) and also compete with capping proteins for binding the barbed ends of filaments (Zigmond et al., 2003).

Of the 15 vertebrate formins known, the most studied are the diaphanous formins, that nucleate or elongate actin filaments from profilin-bound G-actin monomers. The general structure of diaphanous formins consists of a GTPase binding domain (GBD) followed by diaphanous inhibitory domain (DID) at the N-terminus, a formin homology 1 (FH1) domain in the middle, followed by a formin homology 2 (FH2) and diaphanous autoregulatory domain (DAD) at the C-terminus (Figure 1.3) (Paul and Pollard, 2009). The most conserved portions of the protein are the FH1 and FH2 domains (Castrillon and Wasserman 1994), with the FH1 domain only being present in diaphanous formins. The FH1 domain contains multiple binding sites for profilin binding (Watanabe 2007), while the FH2 domain binds G-actin.

*Figure has been removed due to copyright restrictions. Please refer to the original publication at <https://onlinelibrary.wiley.com/doi/full/10.1002/cm.20379>*

**Figure 1.3. Domain map of the diaphanous formin mDia1.** The arrangement of the GTPase-binding domain (GBD), the diaphanous-inhibitory domain (DID), the formin-homology (FH1) domain, the formin-homology (FH2) domain, and diaphanous autoregulatory domain (DAD), are delineated at their approximate, relative scales according to primary sequence of the full-length mDia1 formin molecule. *Figure and legend adapted from* (Paul and Pollard, 2009).

In the inactivated or 'closed' state, the DID binds the DAD, thus preventing G-actin from associating with the FH2 domain (Alberts 2001, Li and Higgs 2005). Binding of active Rho GTPases (Ridley, 2015) to the GBD partially overcomes this inhibition, thus allowing a conformational change of the protein into the activated or 'open' state (Li and Higgs, 2003; Maiti et al., 2012). The FH2 domain then dimerises to form a ring-like structure separated by a flexible linker motif, thus allowing profilin-G-actin to contact the FH1 and FH2 domains, respectively (Li and Higgs, 2005; Otomo et al., 2005a; Rose et al., 2005). Rho GTP-ases recruit and activate formins for localised filament assembly at various sites in cells (Block et al., 2012; Evangelista et al., 1997; Pellegrin and Mellor, 2005b) in addition to membrane phospholipids, that recruit and anchor formins to the plasma membrane (Ramalingam et al., 2015; Ramalingam et al., 2010). The mechanism of formin nucleation is still not well understood; however, studies suggest that activated formins nucleate actin filaments by first stabilising an actin dimer in its FH2 domain (Otomo et al., 2005b; Pring et al., 2003) which provides the actin nucleus necessary for barbed end elongation (Pruyne 2002). The formin then elongates the filament by processive addition of profilin-actin to the barbed ends by random collisions of profilin-actin to the FH1 domain. The FH1 domain acts as a 'lasso', capturing profilin for subsequent transfer of G-actin to the FH2 domain to be added at the growing barbed end. Thus the formins are constantly associated with the growing filament barbed ends as polymerisation continues (Higgs, 2005; Paul and Pollard, 2009). Fluorescence microscopy of activated GFP-tagged diaphanous mDia1 in transfected *Xenopus* cells demonstrated translocation of fluorescence spots at 2  $\mu\text{m}$  per second across the cell cytoplasm, interpreted as single formins associated with the ends of growing actin filaments (Higashida et al., 2004). Subsequently, *in vitro* TIRF microscopy studies demonstrated that mammalian formins mDia1 and mDia2 and yeast formins Bni1p and Cdc12p constantly associate with the barbed ends of single actin filaments attached to glass slides, although elongation occurred at different rates (Kovar et al., 2006). Finally, a more recent study using single molecule microscopy demonstrated that mDia1 rapidly elongates filament barbed ends in a processive manner (Breitspeicher 2012).

In summary, the branched and linear actin filaments and networks are morphologically distinct and are assembled by branched and linear nucleators at various sites in living cells. In addition, these networks coordinate to form functionally distinct higher order structures, thus precise regulation of these filaments are required. The next section will discuss the regulation of actin filaments in cells, mediated by a subset of AAPs dedicated to this purpose.

### **1.3. Tropomyosins: Master regulators of the actin cytoskeleton**

#### **Mammalian actin filament functional diversity is matched by tropomyosin (Tpm) isoform diversity**

The eukaryotic actin cytoskeleton is assembled from a single pool of G-actin derived from only two actin species. Despite this, actin filaments in cells mediate a variety of distinct and complex cellular functions. How is this achieved? Functional specificity of actin filaments is mediated by a class of AAPs known as the Tpm. Tpm are the master regulators of the actin cytoskeleton and associate with the majority of actin filaments in cells. In mammals there are >40 Tpm isoforms derived from four genes, the majority of which associate with cytoskeletal actin. Cytoskeletal Tpm can be categorised into high- and low-molecular weight isoforms (HMW and LMW, respectively), each isoform regulating and conferring a specific function to its associated actin filaments (Gunning et al., 2008; Gunning et al., 2015b).

#### **Tpm structure, dynamics and regulation of AAP access**

Tpm are rod-like, alpha-helical, coiled-coil dimers that form continuous head-to tail polymers. The polymer forms by the binding of the N-terminus of one Tpm dimer, which is a coiled-coil, to the C-terminus of the adjacent Tpm, which has a splayed structure (Greenfield 2003, 2006). Tpm polymers localise to the major groove of actin filaments, thus forming a co-polymer with actin (Figure 1.5) (von der Ecken 2014). The Tpm co-polymer enhances filament stability and prevents depolymerisation (Kawamura and Maruyama, 1970; Fujime and Ishiwata, 1971; Kojima et al., 1994;

Isambertal., 1995; Goldmann, 2000; Wen et al., 2000). In addition, Tpms regulate the interactions of AAPs with actin filaments. This has been well-studied in muscle, where Tpms decide myosin contractility by regulating its Mg ATPase (Chalovich et al., 1981; Sobieszek and Small, 1977). Cytoskeletal Tpms have been shown to recruit and influence the activity of non-muscle myosins (Bryce 2003; Tojkander 2011; Mannstein 2016) as well as protect actin filaments from disassembly by ADF/cofilin (Ono and Ono, 2002; Mazur et al., 2010) and gelsolin by directly binding gelsolin (Khaitlina 2013). Tpms also compete with other AAPs when binding to actin (Gateva et al., 2017).

*Figure has been removed due to copyright restrictions. Please refer to the original publication at <https://www.nature.com/articles/nature14033>*

**Figure 1.4 F-actin interaction with Tpm.** (a) Structural overview of an F-actin filament (green and cyan) decorated with Tpm (yellow) forming the Tpm-actin co-polymer. Half of the filament is shown in surface representation. (b) Surface of F-actin and Tpm (pseudo-repeats 2–6) with the electrostatic Coulomb potentials ranging from 210 kcal mol<sup>-1</sup> to 110 kcal mol<sup>-1</sup> at pH7.5. Tpm was rotated by 180° and shifted to the right to allow a better view on the F-actin–Tpm interface, which is delimited by lines drawn onto the surfaces. The overall negatively charged Tpm interacts with a positively charged groove on F-actin. (c) Several charged residues of actin are within distances that would make it possible to interact with Tpm via putative salt bridges. Different rotamers of the same residue are shown to indicate how F-actin subunits could adjust to the surfaces of different Tpm pseudo-repeats. *Figure and legend adapted from* (von der Ecken et al., 2015).

The Tpm polymer has an overall negative charge and forms electrostatic interactions with specific residues in the major groove of actin filaments, which has an overall positive charge. This causes the polymer to 'float' on the surface on the actin filament (Figure 1.4) (von der Ecken et al., 2015). Hence unlike other AAPs, Tpm's do not bind actin filaments, rather they associate with filaments via ionic or electrostatic interactions in the major groove. Tpm's polymerise on actin filaments in a cooperative manner, where individual Tpm's have a low affinity for actin (Wegner 1980); however, upon addition of more Tpm subunits into the polymer, this affinity is dramatically increased (Wegner 1979, Wegner 1980).

Due to this high cooperativity of binding of Tpm's to actin filaments, it was the general assumption in the field that Tpm polymer dynamics are dependent on actin filament dynamics. Little is known however, regarding the stability of these ionic interactions as well as recruitment kinetics of cytoskeletal Tpm's to actin filaments in cells and there is virtually no data on Tpm dynamics *in vivo*. Martin et al. showed in transfected NIH3T3 cells using fluorescently tagged Tpm's that the isoform 3.1 (Tpm3.1) has an 85% mobile fraction and a higher rate of recovery on actin stress fibres compared to other Tpm's as assessed by fluorescence recovery after photobleaching (FRAP) analyses (Martin et al., 2010). Similarly, Tojkander et al. showed that recruitment kinetics for GFP/YFP-tagged Tpm3.1 and Tpm4.2 on actin stress fibres differ in cultured U2OS cells, where Tpm4.2 has a faster recovery and higher mobile fraction compared to Tpm3.1. Interestingly, a FRAP kinetics study in muscle cells suggested that Tpm's may be exchanging independently of actin filaments (Wang et al., 2014). However, the investigators did not completely abolish actin turnover when assessing Tpm dynamics, thus Tpm interdependency with actin dynamics remained inconclusive. Recently, TIRF analysis revealed that Tpm recruitment was highly dynamic compared to actin filaments. In addition, Tpm dynamics varied amongst different isoforms, with HMW isoforms having lower recruitment rates compared to LMW isoforms which were significantly faster (Gateva et al., 2017). This is supported by another study showing that HMW isoforms have a higher cooperativity for actin compared to LMW isoforms (Janco 2016). These studies were performed *in vitro*; therefore, no study has definitively addressed the interdependency of the dynamics of cytoskeletal Tpm's and actin filaments in cells. This

interdependency is investigated in cell culture and *in vivo*, in the cells of a live animal, in Chapter 4.

### **Tpm sorting and recruitment to branched and linear filaments**

Individual Tpm isoforms have been shown to segregate to distinct cellular locations in various cell types and regulate filaments in a functionally distinct manner (Gunning et al., 2008). Hence, it is possible that individual Tpm isoforms segregate to individual actin filament populations. Recently, an *in vitro* TIRF study supported this hypothesis. Gateva *et al.* demonstrated that Tpm isoforms segregate to distinct actin filament populations and regulated the interaction of these filaments with other AAPs such as  $\alpha$ -actinin and ADF/cofilin. In addition, Tpm isoforms derived from the same gene are able to co-polymerise on individual actin filaments; whereas, isoforms from different Tpm genes did not co-polymerise and instead formed distinct segments on filaments (Gateva 2017). This study revealed novel information about the compatibility for co-polymerisation and regulation of Tpm's in addition to recruitment to specific filaments. However, these experiments were done *in vitro*, hence this property of Tpm isoforms will have to be confirmed in cells. In addition, the study did not provide a mechanism of how the Tpm's are sorted to distinct filaments, as well as the recruitment activity of Tpm's to different populations of branched and linear filaments, generated by different nucleators.

Studies in yeast and cultured mammalian cells provide insights into whether Tpm's segregate to distinct linear actin filament populations in cells. Tojkander et al. demonstrated reduced recruitment of Tpm4.2 to stress fibres in U2OS cells after knocking down mDia2 expression (Tojkander et al., 2011). More recently, Johnson et al. demonstrated that formins determine the isoform composition of Tpm's on yeast actin filaments (Johnson et al., 2014). Therefore, it appears that the formins play a role in sorting Tpm's to specific linear filaments, either by generating filaments that are compatible with the binding of specific isoforms or by incorporating the Tpm into the growing actin filament, directly generating a Tpm-actin co-polymer.

Conversely, Tpm's have also been shown to regulate the activity of formins and stability of formin-mediated linear filaments. In studies using circular dichroism measurements, various Tpm isoforms bound to actin filaments were demonstrated to interact with the FH2 domain of FRL1 and mDia2 formin, resulting in activation of barbed elongation by these formins (Wawro et al., year). In other studies, Tpm's were shown to stabilise the structure of mDia1-bound filaments, making mDia1 filaments more rigid and less dynamic (Ujfalusi 2009, 2012). Furthermore, a study in yeast showed that the yeast Tpm has multiple functions when regulating filament assembly by formin Cdc12p. In the presence of Tpm, Cdc12p is able to overcome inhibition of actin nucleation and elongation and accelerates filament elongation 2-fold. In addition, the yeast Tpm promoted end-to-end annealing of Cdc12p filaments, but also inhibited filament elongation by 'trapping' or dissociating its binding at the barbed end (Skau et al., year).

In contrast, Tpm interaction with the Arp2/3 complex is largely unknown and Tpm's presence on branched actin filaments has been a subject of much controversy. This is largely due to several studies demonstrating that Tpm's are absent from lamellipodia (Blanchoin, Pollard & Hitchcock-DeGregori, 2001; Bugyi, Didry & Carlier, 2010; DesMarais et al., 2002; Gupton et al., 2005; Iwasa & Mullins, 2007; Koestler et al., 2013; Ponti et al., 2004; Skau et al., 2015). In addition, it was shown that Tpm's compete with the Arp2/3 complex for binding sites on actin filaments (Blanchoin, Pollard & Hitchcock-DeGregori, 2001). Coupled with the understanding that branched filaments make up the majority of lamellipodial actin (Blanchoin et al., 2000), it was assumed that branched filaments are devoid of Tpm's.

This view was recently called into question when Hsiao et al. demonstrated that cofilin severing of branched actin filaments produced pointed ends to which Tpm's preferentially bind (Hsiao 2015). This was subsequently confirmed by Brayford et al. (2016), who provided definitive evidence that Tpm's 1.8/1.9 are indeed recruited to lamellipodial actin filaments at the leading edge using a novel antibody (Brayford et al., 2016). In addition, RNAi silencing of Tpm1.8/1.9 resulted in accumulation of Arp2/3 at the leading edge and decreased lamellipodial persistence, while Arp2/3 inhibition resulted in increased Tpm 1.8/1.9 accumulation, in accordance with previous studies (Blanchoin, Pollard & Hitchcock-DeGregori, 2001). In contrast, the absence of cofilin

reduced the presence of Tpm1.8/1.9 on lamellipodial actin (Brayford et al., 2016), in accordance with the study by Hsiao et al. Hence, Tpms play a role in regulating Arp2/3 complex activity and branched filament formation in cells, similar to formins and linear filaments, discussed previously. Furthermore, Tpm insulation of lamellipodial filaments provided an answer to the long-standing conundrum of how multiple filament populations can co-exist at the leading edge of cells.

In summary, Tpms play a central role in regulating linear and branched actin filaments and the activity of their respective nucleators. In addition, it is likely that the actin cytoskeleton consists of multiple distinct populations of actin filaments that recruit specific AAPs such as Tpms for their regulation and homeostasis. Hence, the next section reviews key studies that demonstrate the co-existence of distinct actin populations in cells, as well as evidence of their collaboration and coordination when mediating cellular functions.

#### **1.4. Branched and linear actin networks are independent entities that cooperate in cells**

As mentioned previously, the actin cytoskeleton consists of two filament classes, linear and branched, which are nucleated by formins and the Arp2/3 family of complexes, respectively. Filament homeostasis in eukaryotic cells is regulated by AAPs, with the master filament regulators being the Tpms. It is clear that both these networks are involved in the infrastructure of a variety of different cellular structures, suggesting that they might influence each other. Hence, the dynamics of these networks is a topic of great interest in the field as understanding their kinetic behaviour would provide mechanistic insight into how these networks operate in living cells. The next section of this chapter will focus on key discoveries that illuminate the kinetic differences and interdependence of the branched and linear networks in cells.

One of the first studies that addressed the kinetics of branched and linear networks was performed by Ponti et al. (2004), who utilised novel fluorescence speckle microscopy techniques to demonstrate that two filament networks spatially overlap in the lamellipodia of cells. These networks, comprising branched and linear filaments

had kinetically, kinematically and molecularly distinct properties. The branched filament network had fast retrograde flow and was localised in the lamellipodium, while the linear population had slower turnover and was more rigid, decorated with Tpms and myosins. The authors concluded that the more dynamic branched network appeared to 'surf' on the more rigid and linear lamella network, suggesting that these networks were only weakly coupled to each other. In addition, the advancement of the entire lamellipodia structure was dependent upon the more rigid linear lamella network, which achieved this via formation of protrusions (Ponti et al., 2004). This indicated that the branched and linear networks, despite existing in the same space, were behaving as two separate entities that synergistically collaborate to mediate lamellipodial advancement and cell migration. In addition, cell migration was dependent on activity of the linear network in the lamella.

More evidence of this interdependence between the linear and branched actin networks was recently described by Fritzsche et al. (2013). They demonstrated in a melanoma cell line that cortical actin consists of two kinetically distinct actin populations, one population having rapid turnover dynamics and accounting for 69% of cortical actin, and the other having slower turnover dynamics accounting for the remaining 31%. The slower subpopulation consisted of filaments that were on average much longer than the more dynamic population and were found to associate with formins. Of particular relevance is that the authors demonstrate that cofilin-mediated filament severing of the longer, more stable filament population contributes to the turnover of the more abundant and dynamic filament population. Hence, these subpopulations of filaments are interdependent and the linear formin-associated population determines the integrity of the more dynamic network (Fritzsche et al., 2013).

A subsequent study by the same group showed that formin-nucleated filaments were on average 10 times longer than Arp2/3 branched filaments, although in their estimate these filaments accounted for only ~10% of cortical actin filaments. Remarkably, they show that inhibition of formins and linear filaments, not Arp2/3 and branched filaments, affects cortex integrity in cells, as demonstrated by atomic force microscopy measurements of cortex elasticity. Thus, even though formin-nucleated linear

filaments account for only ~10% of cortical actin filaments, they play a pivotal role in maintaining cortex integrity, likely through dissipating mechanical stresses along the length of the longer, more rigid linear filaments (Fritzsche et al., 2016).

The kinetics studies discussed previously were elegantly supported in a functional assay performed by Ramalingam *et al.* (2010). They demonstrated for the first time that the formins For A and mDia1 in *Dictyostelium* and B16 mouse melanoma cells, respectively, generate a subset of filaments that contribute to a more rigid cortical actin sheath in the rear of cells. This subset of filaments along with actin cross-linkers and myosin II, functions to withstand contractile and hydrostatic forces generated from mechanical stress, thus driving bleb formation at the front and resulting in forward cell movement. Remarkably, mDia1 dynamically relocates to the rear cortex of turning B16 cells, indicating an active sorting mechanism involving membrane phospholipids (Ramalingam et al., 2010). They also demonstrate that cells lacking formin For A migrate at almost double the speed of control cells, likely due to an overall less rigid cortical actin meshwork thus allowing easier compression in the rear and blebbing in the front (Ramalingam et al., 2015). Therefore, actomyosin-mediated cell migration requires a softer cell cortex with presumably low-tensile, highly dynamic branched filaments at the leading edge to drive membrane blebbing, while a more rigid rear cell cortex, comprising formin-generated linear and presumably higher tensile filaments, is required to withstand mechanical forces at the rear of cells.

Another study by Bovellan *et al.* (2014) demonstrated that formin mDia1 and Arp2/3 collaborate to generate *de novo* cortical actin networks in HeLa and M2 melanoma cell blebs, but with differing accumulation kinetics. Inhibition of Arp2/3 with a small molecule inhibitor CK666 resulted in ~60% decrease in cortical actin in the presence or absence of mDia1. In addition, mDia1 localised to the cell cortex in both Arp2/3-depleted and CK666-treated cells, indicating that Arp2/3 contributes to cortical actin density independently of mDia1 and that both nucleators localise independently of each other. Depletion of mDia1 resulted in areas with high filament density with gaps of 100-200 nm between filaments, compared to gaps of ~30 nm in control conditions. In contrast, Arp2/3 depletion led to longer filaments overall, again distinguishable from controls, indicating that both linear and branched filaments co-exist in the same space,

although direct collaboration between these nucleators was still unclear. Cortical actin assembly was also affected. In mDia1-depleted cells, cortical actin assembly was 2-fold slower than controls. In contrast, perturbing the Arp2/3 complex resulted in a ~2-fold increase in actin assembly kinetics. The overall cortex structure was maintained when perturbing or depleting either nucleator separately; however, it was significantly compromised when both nucleators were depleted simultaneously. Inhibition or depletion of the Arp2/3 complex did not significantly affect cell cytokinesis; however, depletion of mDia1 significantly affected cell cycle progression past mitosis. Inhibition of Arp2/3 in mDia1-depleted cells potentiated this effect, indicating that mDia1 appears to act upstream of Arp2/3 during cortical actin network assembly (Bovellan et al., 2014).

In summary, the branched and linear actin filaments are generated as kinetically and functionally distinct networks; however, they cooperate to mediate cellular processes. In addition, the more stable and rigid linear network determines the integrity of the overall actin cortex (Fritzsche et al., 2016; Fritzsche et al., 2013), as well as being the primary effector of cellular processes such as cell migration (Ponti et al., 2004; Ramalingam et al., 2015), even in the absence of a functional Arp2/3 complex (Suraneni et al., 2015). There appears to be a seamless transition between the architecture of the linear and branched actin networks in cells (Bovellan et al., 2014). This is evidenced by the presence of both linear and branched nucleators and filaments in a variety of actin structures (Blanchoin et al., 2014; Bovellan et al., 2014; Campellone and Welch, 2010). In addition, these networks and their respective nucleators are highly dynamic and are able to rapidly relocate to specific sites in cells to generate the required filament architecture (Campellone and Welch, 2010; Ramalingam et al., 2015; Ramalingam et al., 2010). The next section will focus on mechanistic evidence that demonstrates the interdependence of these networks and nucleators during the assembly of actin structures in cells.

## **1.5. Interdependence of actin networks and nucleators**

Previous studies have established that both linear and branched filaments are present in lamellipodia (Campellone and Welch, 2010; Pollard and Borisy, 2003; Ponti et al., 2004) and that the Arp2/3 branched network is essential for lamellipodial formation (Suraneni et al., 2012). However, the mechanism of initiation of the lamellipodial branched network was still unclear, because efficient Arp2/3 branched filament polymerisation requires pre-existing mother filaments (Rouiller et al., 2008). Mechanistic insight into lamellipodial actin assembly was provided by two studies that demonstrated direct collaboration between linear and branched nucleators in generating lamellipodial actin networks (Block et al., 2012; Isogai et al., 2015) and membrane ruffles (Isogai et al., 2015). Using an *in vitro* TIRF assay Block *et al.* showed that formin FMNL2 elongates Arp2/3 filaments at the barbed ends in the presence of profilin. In addition the authors demonstrate that FMNL2 localises to lamellipodial tips and that RNAi knockdown of FMNL2 results in reduced lamellipodial protrusion, thus impairing cell migration (Block et al., 2012). This is consistent with other studies demonstrating the dependence on the linear filament network in migrating cells (Ponti et al., 2004; Ramalingam et al., 2015; Suraneni et al., 2015). Complementary to Block *et al.*, Isogai *et al.* used an *in vitro* TIRF assay to demonstrate that branched actin generation by Arp2/3 is severely impacted in the absence of mDia1 and linear filaments. Addition of mDia1 resulted in dramatically increased generation of branched actin arrays, which occurred in a dose-dependent manner. In accordance with this, inactivation of mDia1 in cells significantly reduced lamellipodia and ruffle formation. However, once the initial mother filaments are assembled the Arp2/3 complex is able to generate more branched filaments in an autocatalytic fashion (Isogai et al., 2015). Taken together, these studies provided mechanistic evidence demonstrating that linear and branched nucleators directly collaborate to generate functional actin networks and structures. In addition, initial Arp2/3 branched network polymerisation efficiency is dependent on mDia1 linear filaments. These observations provided a solution to the conundrum of the branched and linear networks being kinetically and functionally distinct, yet interdependent upon each other as was demonstrated in other studies (Bovellan et al., 2014; Fritzsche et al., 2016; Fritzsche et al., 2013; Ponti et al., 2004).

This interdependency between branched and linear actin networks was further supported by Kage *et al.* (2017), who demonstrated that the FMNL formin linear filaments work independently, although in cooperation with Arp2/3 branched filaments to mediate effective migration of B16 and fibroblast cells (Kage *et al.*, 2017). FMNL loss of function adversely affects network rigidity impeding the ability of cells to exert lamellipodial forces to move beads or facilitate cell migration through a polymer matrix of varying viscosity, indicating that the absence of FMNL linear filaments affects the cell's ability to cope with counteracting forces. The authors hypothesise that this is caused by reduction of filament mass and orientation possibly compromising their ability to exert required pushing forces, also consistent with overexpression of FMNL formins promoting metastasis and invasion of colorectal carcinoma cells (Zheng 2015; Zhu 2011). This was confirmed by FMNL2/3 knockout resulting in reduced lamellipodial width, protrusion frequency and total filament mass which was independent of Arp2/3 polymerisation, strongly indicating that these phenotypic changes were due to loss of FMNL2/3 filaments specifically. In addition, ultrastructural changes to the overall filament network was confirmed by electron microscopy (Kage *et al.*, 2017), also observed in another study (Bovellan *et al.*, 2014). Interestingly, the authors demonstrate that *in vitro* FMNL3 nucleates filaments more potently than FMNL2; however, FMNL2 elongates filaments significantly faster than FMNL3 thus providing kinetic analysis to support the notion that individual formins have distinct behaviour and functions in cells (Kage *et al.*, 2017), also supported by other studies (Bovellan *et al.*, 2014; Isogai *et al.*, 2015; Kovar, 2006; Ramalingam *et al.*, 2015).

In summary, these studies indicate that the linear and branched actin networks are distinct entities that work in synergy to mediate biological functions. Moreover, multiple distinct linear filament populations co-exist in cells, nucleated by different formins (Kage *et al.*, 2017) and are functionally specified by association with distinct Tpm isoforms (Gateva *et al.*, 2017; Johnson *et al.*, 2014). This paradigm could also be extended to the branched filament network as recent discoveries have revealed that the Arp2/3 complex is a family of complexes which can form further hybrid complexes with AAPs (Abella *et al.*, 2016; Chorev *et al.*, 2014; Pizarro-Cerda *et al.*, 2017) and are regulated by Tpm (Brayford *et al.*, 2016). The highly dynamic branched network

appears to be dependent upon the more rigid and stable linear filaments to direct its polymerisation activity (Fritzsche et al., 2016; Fritzsche et al., 2013; Ramalingam et al., 2015).

## **1.6. Assembly kinetics of actin networks in cells**

In previous sections, it was established that multiple kinetically and morphologically distinct actin populations co-exist in various actin structures in cells. In addition, AAPs such as actin nucleators, Tpms, myosins and actin crosslinkers are recruited to nucleate, elongate and regulate filament homeostasis when mediating cellular functions. However, what is not well understood in the field is the assembly kinetics of these networks and recruitment kinetics of AAPs to filaments. What is the mechanism of assembly of these actin networks and structures and how do these molecular players modulate actin *in vivo*? What are the individual functions that these proteins convey to the system and can we assess their interdependence with each other? The answers to these questions are being pursued by many research groups, using a variety of experimental approaches.

One powerful approach is to investigate filament assembly and protein recruitment kinetics *in situ* during the biological process of interest. This would allow observation of the assembly sequence of a functional cytoskeletal network, thereby providing mechanistic insights into how these proteins cooperate to modulate actin as well as the roles and functions they convey to the system. Research groups have used a variety of experimental models to investigate actin assembly and protein recruitment to filaments albeit with significant limitations. In mammalian cell culture models, the actin network is constantly treadmilling (Theriot and Mitchison, 1991), thus making assembly or recruitment kinetics studies extremely challenging because it is difficult to resolve the complete lifetime of a filament or a functional set of filaments. In *in vitro* models, it is possible to assess the dynamics and relationships of individual purified proteins and their influence on filaments (Pollard, 2016); however, these studies lack biological relevance and complexity since they are performed in an artificial, simplified environment.

The ideal model therefore, would be an inducible *in vivo* system whereby the stepwise assembly of cytoskeletal components can be resolved and quantified. In addition, the system should allow for assessment and quantification of phenotypic outcomes resulting from genetic and pharmacological perturbations targeting specific components involved in actin assembly and regulation.

The fission yeast cytokinesis model provided an excellent platform for initial studies on *de novo* actin assembly kinetics. These studies showed that there is a clockwork-style assembly of cytoskeletal components during the formation of the cytokinetic ring. Formins and myosins are first recruited to the ring followed by actin, Tpm's and  $\alpha$ -actinin. This is followed with recruitment of another myosin isoform along with septins, thus finally resulting in ring constriction and cytokinesis (Longtine et al., 1996; Pelham Jr and Chang, 2002; Pollard and Wu, 2010; Vavylonis et al., 2008).

### **1.7 Regulated exocytosis as a model to assess actin assembly kinetics**

Various groups have used regulated exocytosis as a model to investigate *de novo* actin assembly kinetics. Regulated exocytosis is an essential process that occurs in various secretory cell types (Porat-Shliom et al., 2013). Essential biological factors such as proteins and enzymes are produced by these cells and packaged into secretory vesicles (SVs) (~200-350 nm in diameter) or granules (SGs) (1-2  $\mu$ m diameter in mammals and 3-8  $\mu$ m diameter in *Drosophila*) that are stored in the cytoplasm. Upon receiving an extracellular stimulus which triggers the process, SG- or SV-containing cargo are trafficked to the apical plasma membrane (APM) or plasma membrane (PM) in cells, where they fuse and extrude their cargo to the cell exterior. This process is mediated by the actin cytoskeleton, which performs multiple functions.

### **Neurosecretory cells as models for regulated secretory vesicle trafficking, fusion and exocytosis**

Actin involvement in regulated exocytosis has been successfully investigated in cultured bovine chromaffin cells as well as rodent-derived PC-12 cells that are still powerful models in use today. These neurosecretory cells can be triggered to secrete

catecholamines via calcium-dependent exocytosis of SVs using externally applied secretagogues, hence are excellent models to study cytoskeletal and fusion mechanics (Cheek, 1991; Rubin, 1970; Trifaro and Lee, 1980; Trifaro et al., 1992; Vitale et al., 1991; Westerink and Ewing, 2008). The catecholamine cargo is first packaged into SVs formed at the trans-Golgi network (Borgonovo et al., 2006; Tooze and Huttner, 1990) that are 200-350 nm in size (Burgoyne and Morgan, 2003; Oheim et al., 1998). After maturation, SVs are then trafficked to the cortical region for subsequent exocytosis, a process that involves actin, microtubules and motor proteins such as myosin Va that translocates SVs along actin filaments (Rudolf et al., 2003; Rudolf et al., 2001). The membrane phospholipid phosphatidylinositol(4,5)biphosphate (PIP2), that forms clusters at exocytosis sites on the PM, regulates the number of granules available for exocytosis independently of exocytosis kinetics (Milosevic et al., 2005) by governing their translocation from intracellular pools to the PM (Wen et al., 2011). PIP2 clusters also act as beacons that guide SVs to exocytosis sites, facilitating their docking and fusion by bridging the interaction of SNARE proteins on both plasma and SV membranes (Aoyagi et al., 2005; Honigsmann et al., 2013). In addition, they regulate cytoskeletal dynamics through modulation of GTPase and actin nucleator activity (Bader et al., 2004; Di Paolo and De Camilli, 2006; Ramalingam et al., 2010). SNARE proteins mediate fusion by forming a complex between compatible binding partners, that are present on both the SVs and PM. The SNARE complex is then clasped by Munc-related proteins, that stabilise the SNARE complex and fusion of membranes, hence allowing exocytosis to proceed (Südhof and Rothman, 2009). Once SVs are docked and fused to the PM exocytosis occurs very rapidly and is believed to be a passive process, with entire pools of SVs adjacent to the PM being exocytosed within hundreds of milliseconds upon secretagogue stimulation, with single events in 17-19 ms (Ñeco et al., 2004; Oheim et al., 1998). The translocation and exocytosis of SVs is mediated by intricate control and remodelling of the actin cytoskeleton that performs multiple functions as discussed in the next section.

### **Cortical actin regulation of exocytosis in neuroendocrine cells**

Orci *et al.* provided the first evidence of a 'microfilament web' involved in regulating SG access to the PM in rat pancreatic  $\beta$ -cells (Orci *et al.*, 1972). Lee and Trifaró subsequently observed similar structures in chromaffin cells, revealing this microfilament web to be a meshwork of actin filaments highly enriched at the cortical region and providing the first indication of cortical actin involvement in SV exocytosis (Lee and Trifaró, 1981). A further study by Trifaró *et al.* indicated that the cortical actin meshwork likely undergoes contractile activity involving AAPs such as  $\alpha$ -actinin, myosin and tropomyosin, suggesting that it may be dynamically remodelled (Trifaró *et al.*, 1985). This was confirmed by Cheek *et al.* who elegantly demonstrated that cortical actin is indeed able to disassemble and re-assemble upon secretagogue stimulation due to a rise in intracellular calcium (Cheek, 1991; Cheek and Burgoyne, 1986). These discoveries gave rise to the concept of cortical actin functioning as a barrier that regulates SV access to the PM, hence controlling exocytosis and catecholamine release from cells (Aunis and Bader, 1988). In addition to being a barrier, the cortical actin network was also shown to regulate the sequestration of SVs in the vicinity of the PM by housing matured SVs in polygonal actin 'cages', which can be remodelled upon secretagogue stimulation to facilitate exocytosis (Johns *et al.*, 2001; Tchakarov *et al.*, 1998). This suggested that cortical actin may function as both a PM barrier and as facilitator of SV transport to the PM. Giner *et al.* confirmed this by exploiting microscopy techniques as well as actin and myosin inhibitors to demonstrate that the cortical actomyosin network indeed functions as a barrier and carrier system that regulates SV translocation from intracellular pools to the PM for exocytosis (Giner *et al.*, 2005). Furthermore, SV translocation kinetics are dependent upon cytoskeletal organisation and remodelling at sites of calcium influx into cells (Giner *et al.*, 2007; Torregrosa-Hetland *et al.*, 2011), and involves the concerted effort of both actin and microtubules (Maucort *et al.*, 2014). Recently, new intriguing insights into the mechanism of SV translocation by the actomyosin network were revealed. Papadopoulos *et al.* demonstrated that upon secretagogue stimulation, the entire actomyosin network transitions towards the plasma membrane like a 'casting net', enabling tethered SVs to dock at exocytosis sites containing the protein Munc-18-1. The mechanism of this transition is the result of secretagogue-dependent modulation

of myosin II motor activity that relaxes the cortical actomyosin network, hence allowing the entire network to advance to the PM (Papadopoulos et al., 2015).

Delving into the mechanics of cytoskeletal remodelling, various groups investigated the roles and functions of individual AAPs and upstream signalling proteins involved in this process. Vitale *et al.* determined that disassembly of the actin barrier involved the actin-cleaving protein scinderin, and that actin disassembly occurred at sites of SV exocytosis (Vitale et al., 1991). This disassembly is also required for translocation of SVs from the cortical region to the PM, demonstrated by cortical actin disruption directly affecting the SV pool available for exocytosis and catecholamine release from cells (Vitale et al., 1995). This was a key discovery in the field, as prior to this there was no definitive evidence linking cytoskeletal involvement in SV exocytosis and secretion. Rho GTPases were then implicated in this process, through upstream signalling events that activate cytoskeletal exocytosis machinery (Brown et al., 1998; Kowluru et al., 1997). The link between Rho GTPase signalling and actin remodelling was confirmed by Gasman *et al.* who initially used pharmaceutical inhibition to elucidate specific functions for RhoA and Cdc42 GTPases in remodelling cortical actin during SV exocytosis. RhoA was discovered to be involved in remodelling actin filaments in the vicinity of intracellular SV pools in resting chromaffin cells, while Cdc42-mediated cortical actin remodelling preceded catecholamine secretion in secretagogue-stimulated cells (Gasman et al., 1999). The same group subsequently showed for the first time that Cdc42 not only drives disassembly of the cortical actin barrier preventing SV-PM fusion, but also finely remodels the actomyosin network to facilitate trafficking of SVs to the PM from intracellular pools. This involved N-WASP recruitment to the PM as well as Arp2/3 activation which generates *de novo* filaments at the SG-PM interface at sites of exocytosis (Gasman et al., 2004). The remodelled cortical actin network, along with myosin II, regulates fusion pore opening upon exocytosis (Ñeco et al., 2008). Recent evidence shows that actomyosin activity exerts tensional forces on the PM which favours SV-PM integration and cargo delivery (Gauthier et al., 2012), suggesting a mechanism into how SVs are rapidly and passively exocytosed. Remarkably, Wen *et al.* subsequently showed that PIP2 signalling activates Cdc42 independently of secretagogue stimulation, linking phospholipid signalling to Cdc42-

driven cytoskeletal remodelling as well as to SV docking and fusion machinery on the PM (Aoyagi et al., 2005; Honigsmann et al., 2013; Wen et al., 2011).

These studies provided the foundational knowledge on exocytosis mechanics and established that *de novo* generation and remodelling of actin filaments is required for SV exocytosis. Furthermore, these dynamic processes are mediated by a variety of AAPs and signalling factors. However, precise kinetic measurements of *de novo* cytoskeletal assembly as well as AAP recruitment dynamics and modulatory functions are extremely challenging to obtain using this model. This is due to SV exocytosis occurring in a very rapid fashion (17-19 ms per event), the size of SVs being small (200-350 nm) and the cortical actin network being a complex, homogeneous structure with very dynamic behaviour. Hence, other regulated exocytosis models involving large SGs were explored, where SG exocytosis occurs over longer time scales and requires the assembly of an actin scaffold around fused SGs, allowing kinetic mapping of cytoskeletal assembly during this process.

### **Large granule exocytosis models for actin assembly and function**

In secretory cells that exocytose large SGs such as in *Drosophila* larvae salivary glands, SG sizes range from 1-8  $\mu\text{m}$  and take up to 120 s to exocytose (Tran and Ten Hagen, 2017). In the lung epithelium model (AECII cells), lamellar bodies or granules range up to 1-2  $\mu\text{m}$  in size and take 60-90 s to exocytose (Miklavc et al., 2015; Miklavc et al., 2012), while in endothelial models such as HUVECs cells, Weibel-Palade bodies range from 1-2  $\mu\text{m}$  in size and exocytosis takes up to 40 s (Nightingale et al., 2011). Finally, in the acinar cells in rodent pancreas or salivary glands, SGs range from 1-2  $\mu\text{m}$  in size and exocytosis occurs over 60-120 s (Masedunskas et al., 2012b; Masedunskas et al., 2011a). Due to the large sizes of the granules in these models, it is not possible for passive SG-PM integration and cargo expulsion to occur such as in neurosecretory cells, although an actin barrier still prevents uncontrolled SG fusion to the APM of these cells (Meunier and Gutiérrez, 2016; Porat-Shliom et al., 2013; Tran et al., 2015). However upon SG fusion, an actin scaffold is assembled *de novo* around the fused SGs which is essential for driving granule compression and cargo delivery to the cell exterior (Masedunskas et al., 2012b; Masedunskas et al., 2011a). Due to actin scaffold

assembly occurring upon SG fusion, the stepwise assembly and recruitment kinetics of proteins involved can be captured and measured in cells using direct microscopy-based methods, which provides significant advantages over SV exocytosis models described previously. Hence, the regulated large SG exocytosis model is an excellent platform upon which to tease out the functions and recruitment kinetics of individual proteins, as well as the assembly dynamics of actin populations involved.

Recently, Miklavc et al. investigated the role of actin nucleators during actin scaffold formation around fused lamellar bodies or SGs in ATII cells. Chemical inhibition of Rho GTPase and formins resulted in significantly reduced F-actin scaffolds post-fusion. In contrast, inhibition of the Arp2/3 complex did not result in significant reduction of F-actin on SGs, thus indicating that formin-generated linear filaments play a major role in scaffold formation in these cells (Miklavc et al., 2012). In a subsequent live cell study by the same group, they demonstrated that  $\alpha$ -actinin is recruited at the time of actin scaffold formation as detected by dual expression of fluorescent constructs, while myosin II and cofilin are recruited after. The studies also revealed that myosin II inhibition only delays contraction, also described elsewhere (Hoi-Ying and Bement, 2007; Masedunskas et al., 2011a). Inhibition of cofilin and  $\alpha$ -actinin revealed important regulatory roles for these proteins during scaffold contraction, where their inhibition resulted in severely impaired scaffold compression rates (Miklavc et al., 2015).

More recently, Tran et al. demonstrated in *ex vivo Drosophila* salivary glands that upon fusion, the phospholipid PIP2 is redistributed from the APM to the SG membrane, followed by F-actin and finally Arp2/3 recruitment onto the fused SG (Tran et al., 2015). This demonstrates that Arp2/3 complex is recruited to pre-existing filaments generated by other nucleators that form the scaffold upon SG fusion. siRNA knockdown of Arp2/3 both *ex vivo* and *in vivo* showed that *Drosophila* SGs are unable to complete the cargo delivery or membrane integration step of exocytosis. In some cases, the SGs expanded in size and detached from the APM, indicating that the branched actin network plays a pivotal role in membrane integration and structural stability. However, F-actin was still detected on fused SGs post Arp2/3 knockdown, indicating that linear actin was likely still present, nucleated by formins prior to the recruitment of Arp2/3 complex. This is in accordance with the classical behaviour of

the Arp2/3 complex requiring pre-existing mother filaments for branched network generation (Rouiller et al., 2008), as well as PIP2 recruiting and activating actin nucleators at the plasma membrane (Higgs and Pollard, 2000; Ramalingam et al., 2010). Inhibition of both linear and branched actin polymerisation with small molecule inhibitors resulted in compound fusion events, which was not observed with Arp2/3 knockdown. This indicates that the initial filaments are providing a barrier preventing compound fusion events with other SGs, similar to the cortical actin mesh at the APM of cells (Porat-Shliom et al., 2013; Tran et al., 2015).

In summary, the ability to measure protein recruitment kinetics and phenotypic readouts after genetic and pharmacological manipulation yielded unprecedented mechanistic insights into protein function, which had not been possible previously.

## **1.8 The rodent secretory granule exocytosis model**

Studies using the large SG model systems mentioned previously have provided valuable mechanistic insights into cytoskeletal network assembly in living cells and organ-cultures. A significant limitation however, is that these studies did not directly investigate the recruitment of formins and linear actin, which likely precedes Arp2/3 branched network generation on fused SGs. Another limitation is that the physiology and biology of these model systems are substantially different to intact, living mammalian tissue. Thus, the observations from these models may not represent the biology of intact mammalian tissues and hence may not be relevant to humans.

The rodent SG exocytosis model developed by Masedunskas *et al.* provides an elegant solution to these limitations. This model allows the stepwise assembly and recruitment kinetics of actin and associated binding/regulatory proteins to be assessed in a living, intact mammal through visualising the *de novo* assembly of an actin scaffold that drives SG exocytosis in rodent salivary glands (overview described in Figure 1.5) (Masedunskas et al., 2013a). This process can be easily induced in the salivary gland acinar cells of anaesthetised rodents with a chemical agonist delivered by subcutaneous injection (Figure 1.5). This is possible due to recent advances in intravital subcellular microscopy, a powerful imaging modality which allows observation of

biological processes in the cells and tissues of living animals with spatial and temporal imaging resolution that is comparable to cell culture-based imaging methods (Masedunskas 2011). In addition, it is now relatively easy and rapid to genetically modify rodents with technologies such as CRISPR (Clustered Regularly Interspaced Palindromic Repeats) (O'Connell et al., 2014), therefore mice expressing fluorescent tags and knockout/knock-in lines are increasingly available. Furthermore, it is possible to transiently transfect cells/tissues in rats (Sramkova et al., 2014) and mice with plasmid DNA using commercial reagents. This has proven to be a key innovation that allows rather inexpensive and efficient assessment of protein kinetics in actin scaffold assembly *in vivo*. The use of constructs expressing fluorescent-tagged proteins together with refinement of *in vivo* transfection protocols developed and refined during the course of this project is described in Chapter 3.

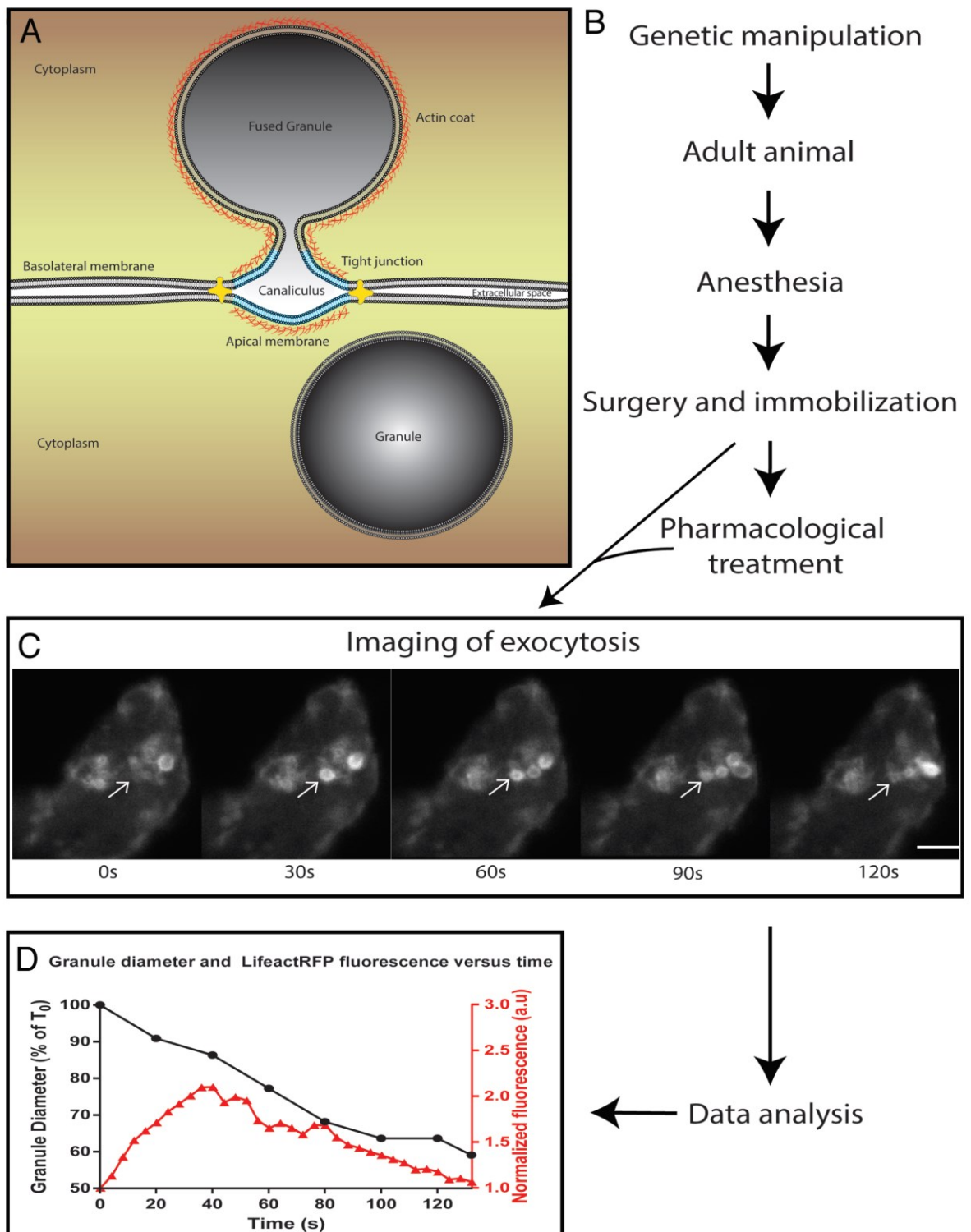


**Figure 1.5 Overview of the *in vivo* granule exocytosis model.** (A) A diagram depicting exocytosis of the secretory granule in the rodent exocrine acinar cell. Two cells are joined by tight junctions that delineate the extracellular space - the canaliculus. Apical membranes are shown in cyan. The dense actin meshwork is maintained at the apical membranes and is assembled on the granule membrane upon fusion with the apical

membrane. The top cell is shown with a fused granule that is starting to undergo the membrane integration phase of exocytosis. The lower cell is shown with a granule adjacent to the apical membrane, but not yet fused. (B) A flowchart showing typical experimental procedures in this model system. (C) Live imaging of a rat salivary gland acinar cell expressing RFP-LifeAct. The rat was transfected with plasmid DNA and allowed to recover for 16 h. The rat was anaesthetised, and the submandibular salivary gland was surgically exposed, stabilised and imaged by confocal microscopy. Five frames were selected from the time-lapse acquisition to show an exocytosis event (arrows) as seen from the recruitment of actin marker and granule shrinkage over time. Scale bar = 5  $\mu\text{m}$ . (D) Data plot showing granule diameter over time (black) and fluorescence intensity of Lifeact-RFP, which depicts actin scaffold formation over time (red). The data was extracted from a single exocytosis event that is highlighted in (C). *Figure and legend adapted from (Masedunskas et al., 2013a).*

## 1.9 Thesis rationale and aims

The eukaryotic actin cytoskeleton is an essential component of living cells and is involved in virtually all cellular functions. Tpm's are AAPs, known as the master regulators of actin filaments and more than 40 isoforms exist in mammals. Tpm's are helical coiled-coil dimers that form co-polymers with actin filaments to stabilise and confer functional specificity to filaments, as well as regulate the recruitment and activity of other AAPs. However, the interdependency between the dynamics of cytoskeletal Tpm's and actin filaments has not been thoroughly investigated in cells and no *in vivo* data exists. Investigating this relationship would provide more insight into how Tpm's modulate cytoskeletal actin in cells and animals. Furthermore, evidence indicates that the actin cytoskeleton is composed of multiple distinct filament populations, which are functionally specified and regulated by various Tpm isoforms. These filament populations appear to co-exist in time and space in cells as independent entities; however, they collaborate to perform diverse biological functions. In addition, the branched and linear actin filament nucleators, Arp2/3 and formins, respectively, appear to have a partially interdependent relationship, while formin isoforms appear to generate distinct actin filaments for specific functions. Much insight into the behaviour and functions of individual components of the actin cytoskeleton has been obtained from a variety of experimental approaches; however, the mechanistic assembly of a functional actin network in a living organism is not well understood. Investigating the *de novo* assembly kinetics of actin filaments and networks, along with the recruitment kinetics of AAPs involved, would provide mechanistic insights into how this complex, versatile and essential cellular component operates. In particular, using recently developed *in vivo* gene delivery and intravital subcellular intravital imaging techniques, it is possible to assess the dynamics of proteins of interest as well as their functional relevance during the assembly of an actin scaffold driving SG exocytosis in the acinar cells of live rodent salivary glands, which has not been possible previously.

Therefore, the aims of this project were to first develop and refine *in vivo* gene delivery methods into the secretory acinar cells in rodent salivary glands. This was

achieved by developing and characterising viral and non-viral delivery techniques, described in Chapter 3. The results yielded successful and efficient long-term viral expression of transgenes as well as development of a novel plasmid DNA transfection procedure in mouse salivary glands using commercial reagents. The second aim was to investigate the interdependency between cytoskeletal Tpm and actin filament dynamics in cells and animals. This was achieved by plasmid DNA transfection of constructs encoding fluorescent-tagged proteins into mammalian cells in culture and *in vivo* in rodents, followed by application of FRAP techniques to elucidate their dynamics, described in Chapter 4. The results revealed that Tpm surprisingly exhibit highly dynamic turnover compared to actin filaments, which has profound implications for Tpm regulation of actin filaments and other AAPs. The final aim of this project was to determine the recruitment kinetics and functions of the actin nucleators Arp2/3 and formins, Tpm, as well as the actin cross-linker  $\alpha$ -actinin during *de novo* actin scaffold assembly during SG exocytosis in rodent salivary glands. This was achieved by using intravital subcellular microscopy to visualise fluorescently-tagged proteins of interest in transgenic or CRISPR knock-in mouse models, as well as in rats or mice transfected with plasmid DNA, described in Chapter 5. The results demonstrated that actin scaffold assembly occurs in a precise, sequential clockwork-style manner, beginning with recruitment of formins, Tpm and actin cross-linkers to generate the initial linear filament network, followed by myosin II recruitment and finally, Arp2/3 generation of the branched network. Intriguingly, the formins displayed dissimilar recruitment kinetics, suggesting that formin isoforms are functionally distinct and that multiple linear actin filament populations co-exist in time and space. Tpm associate with a subset of these filaments, suggesting that Tpm preferentially sort to distinct filament populations to modulate their functions. Finally, a novel function of the Arp2/3 branched network during SG exocytosis was elucidated, which resulted in development of a revised model for SG exocytosis *in vivo*, as well as revealing new insights into the interdependence of the linear and branched actin networks and nucleators.

## Chapter 2. Materials and Methods

### Preparation of plasmid DNA

All plasmid DNA was prepared using Qiagen Endo-free plasmid kits (Qiagen) at a concentration of 4-6 mg/ml, in MilliQ H<sub>2</sub>O according to the manufacturer's instructions.

### List of plasmid DNA constructs

Construct name	Insert	Promoter/vector or	Source
mDia1-Emerald	mEmerald inserted at the C-terminus of human mDia1, separated by a 14 amino acid linker	CMV/mEmerald-N1	gift from Michael Davidson, Addgene plasmid #54157
mDia2-Emerald	mEmerald inserted at the C-terminus of mouse mDia2, separated by a 14 amino acid linker	CMV/mEmerald-N1	gift from Michael Davidson, Addgene plasmid #54159
Arp2-Emerald	mEmerald inserted at the N-terminus of human Arp2, separated by a 14 amino acid linker	CMV/mEmerald-C1	gift from Michael Davidson, Addgene plasmid #53992
$\alpha$ -actinin-NG	mNeonGreen inserted at the N-terminus of human non-muscle $\alpha$ -actinin, separated by a 19 amino acid linker	CMV/pcDNA 3.1	a gift from Jiwu Wang (Shaner et al., 2013)
pCAG-GFP-actin	eGFP inserted at the N-terminus of human $\beta$ -actin	CAG/pCAG	a gift from Ryohei Yasuda, Addgene plasmid

			#21948 (Murakoshi et al., 2008)
Tpm3.1-N/C-mNG	The sequence encoding mNeonGreen (a gift from Jiwu Wang, (Shaner et al., 2013)) was inserted at either the N- or C-terminus of human Tpm3.1, separated by a 10 amino acid linker motif (GGGGSGGGGS)	CMV/pcDNA 3.1	Designed by Mark Appaduray, cloned and generated by GeneArt, Invitrogen
Tpm4.2-mRuby2	The sequence encoding mRuby2 (a gift from Michael Lin, (Lam et al., 2012)) was inserted at the C-terminus of human Tpm4.2, separated by a 10 amino acid linker motif (GGGGSGGGGS)	CMV/pcDNA 3.1	Designed by Mark Appaduray, cloned and generated by GeneArt, Invitrogen
Lifect-RFP	mRFP was conjugated to Lifect, a 17 amino acid peptide which transiently binds F-actin	CMV	gift from Roland Wedlich-Soldner (Riedl et al., 2008))
Farnesyl-TdTomato	TdTomato fluorescent protein was conjugated to human Farnesyl	CMV	A gift from Michael Davidson, Addgene plasmid #58092

### List of viral constructs

All viruses were obtained from Penn Vector Core (University of Pennsylvania).

Virus	Vector name	Promoter	Insert	Titer (particles/ mL)
Adeno-associated virus serotype 9 (AAV9)	AAV9.CMV.P1.eGFP.WPRE.bGH	CMV	eGFP	$5.29 \times 10^{13}$
Lentivirus (LV)	VSVG.HIV.SIN.cPPT.CMV.eGFP.WPRE	CMV	eGFP	$1.24 \times 10^{10}$
Adenovirus serotype 5 (AdV)	H5'040.CMV.eGFP	CMV	eGFP	$5.48 \times 10^{12}$

## Immunohistochemistry

Transfected wild type and B6-*Tpm3*<sup>tm2(Δ9d)Pgun</sup> MEFs (Vlahovich et al., 2009) (mice lack exon 9d of the *Tpm3* gene resulting in the knockout of isoforms Tpm3.1 and Tpm3.2) were fixed in 4% PFA at RT for 30 min, permeabilised in ice cold methanol for 30 min, blocked in 2% BSA in PBS at RT for 60 min. The cells were incubated with CG3 in 2% BSA (mouse monoclonal, 1:25 (Novy et al., 1993)), which recognises the 1b exon from the TPM3 gene (1 h, RT) followed by Alexa-647 conjugated donkey anti-mouse secondary antibodies (1:400 in PBS). Cells were washed 3 times with PBS and imaged using a Zeiss 880 confocal using a 63x/1.4 NA objective and sequential excitation with 488 nm and 633 nm lasers. The raw image data was deconvolved using the Airyscan processing algorithm that is included with the Zeiss Zen software package.

## Cell culture, transfection and drug treatment

MEFs were isolated from day 13.5 embryos and cultured as previously described (Schevzov et al., 2005). WT and Tpm3.1 KO MEFs were derived from mice of two genetic backgrounds: 129/SvJ [129-*Tpm3*<sup>tm1(neo;Δ9d)Pgun</sup>] (Schevzov et al., 2008) and C57BL/6J [B6-*Tpm3*<sup>tm2(Δ9d)Pgun</sup>] (Vlahovich et al., 2009). Cultured cells were maintained in Dulbecco's modified Eagle medium (DMEM) with 10% (v/v) foetal bovine serum (FBS) at 37°C, 5% CO<sub>2</sub>. For imaging experiments, MEFs at passages 1-3 were seeded into Fluorodish™ tissue culture dishes (World Precision Instruments Pty Ltd) and grown to 70-90% confluency. Cell transfections were performed using Lipofectamine 3000 reagent (Life Technologies) and plasmid DNA according to the manufacturer's instructions. Jasplakinolide (Sapphire Bioscience Pty Ltd) was added at a final concentration of 7 μM from a 1 mM stock prepared in DMSO. FRAP analysis was performed within 10 s after addition of drugs.

### **Live cell imaging and FRAP**

Live cell imaging was performed on a Nikon A1 inverted scanning confocal microscope fitted with a Nikon Plan Apochromat λ 60x oil immersion objective with an NA of 1.4 and an Okolab incubation chamber equilibrated to 37°C. The mNeonGreen (λ<sub>em</sub> 516 nm) constructs were excited with a 488 nm laser. For time-lapse imaging, frames were acquired at 516 ms/frame at 256 pixel resolution, 300 nm per pixel, and imaged at 1 Hz. FRAP zones were bleached with a single 120 ms pulse using a 488 nm laser. 3-5 reference frames were acquired per cell, followed by a single bleach pulse, followed by image acquisition at 1 Hz for 120 s.

### **Reporter mouse lines**

Mice were sourced as described below and bred at the Australian BioResources Facility (Moss Vale, NSW, Australia). Mice were imported into the UNSW Biological Resource Centre and allowed to acclimatise for 1 week. Animals were housed in a specific pathogen-free, humidity and temperature controlled facility, under 12 h light-dark cycle and were fed standard laboratory chow *ad libitum*. mTomato C57/BL6 mice were previously generated by Luo's laboratory as a Cre recombinase reporter strain (Muzumdar et al., 2007). Prior to exposure to Cre recombinase all tissues express

tandem dimer tomato fluorescent protein (tdTomato) fused to the plasma membrane targeting peptide from the MARCKS protein making this construct an excellent PM reporter *in vivo* (Masedunskas et al., 2011a). The mTomato mouse strain was purchased from the Jackson Laboratory and used alone or crossed to the Lifact-GFP strain and maintained in the homozygous state. Lifact-GFP and Lifact-RFP transgenic mice were a gift from Roland Wedlich-Soldner (Riedl et al., 2010) and used in crosses in the hemizygous state. GFP-NMIIA knock-in mice were generated as described (Zhang et al., 2012) and used in a homozygous state crossed with Lifact-RFP mice. The genotypes of the mice were confirmed by PCR as described in the original publications.

### **Viral transduction of mouse salivary glands**

All viral transduction procedures were performed in a PC2 certified biosafety cabinet. Mice were anaesthetised with a 100 mg/kg Ketamine/15 mg/kg Xylazine mix in saline via intra-peritoneal injection. For intra-stromal injections, viral particles in 15 µL total volume was delivered by injecting the salivary glands through the skin using a 1 mL syringe and 31G needle (BD Biosciences Cat# 324912). For intra-ductal perfusion, the Wharton's ducts were cannulated and salivary glands were perfused with viral particles in 15 µL total volume using a 1 mL syringe and 31G needle (BD Biosciences Cat# 324912). Mice were then given 300 µL of warm saline via intra-peritoneal injection to aid recovery and allowed to recover in a clean cage on a heat pad. Mice were monitored until ambulant.

### **Mouse salivary gland transfections**

Male mTomato mice (Luo 2007) weighing 28-32 g were anaesthetised with a 100 mg/kg Ketamine/15 mg/kg Xylazine mix in saline via intra-peritoneal injection. Mouse salivary glands were then transfected by cannulating the Wharton's ducts, followed by perfusion of transfection cocktails using a 50 µL Hamilton syringe (Hamilton Company). Lipofectamine reagents used in cocktails were obtained from Invitrogen and PEI (*in vivo*-jetPEI<sup>®</sup>) reagent was obtained from Polyplus Transfection. Transfection cocktails were slowly perfused over 5 min. Animals were then given 300 µL of warm saline via intra-peritoneal injection to aid recovery and allowed to recover in a clean cage on a

heat pad. Animals were monitored until ambulant and imaged via intravital microscopy 16-24 h later to allow adequate plasmid expression.

### **Rat salivary gland transfections**

Male Wistar rats weighing 150–225 g were obtained from the Animal Resources Centre, Perth, Australia and allowed to acclimatise for 1 week. Rats were anaesthetised with a 100 mg/kg Ketamine and 15 mg/kg Xylazine mix via intra-peritoneal injection and salivary glands were transfected as previously described (Masedunskas et al., 2013b) with the following modifications: 10–24 µg of plasmid DNA was mixed with *in vivo*-jetPEI<sup>®</sup> (Polyplus Transfection) with 100 µL of 10% w/v glucose according to the manufacturer's instructions.

### **Staining and imaging of excised salivary glands**

Mice were anaesthetised with a 100 mg/kg Ketamine/15 mg/kg Xylazine mix in saline via intra-peritoneal injection. Salivary glands were surgically excised and imaged within 5 min of excision. Immediately prior to imaging, glands were bathed in a solution containing cold saline with 2 mg/ml Cell Mask Deep Red plasma membrane stain (Thermo Fisher Scientific). Glands were imaged at 1024 pixel resolution on a Nikon A1 inverted scanning confocal microscope fitted with a Plan Apochromat WI DIC N2 60x water objective (NA 1.27), a 20x air objective (NA 0.75) and a 10x air objective (NA 0.45). 700–1000 nm thick confocal slices were taken at 100–150 nm/pixel spatial sampling rate.

### **Western blotting**

Protein was extracted from transfected and non-transfected MEFS in RIPA buffer and analysed by SDS-PAGE and Western blotting as described previously (Schevzov et al., 2011). Protein concentration was estimated using Precision Red (Cytoskeleton, Inc). Equal amounts of protein (30 µg) were resolved on a 12% SDS-PAGE gel before electro-transfer to PVDF membranes. Non-specific binding on the blot was blocked with blocking buffer, 1% BSA in TBST (100 mM Tris-Cl, pH 7.5, 150 mM NaCl with 0.05%

Tween 20). Tpm3.1 was recognised using monoclonal Ab CG3 (1:200 in blocking buffer) (Schevzov et al., 2011) and secondary antibody rabbit anti-mouse Ig-conjugated horseradish peroxidase (Abcam) (1:10,000 in blocking buffer). Primary antibody was incubated overnight and secondary for 2 h with 4 x 15 min washes. Blots were developed with the Western Lightening Chemiluminescence reagent (Perkin Elmer Life Sciences; Boston, MA) and exposed to X-ray film. Equal protein loading was examined by staining the protein gel blots with 0.1% (w/v) Coomassie blue R350, 20% (v/v) methanol and 10% (v/v) acetic acid).

### **Intravital imaging and FRAP**

Animals were anaesthetised with a 100 mg/kg Ketamine/15 mg/kg Xylazine mix in saline via intra-peritoneal injection. Salivary glands were externalised and prepared for intravital imaging as previously described (Masedunskas et al., 2013b). Briefly, the organ was stabilised onto a coverslip on a microscope stage with the vasculature and the innervation still intact. Intravital imaging was performed on a Nikon A1 inverted scanning confocal microscope fitted with a Plan Apochromat WI DIC N2 60x water objective with an NA of 1.27, an Okolab incubation chamber and a custom-made stage insert. mNeonGreen, mEmerald and eGFP constructs were excited with a 488 nm laser. mRFP, tdTomato and mRuby2 constructs were excited with a 561 nm laser. Alexa 647-conjugated 10 kDa dextran (Thermo Fisher Scientific) was excited by a 640 nm laser.

For time-lapse imaging in Chapters 3 and 5, frames were acquired in sequential mode at 943 ms/frame at 256 pixel resolution, 100 nm per pixel and imaged at 1 Hz. Imaging plane with a visible canaliculus / APM was selected as close to the surface of the organ as possible, at a depth of 10-20  $\mu\text{m}$  for the rats and 8-12  $\mu\text{m}$  for the mouse salivary glands. During imaging any noticeable drift was manually corrected in X, Y or Z dimension. For some experiments, the Wharton's ducts of mice were cannulated prior to intravital imaging and a mixture of 1% DMSO/2 mg/ml Alexa 647-conjugated 10 kDa dextran (Thermo Fisher Scientific) in saline was perfused into the salivary glands to visualise fluid in the canaliculi. Perfusions were performed at 1  $\mu\text{L}/\text{min}$  during the imaging using a PHD Ultra Nanomite programmable syringe pump (Harvard Apparatus).

For time-lapse imaging and FRAP in Chapter 4, frames were acquired at 477 ms/frame at 256 pixel resolution, 100 nm per pixel and imaged at 1 Hz. Imaging plane with a visible canaliculus / APM was selected as close to the surface of the organ as possible, at a depth of 10-20  $\mu\text{m}$ . FRAP zones were bleached with a single 120 ms pulse using a 488 nm laser. 3-5 reference frames were imaged per cell, followed by a single bleach pulse at a defined ROI, followed by acquisition at 1 Hz for 120 s.

### **Isoproterenol stimulation**

Exocytosis of secretory granules was stimulated by subcutaneous injection of isoproterenol hydrochloride (Sigma-Aldrich) at 0.025 mg/kg (rats) or 0.01 mg/kg (mice), in 150  $\mu\text{L}$  of saline.

### **Image and data processing**

Images were taken using NIS Elements software. Image processing and data extraction was performed using ImageJ/Fiji software (Schindelin et al., 2012). When necessary drift and motion correction on time-lapse image stacks was carried out with StackReg ImageJ plugin (Schindelin et al., 2012). Diameter measurements were made by measuring the outer diameter of granule membranes or actin scaffolds. To extract fluorescence trace data from single granule fusion events, a circular region of interest (ROI) was drawn over the image area capturing the exocytosis event. Only exocytosis events fully captured in the focal plane were included in the analysis. Integrated pixel fluorescence intensity values from the ROI were extracted and transferred to Microsoft Office Excel for processing as separate channels. Time  $t=0$  for all events was taken as the time point preceding the first significant increase in Lifestat fluorescence above the baseline value. The baseline/background values for each channel were calculated by averaging approximately 5 s worth of data points preceding an increase in fluorescence. The fluorescence intensity values may vary between mice or granules therefore the granule fluorescence traces were normalised by first subtracting the calculated average baseline value and then expressed as fractional values with 1 being the maximum and zero being the minimum/background value. Separate granule

exocytosis events of a given data set were then synchronised to time  $t=0$  with respect to Lifeact fluorescence and mean values were calculated and plotted using Graphpad Prism 7 (GraphPad Software) with standard error of the mean (SEM) shown for each data point. All statistical  $p$  values were obtained from unpaired t-tests using Graphpad Prism 6. FRAP curves were normalised to the minimum and maximum fluorescence values using a value range of 0 (minimum fluorescence) to 1 (maximum fluorescence). Data from normalised FRAP curves were then fitted with a double exponential equation using the IgorPRO6 software complemented with the K\_FRAPcalc version 9 procedure (Kota Miura, EMBL-Heidelberg, Germany). Images for the figures were adjusted for contrast and brightness in ImageJ to have an optimal display range for features of interest, such as secretory granules and then converted to RGB images. In some cases this adjustment for secretory granule visualisation may have resulted in unavoidable “clipping” of the brightest secondary features. The images were then assembled into final figures using Adobe Illustrator CS6 software.

## Chapter 3. Gene delivery into mouse salivary glands

### Introduction

The study of actin assembly is fundamental to our understanding of how this complex and dynamic network of filaments is generated and maintained in cells. In *in vitro* model systems used to study actin assembly, individual protein components can be purified and added to the system with great flexibility and *de novo* assembly kinetics can be obtained (Blanchoin et al., 2014; Mullins and Hansen, 2013). However, the *in vitro* system is an artificial environment, thus crucially lacking biological complexity and potential relevance. *De novo* actin assembly has been studied using large granule exocytosis models in cell culture (Miklavc et al., 2015; Miklavc et al., 2012) and *ex vivo* (Tran et al., 2015). However, these models also lack the multi-dimensional microenvironment present in an intact organ.

Intravital subcellular imaging of exocytosis in the rodent salivary gland (SG) that was developed by Masedunskas et al. (2011a, 2011b) provides a powerful modality to study *de novo* actin assembly *in vivo* in living mammals (Masedunskas et al., 2011a; Masedunskas et al., 2011b). Regulated exocytosis can be triggered in the secretory acinar cells of rodent SGs thus allowing for the quantitation of *de novo* actin scaffold assembly and the recruitment kinetics of associated protein. Importantly, genetic manipulation of rodents is relatively easy such that fluorescently tagged proteins can be expressed to monitor recruitment kinetics and the roles of specific proteins can be determined using knock-out techniques. Many genetically modified (GM) mouse lines already exist that can be used with this imaging method and for this purpose. However, for greatest flexibility and speed it would be best to be able to use a combination of conventional GM mouse lines and *in vivo* DNA transfection into the acinar cells of mouse SGs. However, currently it is only possible to transfect acinar cells of rat SGs (Sramkova et al., 2014). Although rat SGs has proven a powerful model system for imaging subcellular events, rat SGs are inferior to mouse SGs because they are encapsulated in a thicker layer of collagen, thus compromising imaging quality and resolution.

To overcome the aforementioned limitations, we sought to develop an effective method for gene delivery into the SGs of mice to observe *de novo* actin scaffold assembly during regulated exocytosis in mouse secretory acinar cells.

Viral gene delivery methods have been demonstrated to have high transduction efficiency as well as long lasting expression in cells (Walther and Stein, 2000). Previous studies demonstrated that ductal cells in mouse salivary glands can be transduced (Katano et al., 2006) as is the case for secretory acini in rat salivary glands (Timiri Shanmugam et al., 2013). To date however, no viral delivery methods have focused on transduction of the secretory acinar cells in mouse salivary glands. The viral vectors widely used for gene delivery are lentivirus (LV), adenovirus (AdV) and adeno-associated virus (AAV) and each virus has its advantages and disadvantages depending on the target cells, briefly discussed below. The general mechanism of viral-mediated gene transfer occurs by first packaging the transgene DNA into the viral capsid, followed by viral entry into host cells via compatible viral receptors on cell membranes (Kay et al., 2001). LVs are vectors that integrate the transgene into the host genome, thus allowing for long lasting transgene expression. In addition, lentiviral vectors are able to efficiently transduce quiescent cells (Cockrell and Kafri, 2007; Naldini et al., 1996) such as SG secretory acini. A disadvantage however is that LVs have been shown to elicit a strong immune response in tissue which affects the viability of transduced cells (Nayak and Herzog, 2010). Biosafety concerns are also an issue, since LVs are capable of infecting human cells (Trono, 2000). AdVs are classified into seven species and more than 50 known serotypes have been discovered (Harrach et al., 2011). AdV vectors are easy to produce in high titers (He et al., 1998), have a large packaging capacity (Bett et al., 1993) and are able to transduce both dividing and quiescent cells (Benihoud et al., 1999). A disadvantage however is that similar to LVs, AdVs elicit an immunogenic response in rodent tissue (Dai et al., 1995). AAV vectors have significant advantages over LVs and AdVs in that only a mild immune response is observed upon transduction (Chirmule et al., 1999). There are currently 12 described AAV serotypes, each having varying tropism and transduction efficiency depending on the target cell types being transduced (Boerner et al., 2015; Zincarelli et al., 2008). AAVs are also able to transduce both dividing and quiescent cells, however a major disadvantage is that

AAV vectors have a low transgene size packaging capability thus limiting the size of the transgene that can be delivered into cells (Bouard et al., 2009).

A second approach is to develop a transient transfection technique in mouse SGs using synthetic reagents, which would provide a simple and cost-effective means of delivering plasmid DNA of interest into secretory acini. In addition, this could be used in conjunction with genetically modified mouse models thus providing experimental flexibility. This technique has been successfully developed in rat SGs using polyethylenimine (PEI), a commercially available cationic polymer based transfection reagent. PEI forms a complex or polyplex with plasmid DNA thus compacting DNA and allowing its internalisation into cells via electrostatic association with cell membranes (Boussif et al., 1995). As this reagent has been shown to successfully transfect secretory acini in rat SGs (Sramkova et al., 2014), it is likely that successful acini transfection can be also achieved in mouse SGs.

Cationic lipids are another widely used and commercially available transfection reagent. Cationic lipids form DNA/lipid complex or lipoplexes with DNA which are also internalised by cells through electrostatic interactions with the cell membrane (Pires et al., 1999; Simoes et al., 1999). A disadvantage however is that transfection efficiency is much reduced *in vivo*, due to association with serum factors in the vasculature which neutralise the positive charges of the lipoplexes thus adversely affecting efficient entry into cells (Li et al., 1998).

Fortunately, in the case of rodent salivary glands, it is possible to deliver complexed DNA-lipid/polymer or viral particles via two approaches, as depicted in Figure 3.1. The first approach is direct intra-stromal injection of the gland in an anaesthetised mouse (Figure 3.1 A). Viral or synthetic particles delivering DNA would be exposed to the external surface of the parenchyma and the basolateral membranes of acinar cells, that also contain a mixed population of stromal cells, such as fibroblasts and dendritic cells. However, this delivery method exposes gene delivery particles to the serum components and may not allow access to the epithelium behind the basement membranes. The second approach is infusion of the ductal system by cannulation of the Wharton's duct (Figure 3.1 B). This method enables delivery of viral or synthetic

particles to the apical membranes of acinar cells, thus minimising exposure to the serum components and bypassing the basement membrane barrier.

*Figure has been removed due to copyright restrictions. Please refer to the original publication at <https://onlinelibrary.wiley.com/doi/full/10.1111/j.1600-0854.2008.00798.x>*

**Figure 3.1 Ultrastructure of the rodent salivary gland and ductal system with potential gene delivery routes.** The parenchyma of the gland is formed by acinar structures (1), that discharge secreted saliva into the acinar canaliculi (2, magenta lines). The contractions of the myoepithelial cells (5) facilitate the flow of the saliva first into the intercalated ducts (3) and later into the striated ducts (4), which join the interlobular ducts. The surface of the glands is covered by elastic fibres such as elastin (7) and collagen (8), and various populations of fibroblasts and stromal cells are scattered within the fibres and the parenchyma (6). (A) Intra-stromal injection method. Gene delivery particles flood the stroma, thus are able to contact the basolateral membranes of acinar cells. (B) Infusion method via cannulation of the Wharton's duct. Gene delivery particles flood the ductal system thus contacting the apical membranes of acinar cells (2, magenta lines). *Figure and legend adapted from (Masedunskas and Weigert, 2008)*

The focus of this chapter is therefore the development and characterisation of viral and non-viral gene delivery into the secretory acini of mouse salivary glands, that results in successful stimulation of regulated exocytosis and observation of *de novo* actin scaffold assembly revealed by exogenous fluorescent transgene constructs.

## **Results**

### **Viral Gene delivery into mouse salivary glands**

#### **LV does not efficiently transduce cells in mouse salivary glands and elicits an immune response**

We elected to investigate viral gene delivery into mouse salivary glands using both infusion of the ductal system via Wharton's duct cannulation (Figure 3.1 B) and direct intra-stromal injection (Figure 3.1 A). This would allow us to determine if virus particles would more efficiently transduce acinar cells via the stroma or basolateral membranes of cells as delivered via direct intra-stromal injection, or via the apical membranes as delivered via infusion.

To this end, LV particles carrying a plasmid encoding cytoplasmic GFP were obtained from Penn Vector Core (University of Pennsylvania) at  $1.24 \times 10^{10}$  particles per mL. Wild type mice were anaesthetised and  $1.86 \times 10^8$  LV particles in 15  $\mu$ L volume were delivered into the salivary glands either via infusion or direct intra-stromal injection. A control mouse was anaesthetised and 15  $\mu$ L of saline was delivered via intra-stromal injection to assess the effect of fluid delivery into the glands. Transduced mice were allowed to recover and were sacrificed at Days 4 and 12 post-transduction to obtain transduced glands while the control mouse was sacrificed at day 3 post-intra-stromal injection of saline to obtain control glands. Immediately prior to imaging, excised glands were stained with Cell Mask Deep Red (CMDR) membrane dye as described in Materials and Methods to visualise the extracellular tissue.

The control glands (Figure 3.2 A, B) were observed to have normal appearance, indicating that no adverse response was elicited from fluid delivery into the glands. At

Day 4 post-transduction via infusion, no GFP expression was detected (Figure 3.2 E) which is in accordance with the latent expression of lentivirus (Fleming et al., 2001). However, LV particles triggered an immune response, as shown by the recruitment of leucocytes as seen at the surface optical section (Figure 3.2 C, D, arrows) and deeper within the gland (Figure 3.2 E, arrows). Infiltrating leucocytes were identified by their spherical structure and granular appearance of cell membranes (Gleich and Adolphson, 1986; Miller et al., 1966; Williamson and Grisham, 1961). GFP expression was detected in cells at Day 12 post-transduction via infusion (Figure 3.2 F, G); although, only a few transduced acinar cells were detected (Figure 3.2 G, arrow). Acini were identified morphologically by their regular, spherical appearance in the smaller lobes (Figure 3.2 F, arrows), and distinguished from the ducts which are larger structures shaped as irregular ovals (Figure 3.2 F, arrowheads). In addition, no obvious immune cells were observed. GFP expression was detected in glands transduced via direct intra-stromal injection at Day 12; however, no transduced acini were detected. The majority of transduced cells appeared to be stromal cells (Figure 3.2 H, I, arrows) with minor immune cell recruitment (Figure 3.2 I, arrowheads). We conclude that both intra-stromal injection and intra-ductal infusion of LV particles are able to transduce cells in mouse salivary glands; however, they elicit a robust immune response initially which likely adversely affects transduction efficiency and transgene expression.

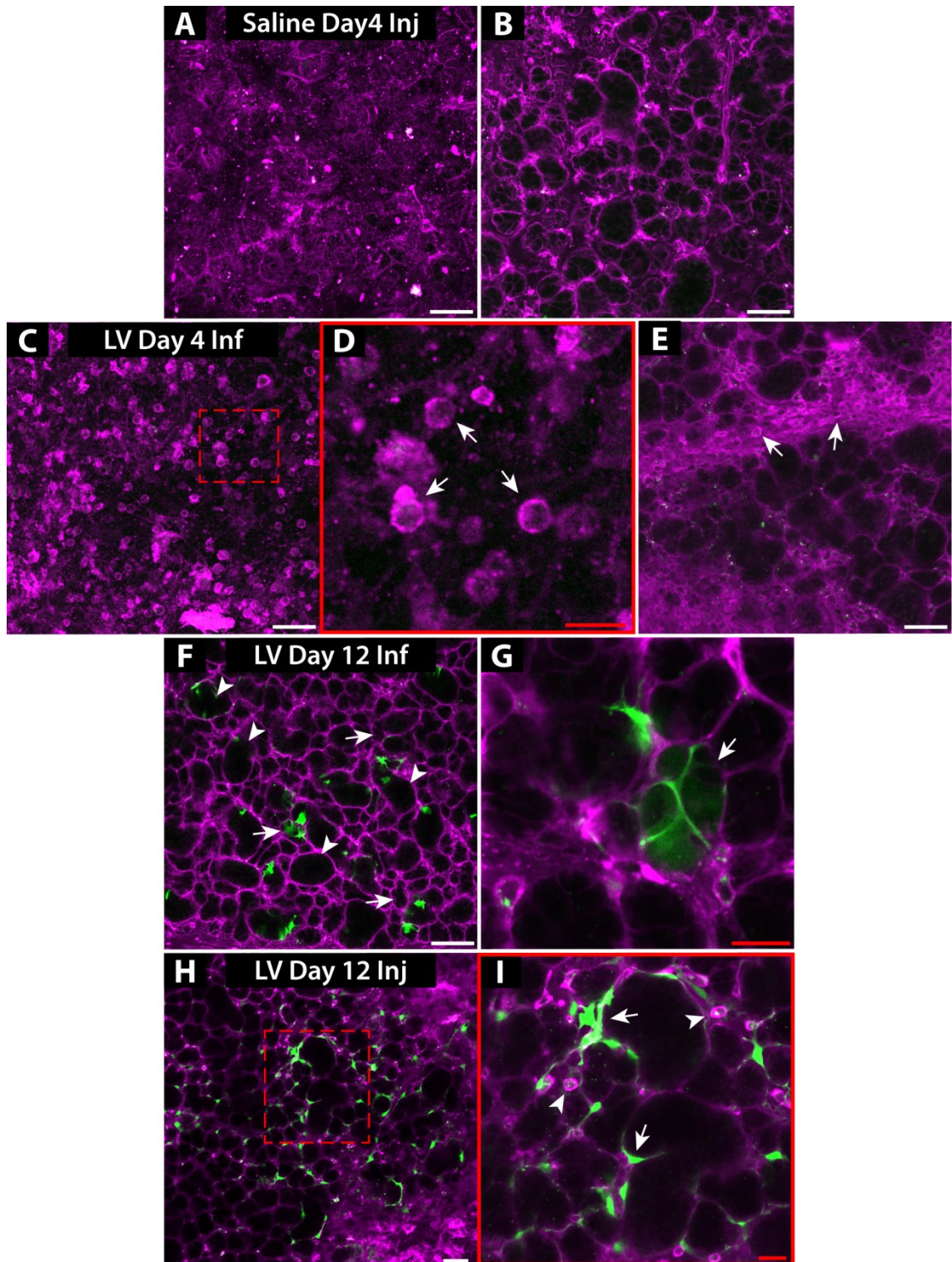


**Figure 3.2 Lentiviral transduction of mouse salivary glands.** Mouse salivary glands were either injected (Inj) directly or infused (Inf) with saline as a control or lentivirus (LV) carrying a cytoplasmic GFP marker. Infusion was performed via Wharton's duct cannulation. Images with a solid red outline are a zoom in of areas marked with a

dashed red outline in the corresponding adjacent image. Prior to imaging, glands were excised and stained with CMDR membrane dye as described in Materials and Methods to visualise the extracellular tissue and immediately imaged by confocal microscopy. Images shown are overlays of GFP (green) and CMDR (magenta) channels and were taken at the surface (A, B) and up to a depth of 20  $\mu\text{m}$  into the gland (B, E, F-I). Control (A, B) and lentivirus transduced glands (C-I) were surgically removed and imaged at Day 4 (A-E) and Day 12 (F-I) post-transduction. Lentivirus carrying a cytoplasmic GFP marker was delivered by infusion via Wharton's duct cannulation (C-G) and direct intra-stromal injection (H, I) in separate animals. A, B: Non-transduced control glands imaged at the surface (A) and  $\sim 5\mu\text{m}$  within the gland (B). C-E: Transduced salivary glands imaged at Day 4 post transduction. No GFP expression observed. Lentiviral transduction elicits an immune response thus recruiting leucocytes at the surface (C, D arrows) and within the gland (E, arrows). GFP expression was detected in the glands transduced via cannulation at Day 12 (F) although only a few acini were transduced (G arrow). Salivary gland acini are identified by their localisation in the smaller parenchymal lobes (F arrows) while the larger lobes are salivary ducts (F arrowheads). GFP expression was detected in glands transduced via intra-stromal injection (H); however, the majority of transduced cells appeared to be dendritic cells or stromal cells (H, I arrows). No transduced acini were observed. White scale bars = 50  $\mu\text{m}$ , red scale bars = 20  $\mu\text{m}$ .

## **AdV efficiently transduces secretory acini in mouse salivary glands however without long lasting gene expression**

To investigate gene delivery using AdV, AdV particles carrying a cytoplasmic GFP marker was obtained from Penn Vector Core (University of Pennsylvania) at  $5.48 \times 10^{12}$  particles per mL.  $8.22 \times 10^{10}$  adenovirus particles in 15  $\mu$ L volume were delivered into mouse salivary glands either via direct intra-stromal injection (Figure 3.3 A, B) or via infusion through cannulation of the Wharton's ducts (Figure 3.3 C-F). Transduced mice were allowed to recover and were sacrificed at Days 3 and 6 post-transduction to obtain transduced glands. Immediately prior to imaging, excised glands were stained with CMDR membrane dye as described in Materials and Methods to visualise the extracellular tissue.

Transduced cells were detected at Day 3 in glands directly injected with AdV particles (Figure 3.3 A, B); although, the transduced cells appeared to be dendritic or stromal cells (Figure 3.3 A, B arrows). AdV particle delivery elicited an immune response as shown by the recruitment of immune cells (Figure 3.3 A, B arrowheads). Transduced cells were also detected in glands infused with AdV; however, in this case the majority of transduced cells were acini (Figure 3.3 C, D arrows) suggesting that AdV particles preferentially transduce acini when in contact with the apical membranes of cells (Figure 3.1 B). At Day 6 post adenoviral infusion, GFP expression was only detected in ductal cells (Figure 3.3 E arrows) as shown by the presence of transfected cells within the larger ductal lobes (Figure 3.3 F, red arrowhead) and absent from acinus (Figure 3.3 F, yellow arrowheads). This suggests that AdV expressing cells were largely lost at Day 6, likely due to the immune response (Thaci et al., 2011). We conclude that AdV is capable of transducing stromal and acinar/ductal cells in mouse salivary glands, depending on whether viral particles are delivered via intra-stromal injection or infused via the ductal system, respectively. However, AdV elicits an immune response which likely affects long lasting expression of transgenes.

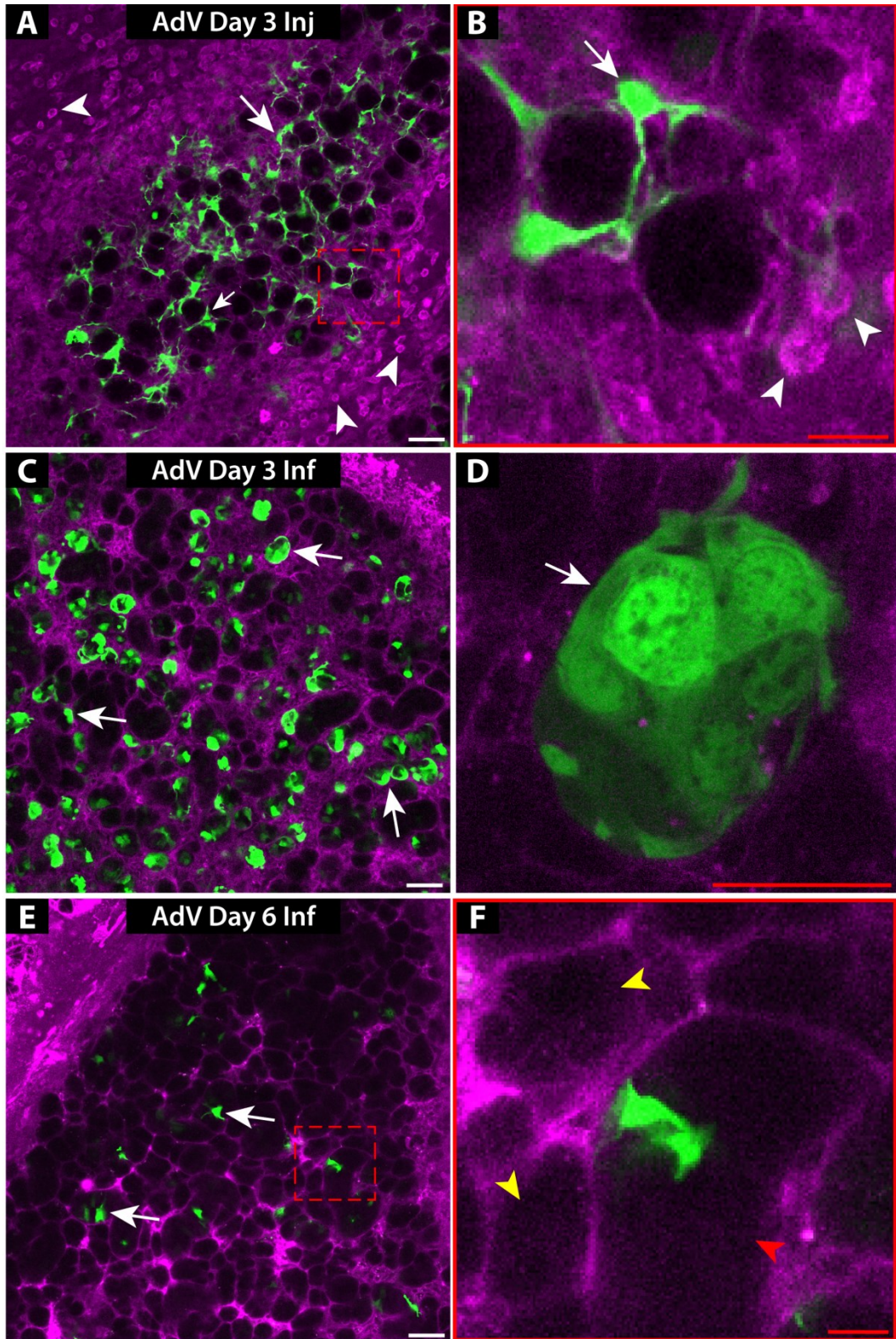


**Figure 3.3 Adenoviral transduction of mouse salivary glands.** Mouse salivary glands were either injected (A,B) or infused (C-F) with adenovirus (AdV) carrying a cytoplasmic GFP marker. Images with a solid red outline are a zoom in of areas marked with a dashed red outline in the corresponding adjacent image. Transduced glands were

surgically removed at Day 3 (A-D) and Day 6 (E-F) post-transduction, stained with CMDR membrane to visualise extracellular tissue and imaged. Images shown are overlays of GFP (green) and CMDR (magenta) channels. Direct injection of AdV elicits an immune response at day 3 as shown by immune cell recruitment (A, B arrowheads). AdV injection at Day 3 primarily transduces stromal cells as shown by expression of cytoplasmic GFP (arrows). No transduced acini were detected. Infusion of AdV primarily transduces acinar cells at Day 3 (C, D arrows) indicating that viral vectors must be delivered to the apical membranes of acinar cells through infusion via the ductal system. At Day 6 post-AdV infusion only ductal cells maintained GFP expression and no transduced acini were detected (E arrows). This is shown by transduced cells (green) present in the salivary duct (F red arrowhead), but absent from adjacent acinus (F yellow arrowheads) indicating that acinar adenoviral GFP expression peaks at Days 3-4 post-transduction and is largely lost at Day 6. White scale bars = 50  $\mu\text{m}$ , red scale bars = 20  $\mu\text{m}$ .

## **AAV transduces secretory acini with high efficiency and long lasting gene expression without an immune response**

We next investigated the transduction capability of AAV in mouse salivary glands. Since other groups have previously demonstrated success with AAV serotype 9 (AAV9) in rat salivary glands (Timiri Shanmugam et al., 2013), we reasoned that AAV9 might effectively transduce salivary gland acinar cells in mice. As our previous attempts with direct intra-stromal delivery of viral particles primarily transduced stromal cells (Figure 3.2 H, I; Figure 3.3 E, F), we elected to focus only on infusion of AAV9 particles which with other viral vectors appeared to efficiently transduce secretory acinar cells (refer to figures), likely due to viral particle exposure to the apical membranes (Figure 3.1 B). To this end, AAV9 particles were obtained from Penn Vector Core (University of Pennsylvania) at  $5.29 \times 10^{13}$  particles per mL.  $7.94 \times 10^{11}$  and  $3.96 \times 10^{11}$  particles in 15  $\mu$ L total volume respectively were infused into the salivary glands of mice via Wharton's duct cannulation and sacrificed at Days 3, 7 and 14 post-transduction. Salivary glands infused with  $3.96 \times 10^{11}$  particles were collected at Days 3 and 7, while salivary glands infused with  $7.94 \times 10^{11}$  particles were collected at Day 14 post-transduction. Immediately prior to imaging, excised salivary glands were stained with CMDR membrane dye to label all cells in the tissue.

Infusion of AAV9 particles resulted in positive transduction of cells at Day 3 with the majority of transduced cells being acini (Figure 3.4 A, B arrowheads). No detectable immune response was detected as shown by the lack of immune cell recruitment, unlike LV (Figure 3.2 D) and AdV (Figure 3.3 B). Transduced cells displayed only low levels of expression, which is in accordance with the delayed expression of AAV vectors (Zincarelli et al., 2008). AAV9-GFP expression in acini was increased at Day 7 (Figure 3.4 C, D, arrowheads) as shown by the increase in expression compared to Day 3 (Figure 3.4 A, B, arrowheads). At Day 14 post-transduction, GFP expression was also detected in ductal and stromal cells (Figure 3.4 E, F, arrows). This indicates that AAV9 has a wide tropism in mouse salivary glands and preferentially transduces acini, at least when delivered via infusion. Hence, robust gene delivery to salivary gland acini can be

achieved with AAV9 viral particles with long lasting transgene expression and without an immune response.

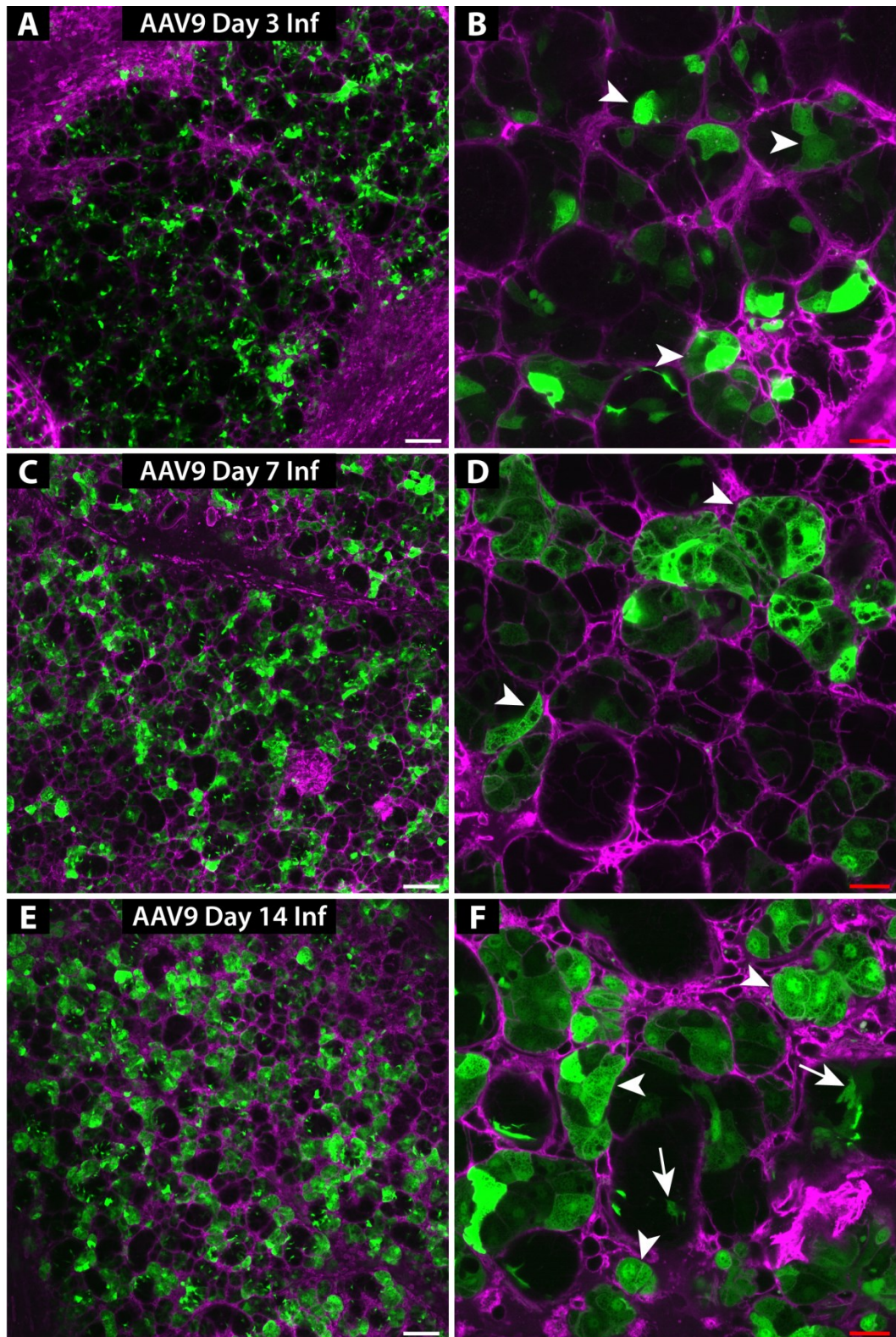


**Figure 3.4 Adeno-associated virus serotype 9 transduction of mouse salivary glands.** Mouse salivary glands were transduced with adeno-associated virus serotype 9 (AAV9) carrying a cytosolic GFP marker via infusion. Glands were surgically removed and stained with CDMR membrane dye to visualise extracellular tissue immediately prior to

imaging at Day 3 (A, B), Day 7 (C, D) and Day 14 (E, F). Images shown are overlays of GFP (green) and CMDR (magenta) channels. AAV9 gene delivery primarily transduced acinar cells (B, D, F arrowheads) without any major immune response, as shown by the absence of immune cell recruitment. GFP expression was detected as early as Day 3 (A, B) with peak expression occurring between Day 7 and 14 (E, F). At Day 14 GFP expression was also detected in ductal cells (F arrows) although expression in acinar cells is more robust (F arrowheads). White scale bars = 50  $\mu$ m, red scale bars = 20  $\mu$ m.

## **Non-viral gene delivery into mouse salivary glands**

Although viral vectors are efficient gene delivery vehicles, there are limitations to this approach. One limitation is that it is expensive and time consuming to generate viral gene delivery vectors for all genes of interest. Although AAV9 proved successful in transducing acinar cells without eliciting an immune response, AAV is limited in the size of insert tolerated. A non-viral, transient transfection technique using synthetic compounds and plasmid DNA would provide a relatively inexpensive, efficient and flexible gene delivery method for mouse secretory acini. We therefore attempted to adapt the method of DNA transfection of rat salivary glands (Sramkova et al., 2014) for mice, using two commercially available transfection reagents, polyethylenimine (PEI) and Lipofectamine.

We elected to use the mTomato mouse as a model to assess transfections as this model expresses a membrane-targeted tdTomato fluorescent protein with nearly ubiquitous expression in all tissues (Muzumdar et al., 2007). This provides us with four important advantages: 1) the acini are clearly identifiable from ductal cells as ductal cells have reduced expression of the mTomato-membrane fusion construct and are localised in the larger ductal structures that lack canaliculi; 2) the plasma membranes of the acini are clearly visible thus making it possible to assess the cellular response to transfections in terms of cell/membrane integrity and viability; 3) immune cell infiltration can be detected due to the ubiquitous expression of membrane-targeting mTomato; and 4) we have a marker of exocytosis that is independent of transfection thus providing an assay to evaluate normal function of the cells. To assess reagent toxicity and cellular integrity in response to transfections, we evaluated levels of intracellular vacuolisation, which is indicative of a cellular stress response and subsequent autophagy (Eskelinen, 2005; Liou et al., 1997). As vacuoles form a plasma membrane bilayer (Eskelinen, 2005), this would be visible in cells in the mTomato mouse, providing us with a means to calibrate and optimise the transfection protocol. This a functional readout which is not possible with membrane dyes such as CMDR. The plasmid DNA used for transfection encoded Tpm3.1 tagged with mNeonGreen which associates with actin filaments (Appaduray et al., 2016). As an actin coat forms

around fused granules undergoing regulated exocytosis (Masedunskas et al., 2011a), the ability to trigger exocytosis in transfected cells provided us with a means to determine if normal cellular functions are maintained. Thus exocytosis events at the apical plasma membrane (APM)/canaliculi could be detected by observing plasma membrane mTomato fluorescence (red channel) and actin scaffold formation around fused granules through Tpm3.1-NG fluorescence (green channel), which is not possible with membrane dyes because they target basolateral membranes exclusively.

### **Cationic polymer (PEI)**

We first tested polyethylenimine (PEI) (Boussif et al., 1995), a cationic polymer-based reagent that has been used to successfully transfect acini in rat salivary glands (Sramkova et al., 2014). To this end, mouse salivary glands were infused with a PEI transfection cocktail containing 4% PEI : 5 µg plasmid DNA : 5% glucose made up to 20 µL in MilliQ H<sub>2</sub>O. Control salivary glands were infused with 5 µg plasmid DNA : 5% glucose : 0.05% Alexa 647 Dextran made up to 20 µL in MilliQ H<sub>2</sub>O without PEI. Successful infusion could be confirmed via Dextran fluorescence, which in turn would determine if infusing plasmid DNA, glucose or H<sub>2</sub>O adversely affects cells. Mice were allowed to recover for 22-24 h at which time intravital imaging was performed.

Dextran fluorescence was detected in the control glands (Figure 3.5 A, arrowheads), likely phagocytosed by stromal cells (Figure 3.1) thus confirming that infusion was successful. Cells in the control gland exhibited normal appearance (Figure 3.5 A, B), thus demonstrating that infusion of plasmid DNA, glucose and H<sub>2</sub>O does not adversely affect cells and does not elicit an immune response, unlike viral delivery methods (cf Figures 3.2, 3.3). Acinar cells were transfected as seen with the green fluorescence signal from the Tpm3.1-NG construct (Figure 3.5 C) and no immune response was observed. However the majority of both transfected and non-transfected acinar cells exhibited extensive intracellular vacuolisation (Figure 3.5 C, D, arrowheads) thus possibly exhibiting a stress response to PEI exposure and internalisation, which has been described previously (Lv et al., 2006). In addition, regulated exocytosis could not be triggered in these cells, indicating that 4% PEI infusion may adversely affect the integrity and normal function of mouse salivary gland acini.

We next tested whether reducing the % PEI 10-fold would ameliorate the adverse impact on cellular integrity and function. Mouse salivary glands were infused with 25  $\mu$ L of a 0.4% PEI : 5  $\mu$ g plasmid DNA : 5% glucose : H<sub>2</sub>O cocktail, allowed to recover and intravital imaging was performed. Cells exhibited a reduced presence of intracellular vacuoles (Figure 3.5 E) compared to the 4% PEI infusion (Figure 3.5 C); however, minor vacuolisation was still evident (Figure 3.5 F, arrowheads), but no transfected cells were detected. We conclude that PEI is not a suitable transfection reagent for mouse salivary glands because cellular integrity and function is compromised at concentrations necessary for successful transfection.

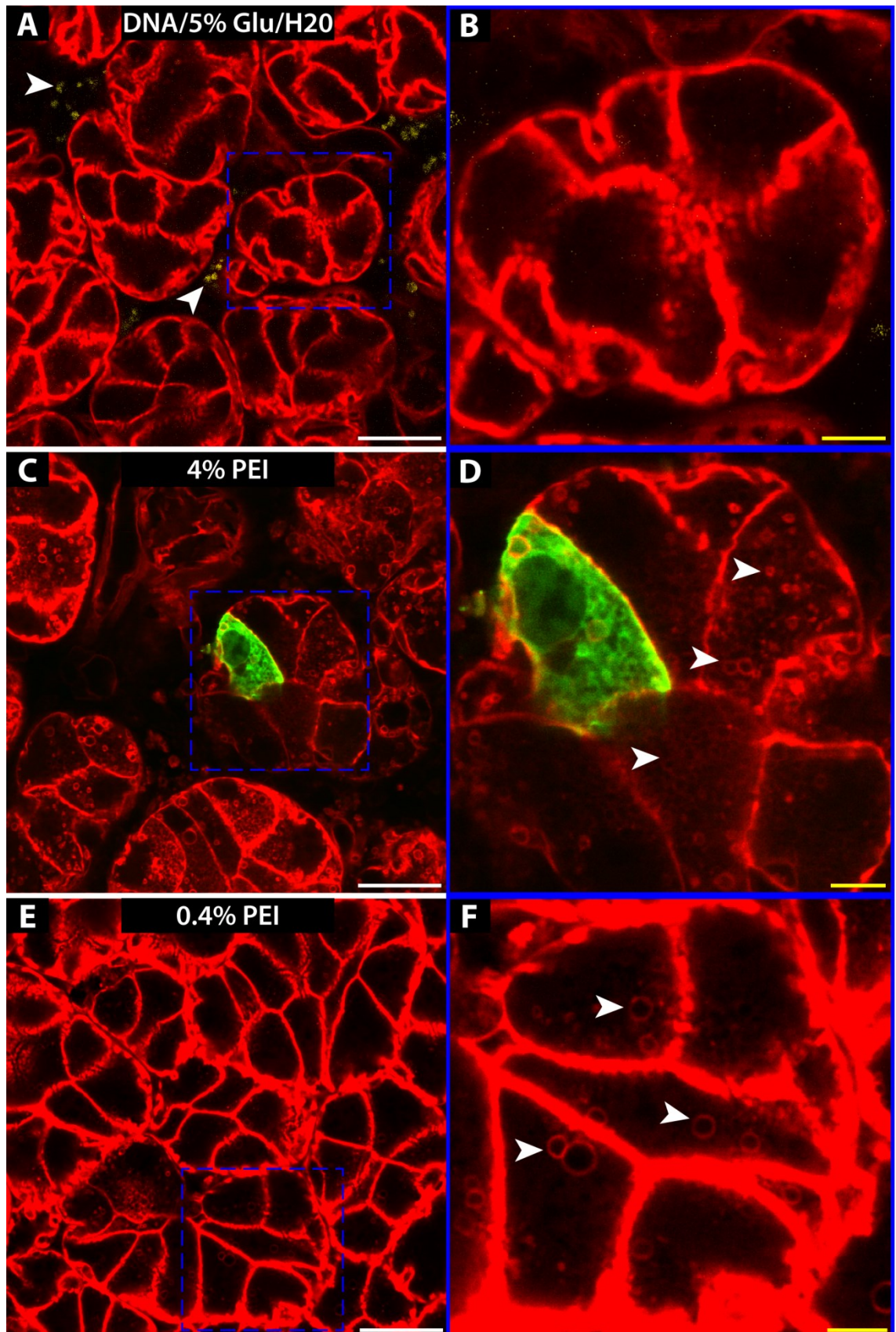


**Figure 3.5** Transfection of salivary glands in mTomato mice with polyethylineimine (PEI). Salivary glands in mice expressing mTomato (plasma membrane marker) were

infused with 20  $\mu$ L of plasmid DNA/H<sub>2</sub>O/5% glucose for controls (A, B) or PEI transfection cocktails (C-F). The plasmid DNA encodes Tpm3.1 tagged with mNeonGreen, that associates with actin filaments. 22-24 h after transfection, mice were anaesthetised and intravital imaging was performed. B, D, and F are enlargements of areas marked with dashed blue boxes in A, C and E, respectively. To ensure the control cannulation/infusion was successful, Alexa 647 Dextran was added to the control mix prior to transfection. Dextran that has been taken up by the stromal cells is visible in yellow (arrowheads) indicating successful cannulation and infusion of reagents into the salivary gland (A). Acini morphology appears to be normal, indicating that the addition of DNA, H<sub>2</sub>O and glucose in a 20  $\mu$ L volume does not affect cellular integrity (A, B). mTomato fluorescence is contrast adjusted to clearly view intracellular structures which are faint. Transfection of a 4% PEI/DNA cocktail per salivary gland results in transfected cells, a representative of which is shown in green (C, D). The majority of acini exhibited intracellular vacuolisation (C, D arrowheads) and regulated exocytosis failed to be triggered in transfected cells, indicating that addition of 4% PEI likely compromises cellular integrity and function. Reducing the concentration of PEI to 0.4% resulted in a much improved cellular phenotype (E) with only a few cells exhibiting intracellular vacuoles (F arrowheads). However, no transfected cells were detected. This indicates that PEI is not a suitable reagent since the concentration necessary for robust transfection compromises cellular integrity. White scale bars = 20  $\mu$ m, yellow scale bars = 5  $\mu$ m.  $n = 2$  glands per condition.

## Cationic lipid (Lipofectamine)

We next tested Lipofectamine LTX (Lipo LTX) and Lipofectamine 3000 (Lipo 3K), which are commercially available cationic lipid reagents (Gao and Huang, 1991). mTomato mouse salivary glands were infused with 20  $\mu$ L of transfection cocktails containing either 10% Lipo LTX or 6-16% Lipo 3K transfection reagents complexed with 2.5  $\mu$ g DNA in Opti-MEM media, shown in Table 3.1. These concentrations were chosen because they were within the range recommended by the manufacturer. Cocktails were mixed according to the manufacturer's instructions. Mice were allowed to recover for 16-24 h and intravital imaging was performed.

**Table 3.1 Mouse salivary gland Lipofectamine transfection trials and outcomes.**

Lipofectamine reagent infused per salivary gland (% v/v)	Transfection cocktail volume per salivary gland ( $\mu$ L)	DNA per salivary gland ( $\mu$ g)	Transfected cells detected per salivary gland	Number of salivary glands transfected	Level of intracellular vacuolisation
Lipo 3K 6%	20	2.5	15-46	6	Moderate
Lipo 3K 8%	20	2.5	5-13	8	High
Lipo 3K 12%	20	2.5	0-1	2	High
Lipo 3K 16%	20	2.5	1-2	2	Very high
Lipo LTX 10%	20	2.5	7-12	2	Light

Both reagents successfully transfected acinar cells as shown by green fluorescence in cells (Figure 3.6 A-D) demonstrating that Lipofectamine can be used to transfect mouse salivary gland acinar cells. In addition, no immune cell infiltration was observed. Lipo 3K had a higher transfection efficiency compared to Lipo LTX, with 15-46 transfected cells detected per gland versus 7-12 cells transfected cells detected per gland, respectively (Table 3.1). Both reagents induced light/moderate intracellular vacuolisation (Figure 3.6 B, D arrowheads) with Lipo LTX being causing marginally less vacuolisation, however with lower transfection efficiency. Lipo 3K titrations resulted in

a dose dependent toxicity where intracellular vacuolisation increased with increasing Lipo 3K with a concomitant reduction in numbers of transfected cells (Table 3.1).

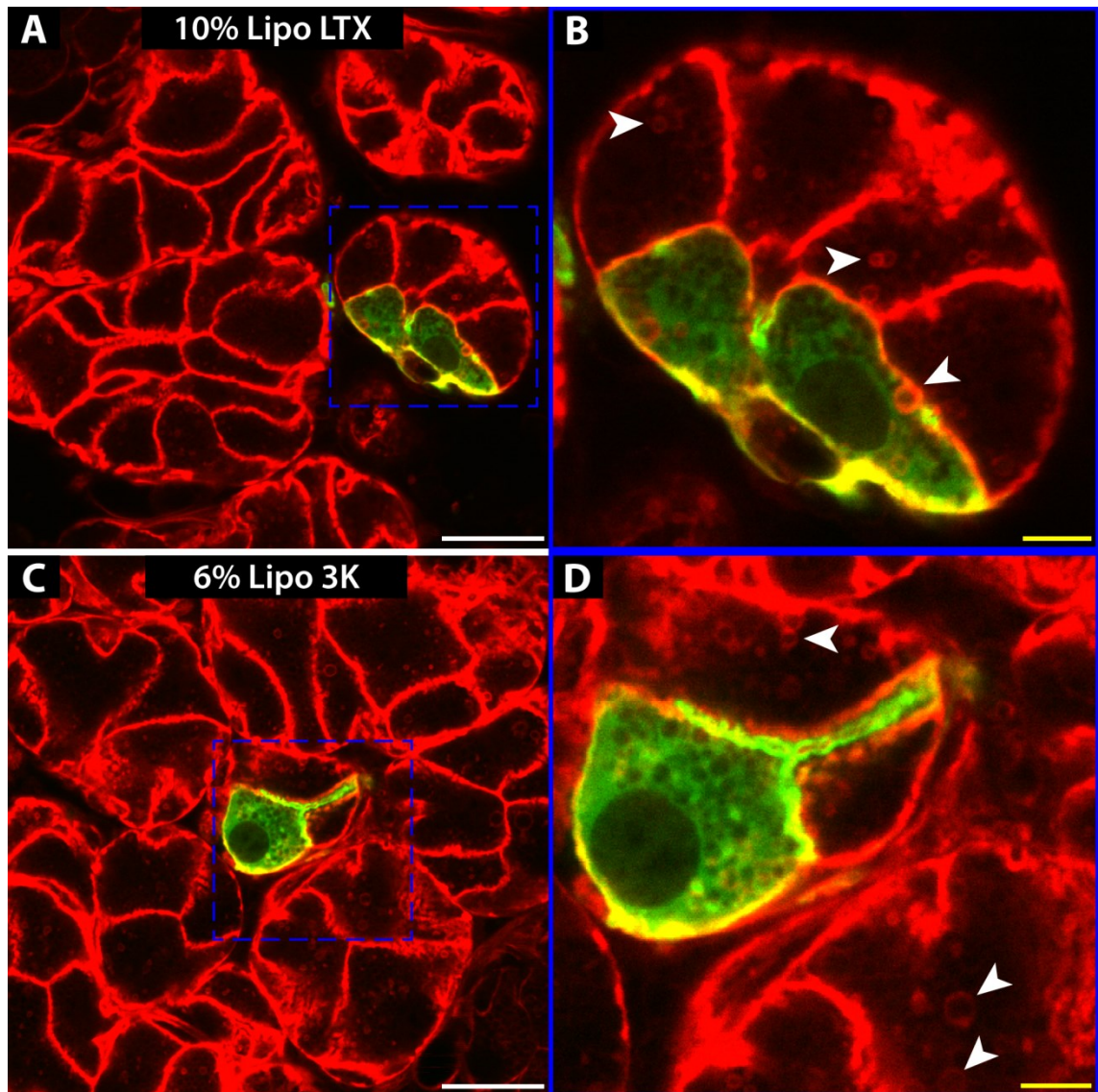


**Figure 3.6 Transfection of salivary glands in mTomato mice with Lipofectamine.** Salivary glands of mice expressing mTomato (plasma membrane marker) were infused with 20  $\mu$ L of Lipofectamine LTX (Lipo LTX) (A, B) and Lipofectamine 3000 (Lipo 3K) (C- F) transfection cocktails delivering plasmid DNA encoding mNeonGreen-tagged Tpm3.1. 22-24 h after transfection, mice were anaesthetised and intravital imaging was performed. B, D and F are enlargements of areas marked with dashed blue boxes in A, C and E, respectively. Lipo LTX resulted in successful transfection with light-moderate intracellular vacuolisation (A, B arrowheads); however, the transfection efficiency was low, with only 7-12 transfected cells detected near the surface in either gland. 6% Lipo 3K resulted in a relatively high transfection efficiency (15-46 cells detected near the surface per gland); however, moderate granulation was present in

cells (C, D arrowheads). White scale bars = 20  $\mu\text{m}$ , yellow scale bars = 5  $\mu\text{m}$ .  $n = 2-8$  glands per condition.

We determined whether acinar cells transfected with 6% Lipo 3K were responsive to isoproterenol stimulation. mTomato mouse salivary glands were transfected with the 6% Lipo 3K cocktail and imaged 16-24 h later upon isoproterenol injection as described in Materials and Methods. Regulated exocytosis was successfully triggered in transfected cells as shown by the appearance of multiple fused granules at the APM in a representative cell (Figure 3.7 A, white arrowheads). A granule undergoing exocytosis as observed by mTomato fluorescence in the adjacent non-transfected cell is shown for comparison (Figure 3.7 A, mTomato panel yellow arrowhead). An actin scaffold marked by Tpm3.1-NG fluorescence is assembled around the fused granules undergoing exocytosis, demonstrating that normal cellular functions are maintained in cells transfected with 6% Lipo 3K (Figure 3.7, A Tpm3.1-NG panel, B arrowhead). In addition, initial granule size upon fusion ranged between 1-1.5  $\mu\text{m}$  and individual exocytosis events lasted approximately 50-90 s (data not shown) indicating that granule morphology and exocytosis kinetics were within the normal range (Masedunskas et al., 2011a). In conclusion, this transfection protocol using Lipo 3K yields functional transfected secretory acini in mouse salivary glands and can be used for exocytosis assays.

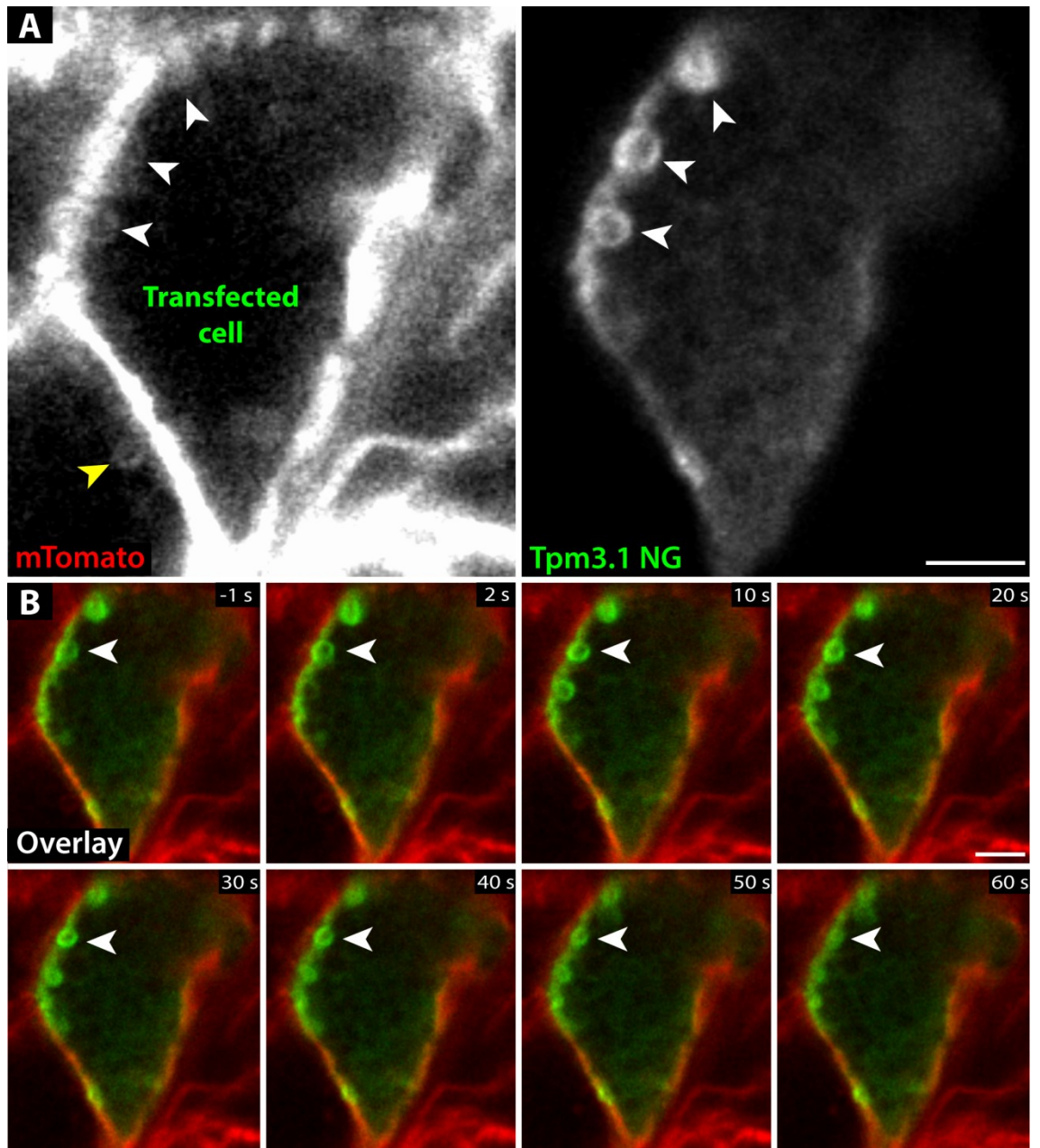


**Figure 3.7 Exocytosis can be triggered in mouse acinar cells transfected with Lipofectamine 3000.** Salivary glands of mice expressing mTomato (plasma membrane marker) were infused with 20  $\mu$ L of Lipofectamine 3000 transfection cocktail delivering plasmid DNA encoding mNeonGreen-tagged Tpm3.1. 22-24h after transfection, mice were anaesthetised, stimulated by subcutaneous injection of isoproterenol to initiate exocytosis and imaged via intravital microscopy. (A) Images showing a transfected cell in mTomato (left panel) and Tpm3.1-NG (right panel) channels. White arrowheads indicate multiple granules undergoing exocytosis in a transfected cell demonstrating that regulated exocytosis can be triggered in transfected cells and observed by time-

lapse microscopy. The yellow arrowhead (left panel) indicates a granule undergoing exocytosis in an adjacent non-transfected cell, visualised by mTomato. (B) Overlay of mTomato and Tpm3.1-NG channels showing a secretory granule undergoing fusion and gradual exocytosis (arrowhead). Scale bar = 5  $\mu$ m.  $n = 4$  glands.

## Discussion

We characterised the efficiency of gene transfer into the secretory acini of mouse salivary glands using LV-, AdV- and AAV-based methods and developed a novel non-viral gene delivery protocol using commercially available transfection reagents (Table 3.2).

**Table 3.2 Summary of results from various DNA delivery methods.**

Delivery method	AAV9	Ad5	Lenti	Lipofectamine	PEI
Efficiency	High	Medium	Very low	Low	Low
Cell types transfected/transduced	Majority are acini, with stromal and ductal cells	Acini, stromal and ductal cells	Majority are ductal cells	Majority are acini	Majority are acini
Immune response	None detected	Yes	Yes	None detected	None detected
Toxicity in transfected/transduced cells	None	None	None	Low	High
Expression duration	At least 14 days	3-6 days	At least 12 days	Approximately 28 hours	Approximately 28 hours
Peak expression	Day 7-14	Day 3-4	Day 4-12	16-20 hours	16-20 hours

We demonstrated that AAV9 efficiently transduces mouse salivary gland acinar cells *in vivo* without eliciting an immune response. In addition, AAV9-mediated gene expression in this tissue peaks between days 7 and 14 and has been shown to last up to at least 7 weeks in other mouse tissue such as cardiac muscle (Piras et al., 2013). Hence, AAV9 would be an excellent vector system for delivering gene editing components, such as CRISPR (O’Connell et al., 2014) for genetic ablation or modification of genes. Recently other groups have successfully used dual AAV9 vectors to deliver CRISPR components to mouse muscle and partially restored dystrophin expression, thus moderately ameliorating muscle dystrophy (Long et al., 2016). Since AAV9 is limited in terms of its capacity to tolerate large inserts, it provides a limited, but viable means to study the activity of proteins of interest. Additionally, data could be obtained in a high-throughput manner from a large number of transduced cells

which lends itself to analyses using flow cytometry. In summary, AAV9 gene delivery to mouse salivary glands provides a limited, but relatively quick, efficient and cost-effective means to genetically manipulate protein expression in mouse salivary glands *in vivo* without the need to generate knock-in/knock-out mice.

Gene delivery using LV and AdV also results in transduced acini, however with varying efficiency and tropism depending on the route of delivery. Interestingly, successful transduction of acini and ductal cells appears to occur only if viral particles are introduced via infusion of the ductal system. This strongly suggests that exposure of viral particles to the APMs of these cells is crucial for successful transduction and points to the existence of compatible viral receptors on these membranes which are likely absent from the basolateral membranes. Alternatively, basement membrane which lines the basolateral surfaces of the epithelial tissues may be preventing viral particles from accessing the parenchyma. Direct intra-stromal injection of LV and AdV particles results in exclusive transduction of stromal cells, thus allowing for selective transduction of these cells for gene delivery in research or therapeutic applications. Although we did not investigate the direct intra-stromal injection of AAV9, since GFP-expression was detected in stromal/myoepithelial cells on Day 14, it is likely that AAV9 would also efficiently transduce these cell types.

A strong immune response was observed for LV and AdV transduction, as evidenced by leukocyte infiltration which likely facilitates removal of infected cells (Bessis et al., 2004; Muruve, 2004). This is a likely contributing factor to the low transduction efficiency observed with LV as well as the loss of expression observed on Day 6 with AdV as has been reported in other studies (Dai et al., 1995). As it is possible to selectively transduce stromal cells via direct intra-stromal injection of viral particles, particularly with AdV, it is worth investigating the effects of immunosuppression to maintain the viability of transduced stromal cells. Previous studies have demonstrated that immunosuppressive techniques successfully increase the duration of expression of LV and AdV transduction in various cell types (Hermens and Verhaagen, 1998; Nayak and Herzog, 2010) and could be a strategy for future work in increasing the efficiency as well as lengthening expression of LV and AdV transduction in mouse salivary gland.

We developed a novel method for non-viral delivery of plasmid DNA into mouse salivary glands using commercially available transfection reagents. A limitation to this method however is the use of ectopically expressed constructs. An overexpressed, exogenous tagged protein may compete with its endogenous counterpart and impact the normal function of the protein. Hence, only cells that have low-medium expression levels should be analysed. Expression levels of ectopic and endogenous proteins could also be compared via antibody staining of transfected cells to optimise the promoter choice in the DNA delivery vector to ensure an adequate expression range. Another limitation is the low transfection efficiencies obtained compared to viral-mediated gene delivery. However despite these limitations, *in vivo* transfections allow for simple, rapid and cost-effective evaluation of DNA constructs of interest without the complications of an immune response or safety concerns associated with viral delivery methods (Nayak and Herzog, 2010). Moreover, the scope of experimental possibilities is now vastly increased as any available genetically modified mouse model can be transfected with constructs of interest. Loss or gain of function studies can be rapidly performed by transfection of fluorescent-tagged constructs into knockout or transgenic mice. Additionally, reporter mouse models such as Lifeact-GFP/RFP mice (Riedl et al., 2010) can be transfected with reciprocal tagged constructs thus allowing investigation into the activity of multiple proteins *in vivo*. This has profound implications for the flexibility and scope of assessing the *de novo* kinetics of proteins involved in actin assembly and regulation which previously has only been possible to a limited extent in the rat transfection model (Sramkova et al., 2014).

Interestingly, only a subset of cells is amenable to transfection despite both PEI and Lipofectamine transfection cocktails being infused extensively throughout the ductal system, as indicated by the presence of intracellular vacuolisation in the majority of cells. What makes these cells in particular more amenable to transfection compared to others is unclear. It is well established that cells undergoing division are more amenable to gene delivery and is a requirement for obtaining high transfection efficiencies using lipo- and polyplexes as exogenous DNA can be translocated into the nucleus during breakdown and reformation of the nuclear membrane (Brunner et al., 2000). It is therefore likely that the transfected cells were undergoing stages of cell

cycle division when the DNA-lipid/PEI complexes were internalised, thus allowing uptake of the plasmid DNA. Further work investigating this phenomenon could help us understand the mechanism of transfection of these cells *in vivo*, which is currently not well understood. This could lead to the development of more efficient and safer non-viral delivery reagents, which would be beneficial for the treatment of diseases such as Sjorgen's syndrome and salivary gland cancer, where viral-based methods are the only currently viable options for delivery of therapeutics (Baum et al., 2015).

## **Chapter 4. Recruitment kinetics of tropomyosin Tpm3.1 to actin filament bundles in the cytoskeleton is independent of actin filament kinetics**

### **Introduction**

In this chapter gene delivery is used in rats as well as primary cell culture to examine the relationship between Tpm and actin filament dynamics. This revealed new insights into how Tpm associate with actin filaments and thus improves our understanding of the physical properties and functions of these co-filaments.

Most non-muscle or cytoskeletal actin filaments are comprised of co-polymers of actin and Tpm. Studies have indicated that the formins specify, at least in part, which Tpm isoform is incorporated into an actin filament (Johnson et al., 2014; Tojkander et al., 2011) which suggests that Tpm polymer formation is dependent on actin dynamics. The current understanding of this relationship is that once the actin-Tpm polymer is formed, Tpm remain bound to the filament until the filament is disassembled. Therefore, Tpm association with filaments is pictured as largely static.

Distinct actin filament populations have been identified in cultured cells (Lin et al., 1988; Weinberger et al., 1996). In U2OS cells there are at least four different categories of stress fibres: dorsal, ventral, transverse arcs and the perinuclear cap (Tojkander et al., 2011). In addition, two actin sub-populations have been identified at the cell cortex distinguished by very different turnover and polymerisation rates (Fritzsche et al., 2013). Analysis of isoform-specific Tpm dynamics associated with stress fibres has been carried out using fluorescence recovery after photobleaching (FRAP) and revealed different recovery rates. When YFP/GFP-tagged Tpm 1.7, 3.1 and 1.9 (previously Tm3, Tm5NM1 and Tm5b, respectively; (Geeves et al., 2015) were compared, Tpm3.1 had a higher rate of recovery on actin stress fibres (Martin et al., 2010). Of the four Tpm isoforms shown to be essential for stress fibre formation, 1.6 (previously Tm2), 1.7, 3.1 and 4.2 (previously Tm4), Tpm4.2 had a faster recovery than the other 3 isoforms (Tojkander et al., 2011). There is no information about the

relationship between actin and Tpm dynamics in filaments of the cytoskeleton; however, recent data on the assembly of pre-myofibrils suggests that there is not an absolute relationship between actin and Tpm turnover (Wang et al., 2014). A secondary question is whether the placement of a tag impacts Tpm dynamics since no comparison has been carried out between N and C-terminal tagged Tpm constructs.

In this chapter FRAP was used to investigate the interrelationship of Tpm and actin dynamics *in vitro* in cultured cells and *in vivo* in tissues. The focus was on isoform Tpm3.1 that is known to stabilise actin filaments by reducing depolymerisation (Stehn et al., 2013b) as well as recruiting myosin motors (Bryce et al., 2003). Fluorescent protein-tagged Tpm3.1 and actin were used to examine Tpm3.1 vs actin recovery in dorsal/ventral stress fibres in mouse embryo fibroblasts (MEFs) and in apical/cortical bundles in rat salivary gland acinar cells. Recovery of Tpm3.1 was determined on actin filaments perturbed with the actin-targeting drug jasplakinolide, that promotes actin filament nucleation and stabilisation (Bubb et al., 2000; Holzinger, 2010). We also investigated the impact of placing a fluorescent tag at either the N- or C-terminus of Tpm3.1 on the fidelity of its localisation and recovery kinetics. Our data is compatible with a continuous dynamic exchange of Tpm3.1 occurring on actin filaments that is independent of actin filament dynamics and the location of the tag on Tpm3.1.

## **Results**

### **Visual characterisation of N- and C-terminal tagged Tpm3.1 constructs**

Tpms exist as  $\alpha$ -helices, therefore fusing a fluorescent protein along its structure would likely affect its flexibility and structure, impeding its ability to bind and regulate actin (Holmes and Lehman, 2008). The fluorescent protein must therefore be placed at either the N- or C-terminus of the protein. Recent studies in yeast have demonstrated that tagging yeast tropomyosin affects proper localisation and behaviour depending on where the fluorescent tag is placed (Johnson et al., 2014), therefore interpretation of tagged Tpm construct activity must be carefully evaluated (Brooker et al., 2016). Hence, we elected to construct both N- and C-terminal fluorescently tagged Tpm

constructs to assess their localisation and dynamics in mammalian primary cell culture as well as *in vivo* in rodent salivary glands.

First, we investigated the effects of placing the fluorescent protein tag in the N- or C-terminus of Tpm3.1 on the fidelity of its activity in primary cell culture. N-terminal (N-Tpm3.1)- and C-terminal (C-Tpm3.1)-tagged Tpm3.1 were transfected into wild type and Tpm3.1/3.2 knockout MEFs as in Materials and Methods. The tagged constructs localised predominantly to stress fibres in both cell types (Figure 4.1 A-D). These cells were co-stained with the CG3 antibody which detects all isoforms expressed from the TPM3 gene as well as both N-Tpm3.1 and C-Tpm3.1 (Figure 4.1 A-E). The CG3 antibody detects stress fibres in both untransfected (Figure 4.1 A arrowheads) and transfected wild type MEFs (arrows Figure 4.1 A). These stress fibres co-localise with the tagged proteins, however there are regions, particularly at the ends of stress fibres and regions of high tag density that do not co-localise with the antibody staining. This is not due to a failure of the antibody to recognise the tagged Tpm3.1 based on both Western blot results (Figure 4.1 E) and detection of the transfected tagged proteins in Tpm3.1/3.2 knock out cells (Figure 4.1 C, D). We hypothesise that there may be steric hindrance of the antibody epitope in these regions and as a result of this only the central region of stress fibres was analysed in further experiments.

*Figure has been removed due to copyright restrictions. Please refer to the original publication at*

*<http://journals.plos.org/plosone/article?id=10.1371/journal.pone.0168203>*

**Figure 4.1 N- and C-terminal tagged Tpm3.1 both localise to stress fibres in mouse embryo fibroblasts.** Tagged Tpm3.1 constructs were transfected into wild type and Tpm3.1/3.2 knockout mouse embryo fibroblasts (MEFs) and visualised by confocal microscopy (A and C) N-terminal tagged Tpm3.1 and (B and D) C-terminal Tpm3.1.

Tpm3.1 was visualised using the CG3 antibody that recognises all isoforms from the TPM3 gene. (E) Western blot showing expression of the tagged Tpm3.1 constructs and endogenous Tpm 3.1 in primary wild type MEFs as detected by the CG3 antibody. Scale bar = 10  $\mu$ m. *Figure and data generated by Nicole Bryce, Christine Lucas and Jeffrey Stear.*

### **Tpm3.1 has a rapid rate of exchange on stress fibres**

Few studies have focused on the kinetics of cytoskeletal Tpm3s in mammalian cell culture and no *in vivo* studies in mammals exist. As Tpm3s are ionically 'bound' to actin filaments (von der Ecken et al., 2015) investigation into their behavioural dynamics on actin filaments would provide insights into how Tpm3s modulate filament activity as well as other AAPs.

Having determined that both tags localised to stress fibres in MEFs, we elected to assess the recruitment dynamics of these constructs to actin filaments to obtain insights into how tag placement affects the behaviour of Tpm3s. A powerful technique for assessing protein dynamics in living cells and tissues is FRAP. Briefly, this technique allows the quantification of protein diffusion/binding/movement dynamics at target sites in living cells by first photobleaching a designated region of interest, followed by measurement of the fluorescence recovery into the bleached region over time (Reits and Neefjes, 2001) using downstream processing software such as ImageJ (Abràmoff et al., 2004). FRAP could therefore be used to assess Tpm3 dynamics on actin structures such as stress fibres in cell culture or actin filament bundles at the apical junctions of acinar cells *in vivo* in rodents.

Hence, we elected to use the FRAP assay to assess the dynamics of recruitment of Tpm3.1 into actin filament bundles in relation to actin dynamics using constructs tagged at either the N- or C-termini. By photobleaching zones containing stress fibres in the interior of the cell and monitoring the fluorescence recovery we are able to characterise the kinetics of Tpm3.1 recovery on a cell-by-cell basis. Laser power was optimised to ensure complete photobleaching occurred while also maintaining structural integrity, confirmed by visual comparison of stress fibre structures pre- and post-bleach.

In a typical FRAP experiment, the fluorescence will recover due to movement of unbleached molecules into the bleached zone and eventually reach a plateau. The level of the plateau provides information about the fraction of molecules that are mobile in the bleached zone (the 'mobile fraction') while the shape of the recovery provides information about the number and rates of the dynamic processes leading to

recovery, for example diffusion and exchange with a cytoplasmic pool. Initial preliminary data using cells transfected with Tpm3.1-YFP were acquired for 5 min, but no stable plateau was observed. This is due to the inevitable movement of the cells during imaging (typically at 1.5 to 2 min), resulting in unbleached structures being imported into the FRAP zone with time. Therefore, to minimise motion artefacts in the FRAP recovery data, all photobleaching experiments were performed for 2 mins post-bleach. Although the recovery is not fully complete at 2 mins, we found that the data recorded up to this point was able to sufficiently constrain the model and so obtain an accurate estimate of the mobile fraction; for N- and C- terminal tagged Tpm3.1 the spread of the 95% confidence interval on the estimated mobile fraction ranged from  $\pm 1\%$  to  $\pm 5\%$ .

Representative examples of a FRAP sequence from either N- or C-terminal Tpm3.1 construct transfections are shown in Figure 4.2 A and B. Zones containing stress fibres were bleached at time 0 followed by image acquisition at 1 fps for 2 min to acquire FRAP profiles (Figure 4.2 A, B, inset), which were measured by drawing a region of interest within the bleach zone using ImageJ data processing software (Abràmoff et al., 2004). We fitted recovery curves from both N- and C-terminal tagged constructs to a single- and double-exponential FRAP recovery models. We found that the double exponential model provided a statistically significant improvement in the quality of the fit compared the single exponential model. The C-terminal fit  $R^2$  values were calculated at 0.9835 for the single exponential fit compared with 0.999 for the double exponential fit ( $p < 0.0001$ ) with the N-terminal  $R^2$  values calculated at 0.9860 and 0.9995 for the single and double exponential fits respectively ( $p < 0.0001$ ), suggesting there are two dominant processes contributing to the recovery. We hypothesised that there are three candidate processes potentially contributing to the recovery; (1) diffusion of unbound tropomyosin molecules in the cytoplasm, (2) exchange of tagged- for untagged-Tpm3.1 on actin filaments which are exposed to the cytoplasm and (3) relatively slower exchange of tagged- for untagged-Tpm3.1 on actin filaments located in the interior of stress fibre filament bundles which are not in direct contact with cytoplasm. To determine whether the fast recovery component observed was associated with diffusion or exchange of Tpm3.1 between actin filaments and the

cytoplasm we examined in more detail the spatial profile of the recovery process. These processes will produce distinct spatial recovery profiles (Figure 4.3 A, B). Recovery due to diffusion will show an increase in the width of the bleached region over time as bleached and unbleached molecules diffuse, while the width of the bleached region will remain unchanged in an exchange process (Coscoy et al., 2002; Erami et al., 2016). We computed radially averaged spatial recovery profile by averaging over the bleached regions of a number of N- and C-terminal tagged Tpm3.1 transfected cells (Figure 4.3 C, D). In both cases the spatial recovery profile is consistent with an exchange based recovery. In line with this, we calculated the width of the bleached region over time in both cases by fitting to a Gaussian profile and found no increase in the width over time. We therefore concluded that diffusion does not contribute significantly to the observed recovery and the two recovery processes are associated with exchange of Tpm3.1 between cytoplasm exposed and shielded filament bundles respectively. This conclusion is supported by visual inspection of the movies and micrographs (Figure 4.2 A, B); association of tagged-Tpm3.1 with filament bundles starts almost immediately after bleaching. We hypothesise that the relatively slower recovery process is due to packing of filaments in the interior of stress fibres leading to potential steric impediments to complete exchange, independent of filament turnover.

Recovery curves for C-Tpm3.1 and N-Tpm3.1 showed identical mobile fractions of 66% in MEFs (Figure 4.2 C, D), and no statistical difference between the rate of fast exchange or relative contributions of slow and fast exchange, indicating that the fast exchange process is not affected by the tag location. N-Tpm3.1, however, exhibited a significantly longer slow recovery half time than C-Tpm3.1 ( $64.6 \pm 14.9s$  vs  $40.2 \pm 3.2s$ ,  $p=0.017$ ), indicating that this slower exchange process is inhibited by the N-terminal tag.

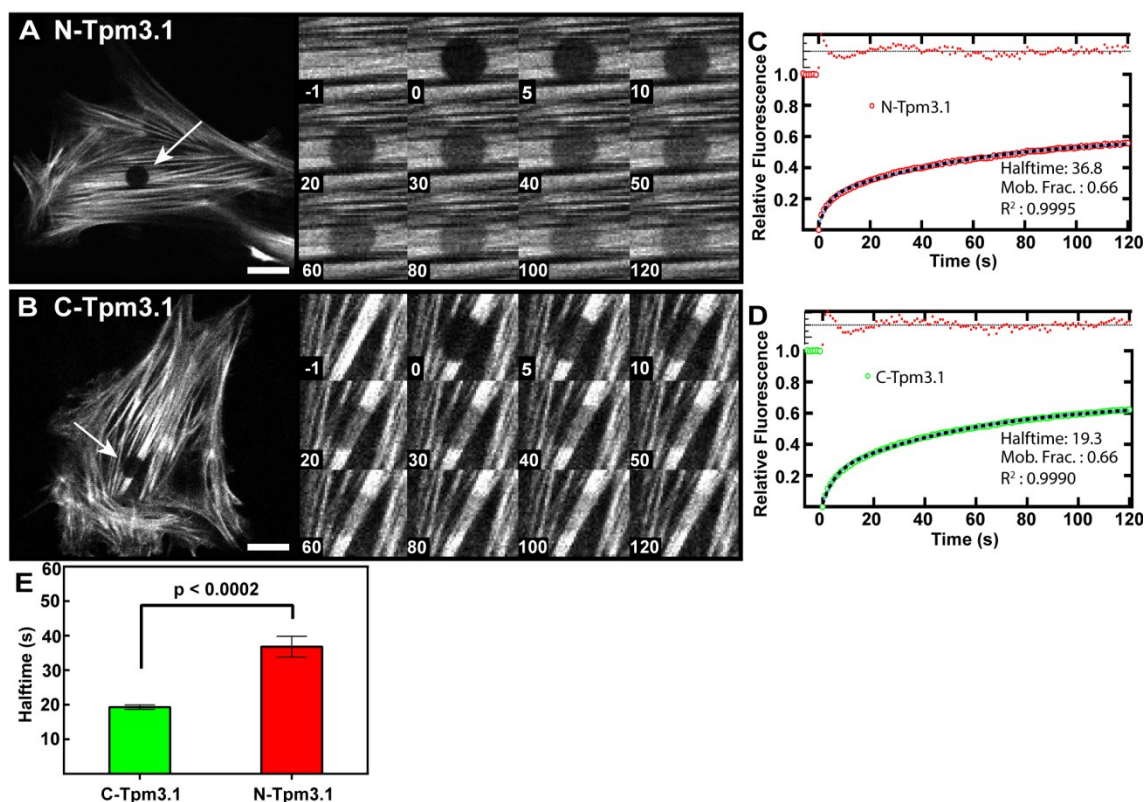


**Figure 4.2 N- and C-terminal tagged Tpm3.1 constructs have similar mobile fractions but dissimilar recovery rates.** (A, B) Representative images of FRAP assay in MEFs transfected with either N- or C-Tpm3.1. FRAP zones (white arrows) were bleached and cells imaged at 1 fps for 2 min. Both constructs continuously enrich stress fibres, but at different rates. Inset (A, B) Enlarged images of FRAP zones over time (s). (C, D) FRAP curves of N- or C-Tpm3.1 transfected MEFs. (E) Half-times of N- and C-Tpm3.1 recovery (see also Table 4.1). Data obtained from 6 experiments, 3-15 cells per experiment. Error bars are +/- S.E.M. Scale bars = 10  $\mu$ m

**Table 4.1 Half-times from double-exponential fits of N- and C-Tpm3.1 recovery in transfected MEFs.**

Half-times	N-Tpm3.1	Fractional contribution (%)	C-Tpm3.1	Fractional contribution (%)
$\tau_1$	3.1 s ( $\pm$ 0.6)	24	3.3 s ( $\pm$ 0.8)	31
$\tau_2$	64.6 s ( $\pm$ 14.9)	76	40.2 s ( $\pm$ 3.2)	69

*Figure has been removed due to copyright restrictions. Please refer to the original publication at <http://journals.plos.org/plosone/article?id=10.1371/journal.pone.0168203>*

**Figure 4.3 Spatial recovery of tagged Tpm3.1 is consistent with exchange rather than a diffusive transport process.** (A, B) Simulated spatial recovery profile for (A) diffusion and (B) exchange reaction based recovery showing (top) kymographs of fluorescent intensity and (bottom) spatial profile of recovery at selected timepoints with cartoon

illustrating relationship to bleached region. Black arrows indicate change in fluorescent intensity over time. Recovery due to diffusion shows an increase in the width of the bleached zone during the recovery due to motion of bleached and unbleached molecules from the surrounding areas while recovery due to an exchange reaction shows no change in the width of the bleached zone during the recovery. (C, D) Measured radially averaged spatial recovery profiles, for (C) N-Tpm3.1 and (D) C-Tpm3.1 averaged over  $n = 13$  and  $n = 9$  cells, respectively. (E, F) Fitted width of recovery profile over time for (E) N-Tpm3.1 and (F) C-Tpm3.1. Error bars indicate confidence interval on fit. *Data analysis and figure generated by Sean Warren and Paul Timpson.*

## **Intravital imaging and FRAP analysis of Tpm3.1 recruitment in transfected rat salivary glands**

To confirm these observations *in vivo*, we applied FRAP analysis to transfected salivary gland acinar cells in live rats using intracellular intravital microscopy. We chose the rat salivary gland as our *in vivo* model because of its tractability for intravital imaging and genetic manipulation (Masedunskas et al., 2013b). Salivary acinar cells express endogenous Tpm3.1 which is highly enriched at the apical membranes that are arranged into canaliculi (Figure 4.4 A, white arrow). Therefore, intravital FRAP assay was carried out on the apical regions of transfected cells (Figure 4.4 B, C). Both N- and C-terminally tagged proteins were localised at the apical membranes of acinar cells (Figure 4.4 D, E, white arrows). FRAP recovery kinetics showed similar trends to that seen in cultured MEFs; although, C-Tpm3.1 has a significantly higher mobile fraction (66%) compared to N-Tpm3.1 (55%) (Figure 4.4 F, G, I, J and Table 4.2). Therefore, the tagged proteins display similar, but distinct activities *in vitro* and *in vivo*, in quite dissimilar actin filament structures – stress fibres vs apical filament meshwork. As observed with MEFs, the half-life of recovery of C-Tpm3.1 was half of that seen with N-Tpm3.1 (Figure 4.4 H).

The slower recovery half-time observed for N-Tpm3.1 both in primary culture (Figure 4.2 E) and *in vivo* in rats (Figure 4.4 G) is consistent with the finding that muscle Tpm with an 80 residue N-terminal fusion peptide binds with an affinity slightly greater than a non-fusion variant and many-fold greater than unacetylated Tpm (Heald and Hitchcock-DeGregori, 1988). Additionally, tagging the N-terminus of yeast Tpm causes the construct to mis-localise (Johnson et al., 2014). Inserting the tag in the N-terminus therefore appears to alter normal Tpm regulation and binding possibly through steric hindrance, thus reducing the rate of N-Tpm3.1 incorporation into actin filaments. In contrast, recent studies in yeast have shown that tagging the C-terminus of the yeast Tpm also disrupts its ability to bind actin filaments (Brooker et al., 2016); however as shown here C-Tpm3.1 constructs are able to bind actin filament bundles both in MEFs and *in vivo* in live rodents. In addition, the C-Tpm3.1 construct was used to successfully generate a functioning knock-in mouse model (Masedunskas et al., 2017 submitted),

suggesting that in mammalian cell culture and *in vivo* in rodents, tagging the C-terminus of Tpm3 does not appear to perturb its localisation or function. For these reasons we selected C-Tpm3.1 as the construct of choice for subsequent cellular experiments.

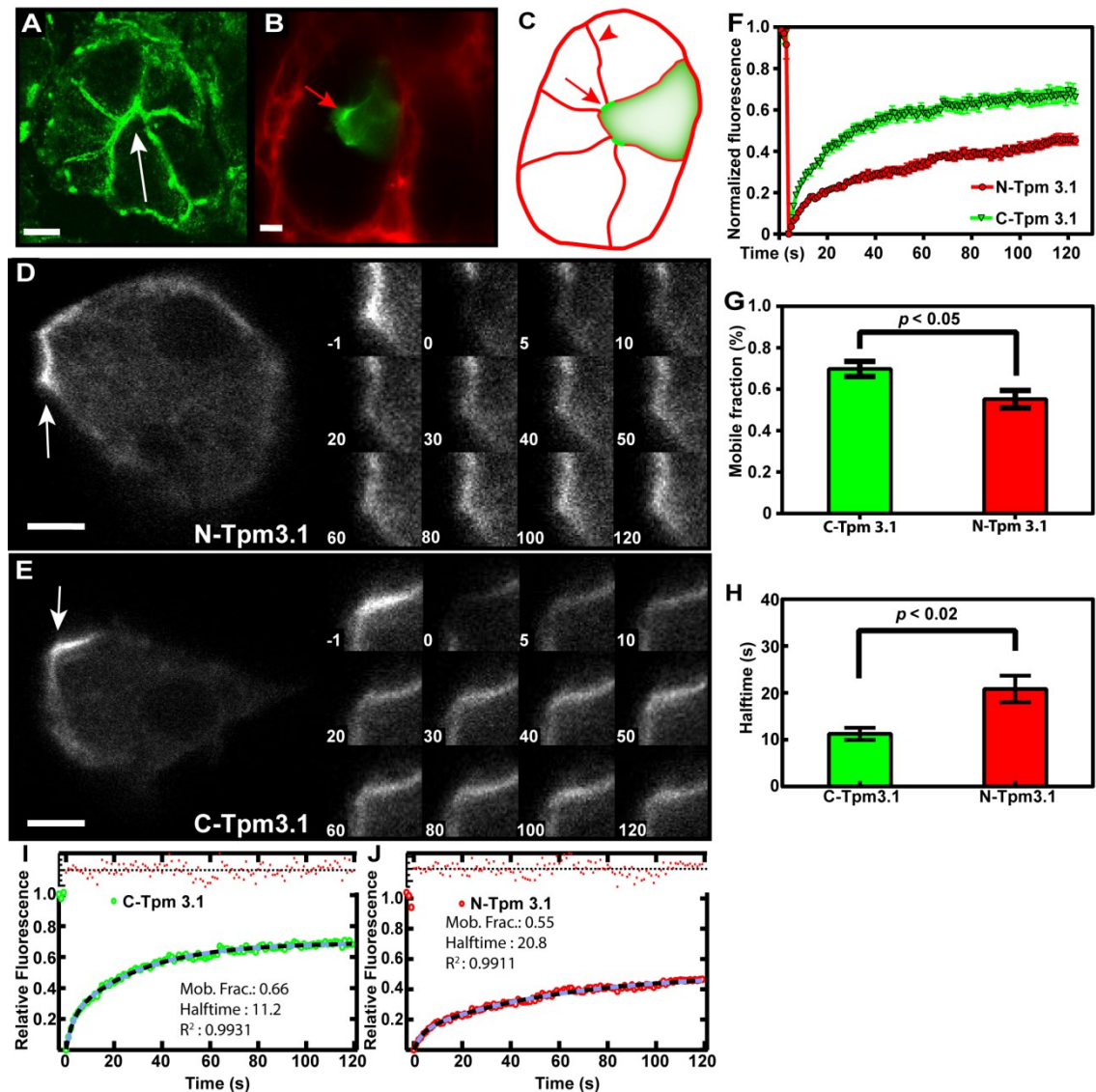


**Figure 4.4 Intracellular intravital imaging of the kinetics of N- and C-terminal tagged Tpm3.1 constructs transfected into rat salivary gland acinar cells.** (A) Confocal image of an acinus from rat submandibular salivary gland section stained with an anti-Tpm3.1 antibody. Tpm3.1 is enriched on the apical plasma membranes that form the canaliculi of acinar cells (white arrow). (B) Confocal image of a C-Tpm3.1 transfected cell in a single acinus of a rat salivary gland *in situ*. Extracellular space outside the acinus stained with 10kDa dextran Alexa 647 conjugate. Apical membrane is enriched with C-Tpm3.1 (red arrow). (C) Illustration of the transfected acinar cell in (B) showing Tpm3.1 enrichment at the apical membranes (arrow), but not at the basolateral membrane (arrowhead). (D, E) Intravital microscopy and FRAP analysis of N- and C-Tpm3.1 constructs in live transfected rats. Both constructs continually enrich filaments at

apical membrane with C-Tpm3.1 having a higher mobile fraction and lower halftime compared to N-Tpm3.1 (G, H). Numbers indicate time in seconds. White arrows indicate FRAP zones on the canaliculi of acinar cells. (F) FRAP curves for N- and C-Tpm3.1 from rat acinar cells. (G) Mobile fraction of N- and C-Tpm3.1. (H) Halftimes for N- and C-Tpm3.1 from rat acinar cells (See also Table 4.2). (I, J) Curve fits for N- and C-Tpm3.1 from rat acinar cells. Error bars are S.E.M. 11-19 cells assayed from at least 3 animals per construct. Scale bars = 5  $\mu$ m. *Data in (A) was generated by Christine Lucas.*

**Table 4.2 Half-times from double-exponential fits of N- and C-Tpm3.1 recovery in transfected rat acinar cells.**

Half-times	N-Tpm3.1	Fractional contribution (%)	C-Tpm3.1	Fractional contribution (%)
$\tau_1$	2.9 s ( $\pm$ 0.7)	31	1.9 s ( $\pm$ 0.9)	26
$\tau_2$	45.3 s ( $\pm$ 6.8)	69	20.5 s ( $\pm$ 5.9)	74

## **Impact of the actin-filament stabilising drug jasplakinolide on Tpm3.1 recruitment into stress fibres**

Having determined that C-Tpm3.1 appears to more faithfully represent endogenous Tpm3.1 behaviour, our next objective was to investigate the dynamics of Tpm3.1 interaction with actin filaments. Wang et al. (Wang et al., 2014) recently showed that C-terminal tagged muscle Tpm exchange is much less sensitive to jasplakinolide than tagged actin in pre-myofibrils suggesting that Tpm's can exchange independent of actin. Since our results suggest a similar conclusion we tested this in the MEF cytoskeleton by examining the cytoskeletal Tpm3.1. Our approach was to inhibit actin filament kinetics in MEFs using jasplakinolide to stabilise the actin filaments and measuring Tpm3.1 kinetics in stress fibres using FRAP analysis. Using this strategy, we specifically manipulated the kinetics of actin filaments; therefore, any recovery following photobleaching should reflect Tpm3.1 dynamics independent of actin dynamics. First, we established the conditions under which actin filaments were disrupted with drug treatment. We found that FRAP analysis of MEFs transfected with GFP- $\beta$ -actin showed very weak recovery into stress fibres (Figure 4.5 A, B) and treatment with 7  $\mu$ M jasplakinolide eliminated the minimal recovery of fluorescent actin into the FRAP zone (Figure 4.5 A, inset). Although the recovery curve (Figure 4.5 B) shows an  $\sim$ 50% reduction in the mobile fraction (Figure 4.5 B, D, E, F and Table 4.3) this does not reflect true recovery into stress fibre bundles, but rather a recovery in fluorescence of the cytosolic G-actin pool (Figure 4.5 A inset). Thus, treatment with jasplakinolide essentially eliminates the small amount of recovery of actin into stress fibres after photo-bleaching (Figure 4.5 A).

We then investigated the kinetics of continuous diffusion as opposed to active binding of a tagged construct in our assay using Lifeact-RFP, which has extremely transient binding to actin (Riedl et al., 2008). MEFs were transfected with Lifeact-RFP and FRAP analysis was performed on stress fibre regions in the presence and absence of 7  $\mu$ M jasplakinolide. FRAP of Lifeact-RFP results in an almost instantaneous recovery in both control and drug treated conditions (Figure 4.5 C). This is in agreement with the highly diffusive behaviour and transient binding of Lifeact constructs to its target site on actin

(Riedl et al., 2008). Interestingly, a small reduction in the mobile fraction from control to drug treated cells was observed (Figure 4.5 C, D). This perhaps suggests the existence of a sub-population of Lifeact bound to actin filaments in the interior of stress fibres which cannot as readily exchange as Lifeact at the periphery of stress fibres.

Comparison of recovery curves for the C-terminal tagged Tpm3.1 with Lifeact in MEFs indicates that Tpm3.1 has a high mobile fraction although not as high as Lifeact (Figure 4.2D, 4.5C). Because Lifeact engages in rapid exchange binding to actin filaments the mobile fraction is over 90% and has a very short half-time (Table 4.4). However, the fact that Tpm3.1 also has a short half-time and a high mobile fraction both in MEFs and in acinar cells *in vivo* suggests that most of the Tpm3.1 associated with actin is engaging in rapid exchange with a soluble pool. In contrast, GFP-actin shows a relatively slow recovery curve (Figure 4.5 A, E and Table 4.3) that raises the possibility that Tpm3.1 may be exchanging independently of actin filament turnover.

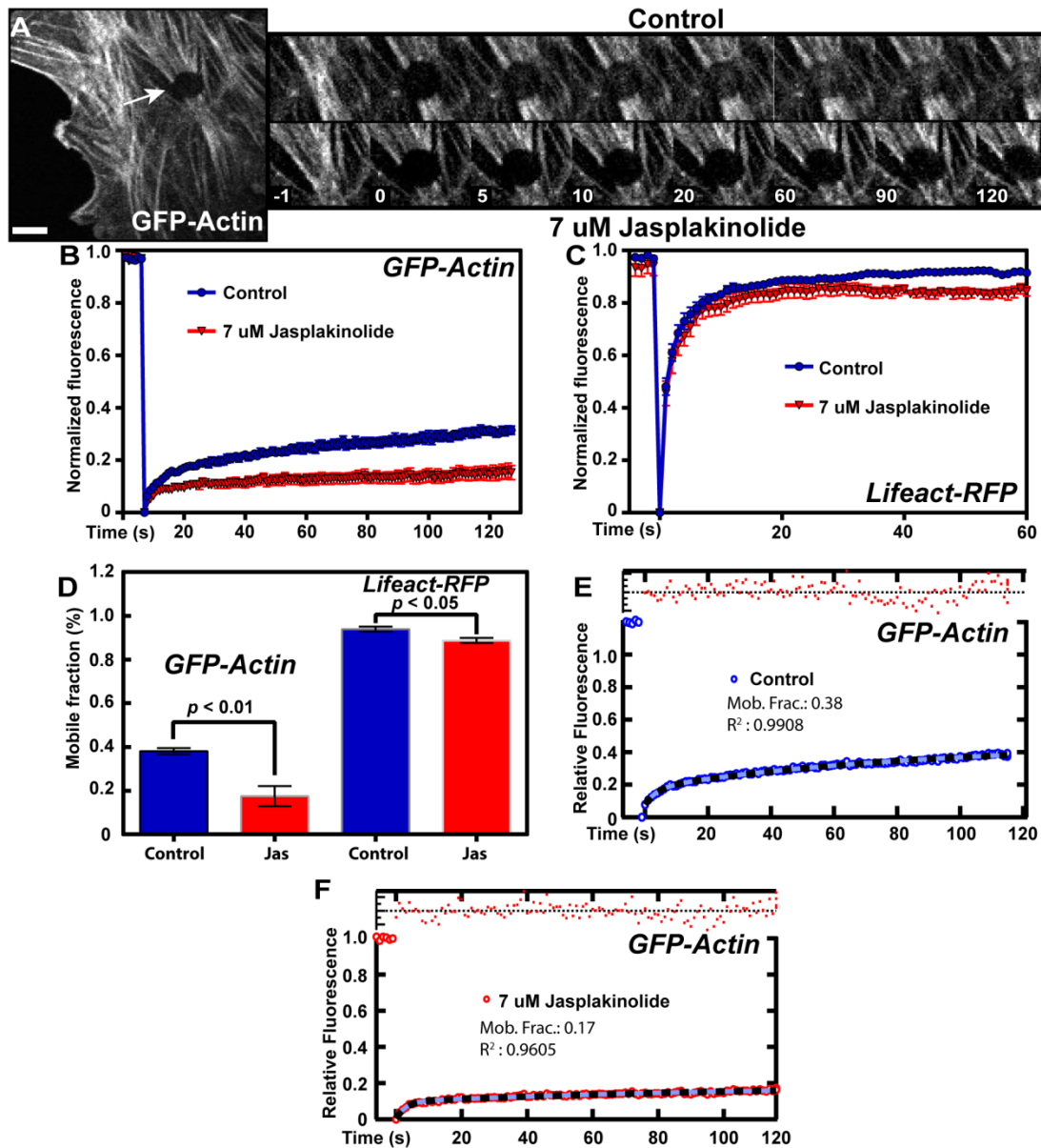


**Figure 4.5 The majority of actin in stress fibres is stable.** (A) Representative image and FRAP sequence of MEFs transfected with GFP- $\beta$ -actin. FRAP zone indicated by white arrow. Top panel: FRAP sequence of untreated control cells. Bottom panel: FRAP sequence after treatment with 7  $\mu$ M jasplakinolide. Actin filament turnover is completely inhibited by treatment with 7  $\mu$ M jasplakinolide, as shown by lack of GFP- $\beta$ -actin FRAP compared to untreated control. (B) FRAP curves for GFP-actin in control and jasplakinolide treated condition. (C) FRAP curves for Lifeact-RFP in control and jasplakinolide treated condition. A small but significant reduction in the Lifeact-RFP mobile fraction is observed with 7  $\mu$ M jasplakinolide treatment, suggesting that a sub-population of filaments exist in the interior of stress fibres that does not readily allow

bound Lifeact-RFP to exchange with the cytoplasmic pool. (D) Mobile fractions of control and drug-treated GFP-actin and Lifeact-RFP (see also Tables 4.3 and 4.4). (E) Curve fits for GFP-Actin control. (F) Curve fit for GFP-Actin treated with jasplakinolide. Data obtained from 3 separate experiments, 2-8 cells per experiment. Error bars are +/- S.E.M. Scale bars = 5  $\mu$ m

**Table 4.3 Half-times from double-exponential fits of GFP-actin recovery in control and drug-treated conditions.**

Half-times	Control	Fractional contribution (%)	Jasplakinolide	Fractional contribution (%)
$\tau_1$	2.4 s ( $\pm$ 0.4)	36	1.4 s ( $\pm$ 0.9)	33
$\tau_2$	65.5 s ( $\pm$ 12)	64	35.7 s ( $\pm$ 22)	67

**Table 4.4 Half-times from double-exponential fits of Lifeact-RFP recovery in control and drug-treated conditions.**

Half-times	Control	Fractional contribution (%)	Jasplakinolide	Fractional contribution (%)
$\tau_1$	0.6 s ( $\pm$ 0.2)	64	0.4 s ( $\pm$ 0.38)	52
$\tau_2$	5.9 s ( $\pm$ 1.5)	36	3.9 s ( $\pm$ 2.6)	48

Having determined that treatment with 7  $\mu$ M jasplakinolide significantly impacts actin recovery into stress fibre structures, we then sought to determine the recruitment kinetics of tagged Tpm3.1. MEF cells were transfected with constructs encoding C-Tpm3.1. Regions containing stress fibres were photobleached prior to addition of jasplakinolide to obtain control curves (Figure 4.6 A, inset). jasplakinolide was then added to cells and the same cells were immediately photobleached at a different site (Figure 4.6 A, inset). Intriguingly, jasplakinolide had a minimal effect on tagged Tpm3.1 recruitment into stress fibres (Figure 4.6 A, inset), where only a small but not significant reduction in the mobile fraction was observed (Figure 4.6 B-E and Table 4.5). As global actin turnover is significantly inhibited in the presence of the drug (Figure 4.5 A, B), we conclude that Tpm3.1 is constantly undergoing dynamic exchange on actin filaments that is independent of actin filament dynamics. This is also apparent from inspection of the images of actin and Tpm3.1 recovery in Figure 4.4 A vs 4.5 A. Since Tpm3s bind actin through weak ionic interactions (Barua et al., 2012; Wegner, 1979) it may be logical that Tpm3.1 on filaments undergoes exchange independent of actin. The small reduction in mobile fractions of tagged Tpm3.1 (Figure 4.6 B, C) and Lifeact-RFP (Figure 4.5 C, D) in the jasplakinolide treated conditions perhaps suggests that jasplakinolide is inhibiting the translocation and/or polymerisation of a dynamic sub-population of actin filaments that operates in stress fibres, a hypothesis which is in agreement with what has been reported for cortical actin (Fritzsche et al., 2013).

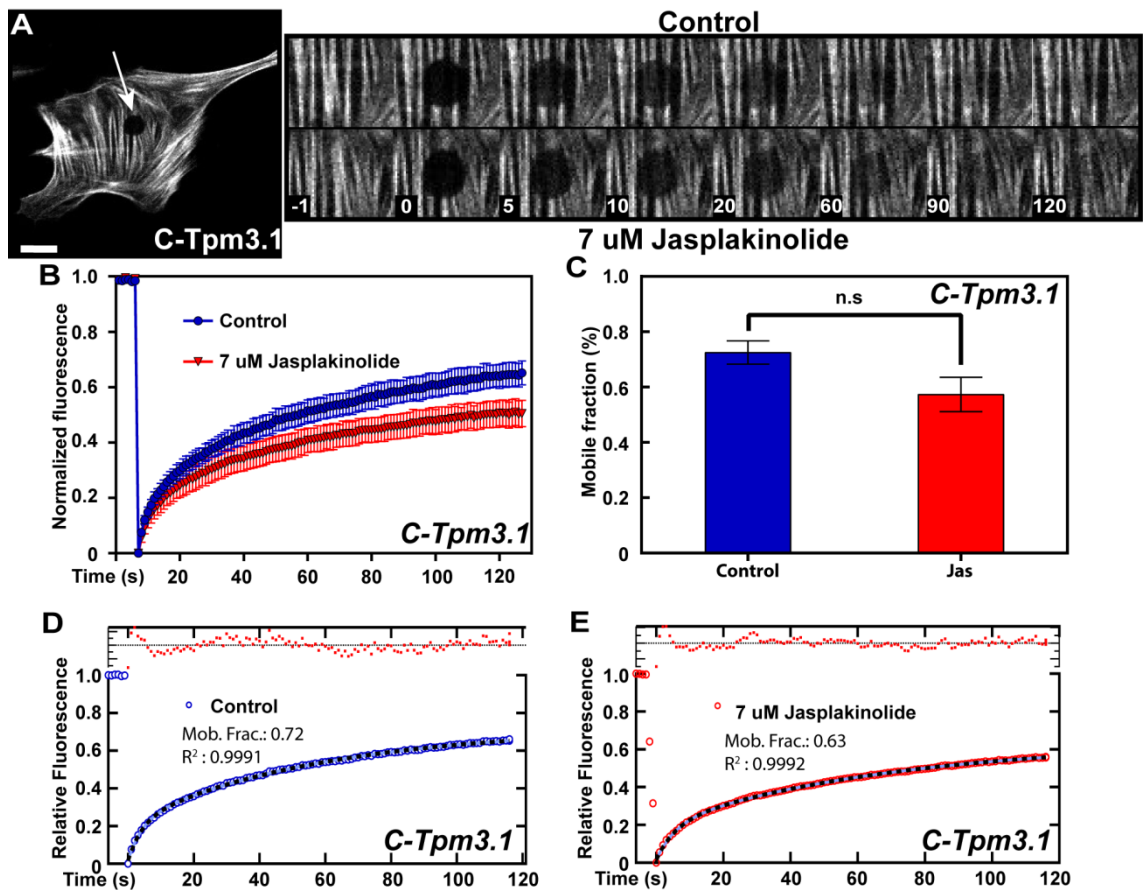


**Figure 4.6 Tpm3.1 maintains constant and rapid cycling on stress fibres in the presence of jasplakinolide.** (A) Representative image and FRAP sequence of MEFs transfected with C-Tpm3.1. FRAP zone indicated by white arrow. Top panel: FRAP sequence of untreated control cells. Bottom panel: FRAP sequence after treatment with 7  $\mu$ M jasplakinolide. C-Tpm3.1 exhibits constant exchange on filaments when actin filament turnover is inhibited with 7  $\mu$ M jasplakinolide treatment, indicating that Tpm3.1 binding dynamics are independent of actin filament turnover. (B) FRAP curves of C-Tpm3.1 in control and drug-treated conditions. (C) Mobile fraction of control and drug-treated condition (see also Table 4.5). (D, E) Curve fits for C-Tpm3.1 in control (D) and drug treated condition (E). Data obtained from 3 separate experiments, 3-8 cells per experiment. Error bars are +/- S.E.M. Scale bars = 10  $\mu$ m

**Table 4.5 Half-times from double-exponential fits of C-Tpm3.1 recovery in control and drug-treated conditions.**

<b>Half-times</b>	<b>Control</b>	<b>Fractional contribution (%)</b>	<b>Jasplakinolide</b>	<b>Fractional contribution (%)</b>
<b><math>\tau_1</math></b>	3.0 s ( $\pm$ 0.4)	28	3.1 s ( $\pm$ 0.4)	30
<b><math>\tau_2</math></b>	42.3 s ( $\pm$ 7)	72	43.9 s ( $\pm$ 13)	70

## Discussion

The observation that both types of tagged Tpm3.1 proteins have very similar localisation patterns to each other is surprising because there is extensive evidence that the N-termini of Tpm3s are crucial for Tpm3 function. From studies on muscle Tpm3s, it is known that the N-terminal residues are highly conserved (Helfman et al., 1984; Sanders and Smillie, 1985) and that acetylation of a methionine is required for normal function (Cho et al., 1990), regulation of actomyosin ATPase with troponin (Heald and Hitchcock-DeGregori, 1988) and Tpm3 dimer formation (Palm et al., 2003). Mammalian cytoskeletal Tpm3s in contrast do not require acetylation to bind actin (Pittenger and Helfman, 1992). In yeast, tagging the N-terminus of Tpm3 prevents acetylation of the N-terminal methionine causing the tagged protein to mis-localise (Johnson et al., 2014) and recent studies indicate that care must be taken in interpreting functional outcomes using tagged Tpm3s (Brooker et al., 2016). Nevertheless, expression of transfected N-terminally tagged Tpm3.1 shows biological activity in a cell motility assay in MEFs, but proving biological equivalence of tagged and untagged Tpm3.1 has not been established (Bach et al., 2009). In contrast, the C-terminus has a more variable amino acid sequence and a more flexible structure (Greenfield et al., 2003; Li et al., 2002), thus tagging the C-terminus of Tpm3.1 is expected to cause less perturbation to the normal activity of the protein, however in this study we observed localisation of both constructs to stress fibres in MEFs and to the apical membranes of acinar cells *in vivo* in rodents.

It is also possible that the replacement kinetics we observe primarily reflects the addition of tagged Tpm3.1 to the ends of actin filaments within filament bundles; however, the similar levels of accumulation of the tagged and endogenous Tpm3.1 make this unlikely (Figure 4.1 B, D). Thus, it appears that Tpm3.1 dimers located within a filament are able to break two head-to-tail overlap interactions with adjacent dimers in the polymer together with their interaction with actin in order to exchange with 'free' Tpm3.1. While each of these interactions is of low affinity (Tobacman, 2008; Wegner, 1979), it seems likely that a source of energy may be required to weaken these interactions and promote the exchange reaction.

The unexpected finding that Tpm s appear to exchange independently of actin filaments is shown by the constant dynamic exchange of Tpm3.1 in the presence of jasplakinolide that inhibits actin turnover (Figure 4.6). This provides interesting new mechanistic insights into how Tpm s specify actin filament function as well as regulating the activity of other AAPs. In eukaryotes a single pool of actin filaments performs multiple biological functions, unlike other organisms which have multiple distinct filament types for specific tasks. It has been proposed that the multiple biological functions achieved by this single filament network is directed and regulated by binding of the >40 Tpm isoforms, each conferring a different function to their respective bound filament within the network (Gunning et al., 2015a). Dynamic exchange of Tpm s on actin filaments provides a possible mechanism into how a single filament type can perform multiple functions in the cell, specified by various Tpm s. It is possible that a particular Tpm isoform is recruited onto filaments thus directing the filament to perform a particular function, then subsequently detaches following a molecular switch to allow binding of another Tpm isoform which specifies a different function to the same filament. On the other hand, recent studies have demonstrated that the formins specify the Tpm isoform bound to filaments (Johnson et al., 2014; Tojkander et al., 2011). Hence, formins could mediate the generation of isoform-specific actin-Tpm co-polymers for specific functions such as cell motility, cytokinesis and vesicle transport. A model has been proposed whereby newly generated filaments have a specific actin-Tpm pairing for a specific function, however as the filament matures, they could be allosterically regulated by post-translation modifications, ligand binding or switching of AAPs such as Tpm s by dynamic exchange (Manstein and Mulvihill, 2016a). Tpm s recruit and modulate the activity of specific myosin isoforms on filaments in an isoform dependent manner (Barua et al., 2012; Bryce et al., 2003; Hundt et al., 2016; Tojkander et al., 2011). Hence, dynamic exchange of Tpm s would be an efficient method to regulate acto-myosin contractility by recruiting and regulating specific myosin isoforms on filaments for diverse functions (Manstein and Mulvihill, 2016a). Further work could involve genetically manipulating the expression of formins and other actin nucleators in cells to assess the impact on the dynamic exchange of

different Tpm isoforms and their regulation of respective downstream myosin isoforms.

Tpm dynamic exchange could also influence the relationship of other AAPs to filaments. When in a co-polymer with actin filaments, Tpm could be blocking the binding sites for other proteins and when they exchange, they create gaps allowing other proteins to bind, thereby regulating the interaction of other proteins with actin. One such example is the mutually exclusive binding of  $\alpha$ -actinin and tropomyosin to filaments (Zeece et al., 1979), hence it is possible that  $\alpha$ -actinin binding to filaments could be regulated in such a manner by Tpm. Future work could therefore assess the impact that Tpm have on recruitment kinetics of AAPs by comparing their WT recruitment kinetics to kinetics obtained from Tpm KO models.

It is possible that the balance of dynamic exchange of Tpm isoforms on filaments varies during specific points in the lifetime of a filament or a particular biological process, for example during cytokinetic ring contraction in yeast or exocytosis and endocytosis. Recruitment levels of particular Tpm isoforms could vary during specific phases of a cellular process, which in turn regulates the activity of downstream AAPs at key points in the event. This is addressed in Chapter 5 of this thesis using the rodent salivary gland endocytosis model developed by Masedunskas et al. which allows kinetic investigation of different molecular players during *de novo* actin coat formation required for large granule exocytosis (Masedunskas et al., 2011a).

## **Chapter 5. Recruitment kinetics of AAPs during *de novo* assembly of actin scaffolds that drives regulated SG exocytosis in rodent salivary glands**

### **Introduction**

Previous chapters focused on the development of gene delivery techniques into mouse salivary glands, as well as the dynamics of Tpm on filaments comprising stress fibres in cultured MEFs and actin bundles *in vivo* in the acinar cells of rodent salivary glands. It is now possible to perform plasmid DNA transfections in rat and mouse salivary glands, allowing us to utilize genetically modified mouse models and plasmids encoding fluorescent-tagged proteins together with intravital subcellular imaging to assess SG exocytosis *in vivo*. The work presented in this chapter will demonstrate the application of these techniques and observations of Tpm dynamics to investigate cytoskeletal assembly kinetics in an effort to obtain mechanistic insights into the assembly of actin scaffolds in cells of live mammals.

The mediators of actin assembly and regulation are the AAPs, which are employed by cells to nucleate, modulate and impart specific functionality to actin filaments (Blanchoin et al., 2014; Gunning et al., 2015a; Pollard, 2016). Unbranched filament nucleators such as the formins nucleate and elongate linear filament networks, while the Arp2/3 family of complexes nucleates the branched filament network (Campellone and Welch, 2010; Pizarro-Cerda et al., 2017; Pollard, 2016). AAPs such as myosins bind filaments to facilitate filament contraction, crosslinkers such as  $\alpha$ -actinin mediate filament bundling and organisation (Blanchoin et al., 2014; Pollard, 2016) and filament regulatory proteins such as the Tpm stabilise, confer specific functions to filaments as well as regulate the binding of other AAPs to filaments (Gunning et al., 2008; Gunning et al., 2015a; Gunning et al., 2015b). Previous studies indicate that the linear and branched filament networks consist of multiple functionally distinct filament populations that interdependently operate in cells, nucleated by distinct linear and branched nucleators (Bovellan et al., 2014; Fritzsche et al., 2016; Fritzsche et al., 2013; Miklavc et al., 2012; Ponti et al., 2004; Ramalingam et al., 2015; Tran et al., 2015).

These filament populations in turn recruit AAPs such as Tpms to regulate their functions as well as the binding and activity of other AAPs such as myosins and  $\alpha$ -actinin (Bryce et al., 2003; Gunning et al., 2015a; Miklavc et al., 2015; Tojkander et al., 2011).

What are the functions and recruitment kinetics of the actin nucleators, Tpms and other AAPs during actin filament assembly? How do the branched and linear actin filament populations coordinate to perform cellular functions? A powerful method to answer these questions is to investigate the recruitment kinetics of AAPs and *de novo* actin assembly in living cells. The rodent secretory SG exocytosis model provides a robust, flexible and reproducible system to assess these dynamics in mammals (Masedunskas et al., 2013a; Masedunskas et al., 2012b; Masedunskas et al., 2011a). This is possible by using live subcellular intravital imaging techniques to visualise *de novo* assembly of actin scaffolds that drive SG exocytosis in the secretory acini of rodent salivary glands. In addition, widely available reporter mouse models in combination with *in vivo* gene delivery techniques (Chapter 4) (Masedunskas et al., 2012a; Sramkova et al., 2014) can be utilised. Observing *de novo* recruitment and assembly kinetics would provide functional insight into the molecular players involved, as well as mechanistic insight into the interdependence and collaboration between the branched and linear actin populations.

Hence, in this this chapter we employ the aforementioned approaches to investigate recruitment kinetics of Tpms, myosins, actin crosslinkers and the linear and branched actin nucleators during actin assembly *in vivo* in rodent salivary glands. The findings in this chapter suggest a mechanism of filament co-polymerisation with Tpms on distinct actin populations, as well as the stepwise recruitment kinetics of linear and branched nucleators, Tpms, myosins and actin crosslinkers during the *de novo* assembly of the actin scaffold. The work culminates by describing a novel, uncharacterised mechanism of regulated SG exocytosis in mammals by distinct actin populations.

## Results

### **Actin polymerisation at the scaffold interior drives membrane compression and cargo delivery into canaliculi prior to scaffold constriction and disassembly**

A major advantage of using the *in vivo* SG exocytosis system to assess actin dynamics is that the activity of various molecular players involved in actin scaffold assembly can be assessed with the use of fluorescently tagged constructs. Transgenic and knock-in mouse models can be exploited for this purpose, in addition to the ability to transfect the acinar cells of rodent salivary glands (Chapter 3, (Sramkova et al., 2014)). However, in order to coherently investigate the recruitment kinetics of these molecular players, it was important to employ a reliable standard that would allow us to make relevant and accurate comparisons between experiments and recruitment profiles generated. As an actin scaffold forms around fused SGs and is required to complete exocytosis (Masedunskas et al., 2011a), we elected to use actin recruitment, marked by Lifeact-RFP/GFP, as the global standard with which to compare all other recruitment curves from tagged proteins in different mouse models and transfections. The first experiment was therefore to determine the timing of SG fusion to the APM and subsequent membrane remodelling events versus actin filament assembly.

To this end, mice co-expressing Lifeact-GFP and MARCS-tdTomato (Membrane-tdTomato, denoted as mTomato), a membrane marker tagged with tdTomato fluorescent protein were cannulated, infused with Alexa 647 dextran and imaged using intravital microscopy with isoproterenol stimulation to induce SG exocytosis, as described in Materials and Methods. Lifeact-GFP fluorescence indicates the presence of filamentous actin while dextran and mTomato fluorescence indicate the precise time of SG fusion to the APM, as both dextran and membrane markers would transfer to the lumen or the membrane of fused SG, respectively, immediately after fusion (Masedunskas et al., 2011a).

The time-lapse images reveal that Lifeact-GFP (which marks the actin scaffold) appears on SGs after mTomato and dextran appearance on and inside the SG, respectively (Figure 5.1 A, panel 5-7 s). Remarkably, upon closer inspection of the time-lapse images (Figure 5.1 A), the majority of SG cargo (as labelled by dextran) appears to be delivered into the canaliculus and APM, respectively, at approximately 30 s after fusion, long before the actin scaffold structure is disassembled (5.1 A, panel 30 s). This is coupled with a reduction in SG diameter from 10-30 s (Figure 5.1 A, mTomato panel). After SG cargo delivery, a small sliver of membrane lingers on and is gradually integrated into the APM while the scaffold structure is gradually constricted and disassembled (Figure 5.1, panel 30-65 s). The observations demonstrate that membrane diameter and cargo dynamics are closely coupled, however both are uncoupled from actin scaffold dynamics during the later phase of exocytosis. This was unexpected since it indicates that large granule exocytosis occurs in two distinct phases, which has not been described previously in classical models (Porat-Shliom et al., 2013). We refer to the SG cargo delivery/membrane diameter reduction step as the membrane compression phase, which occurs at approximately 5-30 s and the subsequent step as the scaffold constriction and disassembly phase, where the remaining membrane sliver is gradually integrated into the APM with simultaneous gradual constriction and disassembly of the actin scaffold (approximately 30-65 s). The driver of the membrane compression phase appears to be actin itself, via a polymerisation mechanism at the scaffold interior, as shown by the increase in thickness of Lifeact-GFP from 5-30 s progressing inwards from the scaffold structure.

This is also clearly illustrated in the kymographs showing separate Lifeact-GFP, mTomato and dextran channels (Figure 5.1 B). SG cargo is delivered and most of the SG membrane is compressed into the APM in the first 30 s of exocytosis, with peak actin enrichment occurring just after, as shown by complete enrichment of the actin scaffold with Lifeact-GFP (Figure 5.1 A, panels 30-40 s, B overlay and actin kymographs). From approximately 30-65 s, the actin scaffold, now enriched with actin, gradually decreases in size to complete exocytosis while simultaneously dispersing actin, as shown in the time-lapse images (Figure 5.1 A) and reduction in Lifeact-GFP fluorescence (Figure 5.1 C).

Fluorescence profiles were also acquired by drawing a region of interest around individual SGs undergoing exocytosis, normalised with respect to their minimum and maximum values and averaged across multiple events. The fluorescence recruitment data shows that Lifeact-GFP appears on SGs 1-2 s post mTomato and dextran appearance on and inside the SG, respectively (Figure 5.1 C, inset). Dextran peak fluorescence occurs rapidly at approximately 10 s before peak membrane mTomato and approximately 20 s before peak Lifeact-GFP fluorescence (Figure 5.1 C). This is expected, as upon SG fusion to the APM, SG cargo and fluid from the canaliculi mix via the open fusion pore and dextran enters the fused SG at a rapid rate, as shown in Figure 5.1 A (top panel). Corresponding with visual assessment of the time-lapse images, dextran fluorescence intensity is rapidly reduced from 10-30 s, while in contrast Lifeact-GFP fluorescence is rapidly increased to its peak at approximately 18 s, followed by gradual reduction in intensity as the scaffold decreases in size to complete the exocytosis event (Figure 5.1 C).

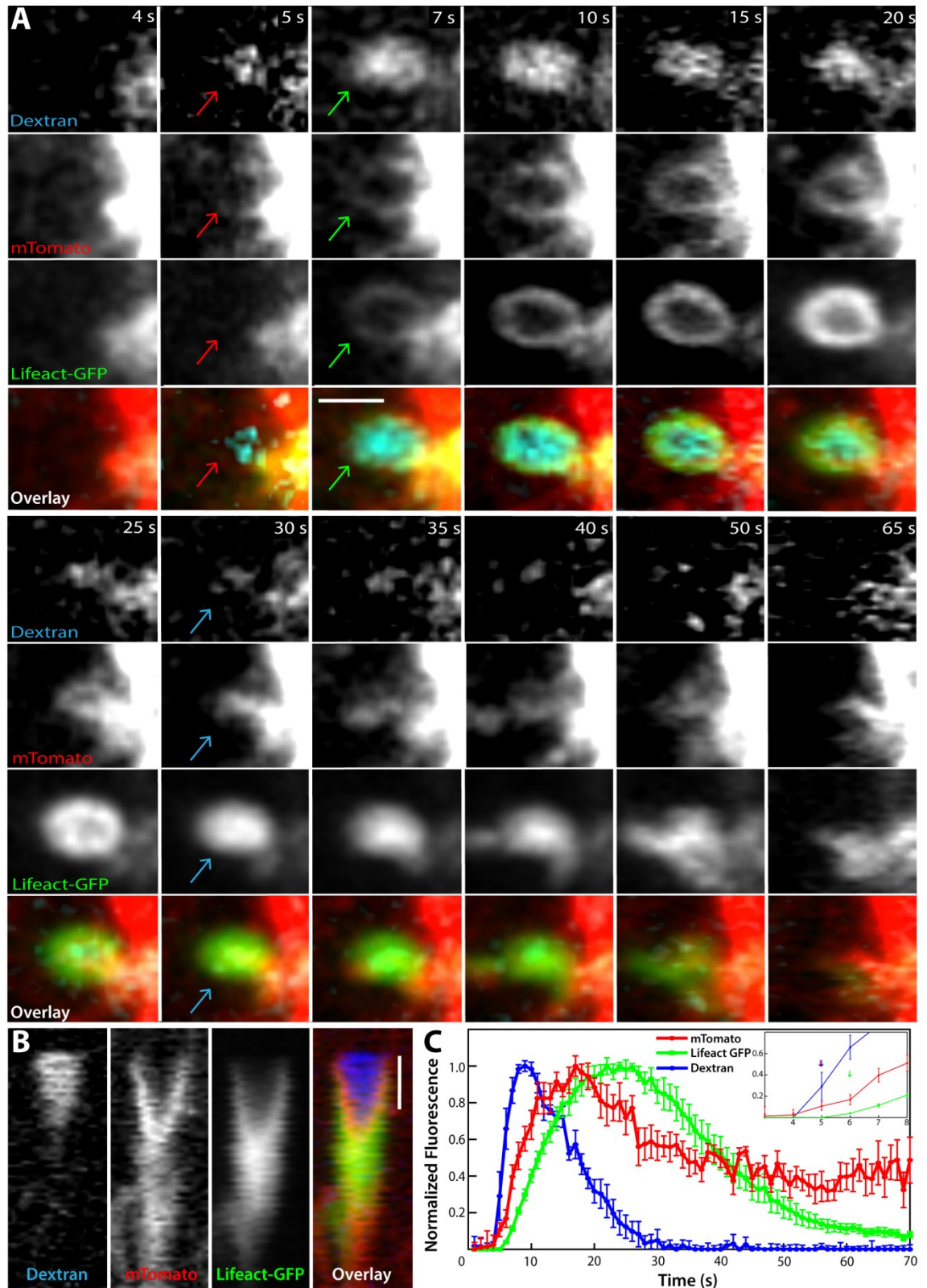


**Figure 5.1** SG membrane is integrated into the APM by an actin population at the interior of the actin scaffold. The Wharton's duct of a mouse co-expressing Lifeact-GFP and mTomato was cannulated and infused with DMSO/Alexa 647 Dextran during

intravital imaging and SG exocytosis was stimulated with subcutaneous injection of isoproterenol as described in Materials and Methods. (A) Time-lapse imaging of a SG undergoing fusion and exocytosis. Upon fusion, the SG and apical membranes become continuous and Dextran enters the fused granule through an open fusion pore thus labelling the cargo space (→). Approximately 1 s later filament polymerisation starts to form the actin scaffold around the granule membrane (→). Actin polymerisation directed towards the SG membrane drives the fused SG and cargo/Dextran into the canaliculi as shown by Lifeact-GFP enriching the scaffold interior with simultaneous reduction in SG diameter (panels 10-30 s, →). After cargo/dextran delivery, a small sliver of membrane remains and is gradually integrated into the APM while the actin scaffold is gradually constricted and disassembled (panels 30-65 s). Numbers denote time in s. Scale bar = 2 μm. (B) Kymographs showing the exocytosis event in separate channels. Scale bar = 20 s. (C) Normalised mean fluorescence intensity of Lifeact-GFP, mTomato and cargo/Alexa 647 Dextran. Dextran fluorescence peaks starts to decline in intensity (at approximately 10 s) as Lifeact-GFP fluorescence reaches peak recruitment (at approximately 28 s). Dextran fluorescence reaches baseline at approximately 30 s after peak recruitment of actin which coincides with interior filling of the scaffold with actin to drive membrane integration. We refer to this phase as the membrane compression phase which corresponds approximately to 10-30 s in the sequence as shown in A. Inset: Zoom of the first 8 s of exocytosis showing SG fusion/Dextran filling (4 s) occurs 1-2 s before the appearance of actin (6 s). n = 5 events from 1 animal, error bars are S.E.M.

These data allow us to propose a novel mechanism driving regulated exocytosis *in vivo*, which separates regulated SG exocytosis into two distinct phases and places actin polymerisation itself as a driving force for membrane compression/cargo delivery. The membrane compression phase occurs in the first 5-30 s after actin scaffold formation, followed by the scaffold constriction and disassembly phase which occurs from 30-65 s. The data indicates that the actin scaffold assembled around fused SGs functions as a support structure which facilitates actin polymerisation-driven membrane compression within the scaffold. How is the scaffold assembled and what drives actin polymerisation at the inner part of the scaffold? Furthermore, when are molecular players such as Tpm, myosins, actin crosslinkers and nucleators recruited and what functions do they carry out? We next sought to answer these questions, starting with investigating Tpm recruitment kinetics during actin scaffold assembly.

### **Tpms are enriched on a subset of actin filaments indicating multiple actin filament populations cooperate to build a functioning actin scaffold**

It is well established that Tpm confer specific functions to actin filaments in addition to regulating the binding and activity of downstream actin associated proteins such as myosins (Bryce et al., 2003; Hundt et al., 2016). In cells, Tpm form a co-polymer with actin filaments and localise to the major grooves on the side of the actin filament (von der Ecken et al., 2015). However, what is not understood is the mechanism of co-polymer formation. Are actin filaments first nucleated and Tpm subsequently recruited or do they simultaneously assemble by co-polymerisation? Studies have shown that two major Tpm isoforms in cells, Tpm 3.1 and 4.2, similarly localise to stress fibres in cell culture (Schevzov et al., 2011; Tojkander et al., 2011). To date however, there has been no data on the temporal recruitment of these Tpm to filaments, and whether different Tpm isoforms form hetero or homo-polymers on filaments. This is an important issue to address since Tpm confer different functions to actin filaments (Gunning et al., 2015b) therefore information regarding their temporal and spatial properties during filament assembly would provide valuable

insights on how Tpm3s regulate actin filaments, as well recruitment and activity of other AAPs.

The *in vivo* rodent SG exocytosis model is an ideal system to address these questions as individual Tpm recruitment kinetics to filaments can be measured during *de novo* actin scaffold formation. Here we investigate the recruitment kinetics of Tpm3.1 relative to Tpm4.2, as well as Tpm3.1 relative to actin. In addition to Tpm recruitment kinetics onto filaments, we examined where the Tpm3s localise on the SG and whether they are involved in the membrane compression phase or during the subsequent scaffold constriction and disassembly phase. This would provide mechanistic insights into how Tpm3s modulate actin during the phases of SG exocytosis.

To investigate the recruitment kinetics of Tpm3.1 vs actin, Wistar rats were co-transfected with Lifeact-RFP and Tpm3.1-NG, injected with 0.025 mg/kg isoproterenol to stimulate SG exocytosis and imaged using intravital microscopy as in Materials and Methods. The data show that Tpm3.1-NG and Lifeact-RFP appear simultaneously on fused SGs (Figure 5.2 A, panel 7 s; C, inset) demonstrating that Tpm3.1 is enriched on the initial actin filaments and suggesting a mechanism of co-assembly and polymerisation of the Tpm-actin co-polymer. Interestingly, the peak of Lifeact-RFP recruitment occurs approximately 10 s prior to the peak of Tpm3.1-NG (Figure 5.2 C). Inspection of the time-lapse images shows that Tpm3.1-NG is indeed highly enriched at the later phase of exocytosis, as indicated by the increase in average density of Tpm3.1-NG and declining Lifeact-RFP fluorescence on SGs at approximately 50 s (Figure 5.2 A, panel 50 s). Inspection of the kymographs shows that Tpm3.1-NG is primarily enriched on the outer edges of the scaffold and not at the interior, while Lifeact-RFP completely fills the interior of the scaffold at 20-25s (Figure 5.2 B). The similar initial recruitment but dissimilar peak fluorescence of Lifeact-RFP and Tpm3.1-NG indicates that multiple actin filament populations exist and are possibly nucleated simultaneously upon SG fusion to the APM, however only a subset of filaments are decorated with Tpm3.1. Tpm3.1 enriched filaments appear to be primarily involved in building the actin scaffold around the fused SG whilst a distinct, Tpm3.1 free filament population exists and functions to drive membrane compression within the scaffold. In addition, peak Tpm3.1 enrichment occurs approximately when the scaffold

constriction and disassembly phase begins, possibly indicating that Tpm5 are enhancing the process.

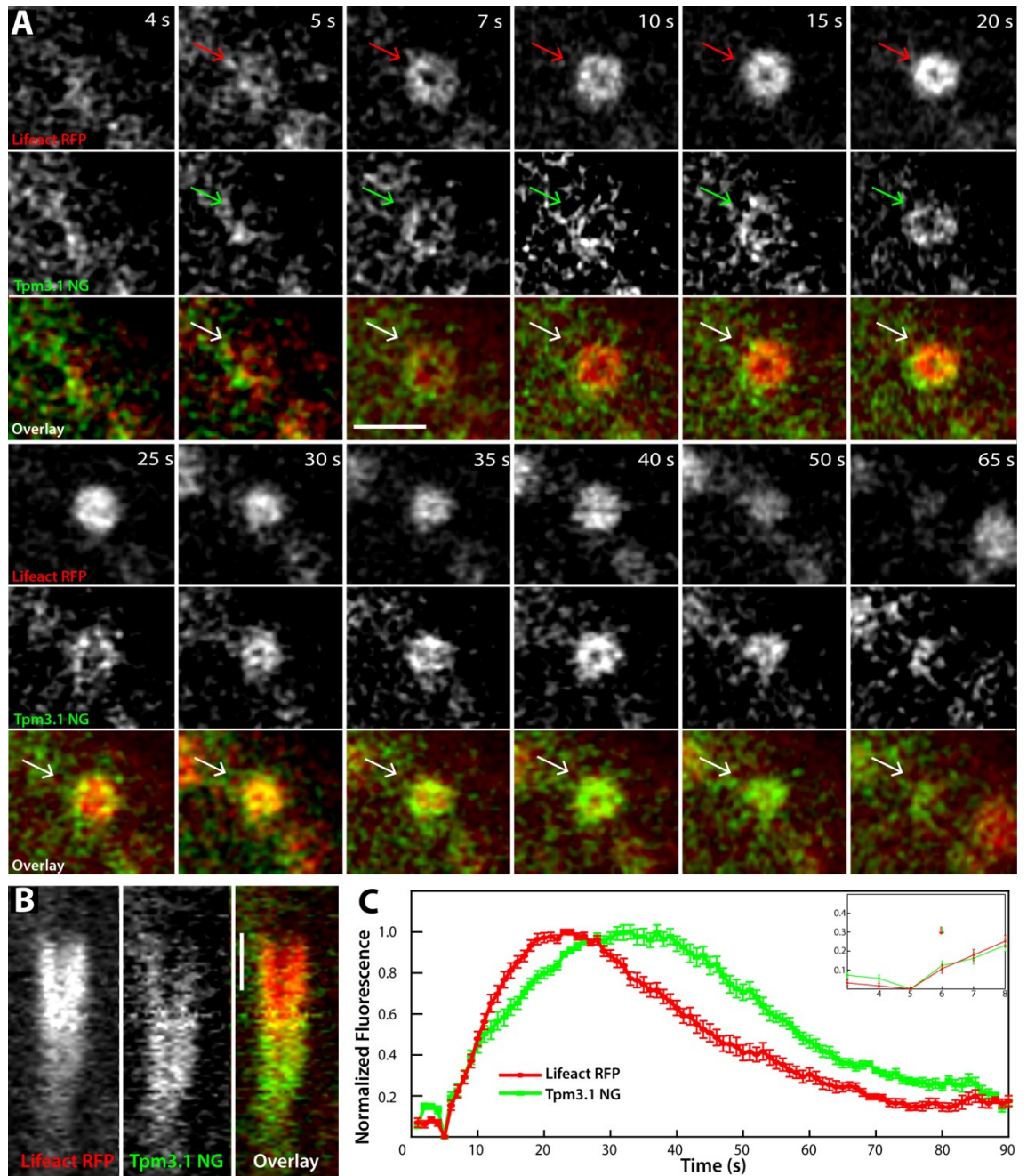


**Figure 5.2 Tpm3.1 is co-recruited with actin and is enriched on a subset of actin filaments.** Wistar rats were co-transfected with Lifact-RFP and Tpm3.1-NG, SG exocytosis was stimulated with subcutaneous injection of isoproterenol and intravital microscopy was performed as described in Materials and Methods. (A) Time-lapse imaging of a SG fusion and exocytosis event. Tpm3.1-NG is recruited simultaneously with Lifact-RFP (panel 7 s). Lifact-RFP enrichment occurs rapidly at the earlier phase of the event (panels 7-25 s) while Tpm3.1-NG is highly enriched at the later phase (panels 30-45 s). Numbers denote time in s. Scale bar = 2  $\mu$ m. (B) Kymographs showing

the exocytosis event in separate channels. During the membrane compression phase Lifeact-RFP is enriched within the interior of the scaffold however Tpm3.1 only appears to localise the outer edges of the structure. Scale bar = 20 s. (C) Normalised mean fluorescence intensity of Lifeact-RFP and Tpm3.1-NG. Tpm3.1-NG and Lifeact-RFP are recruited simultaneously at 6 s and similar recruitment rates continue until approximately 10 s where Tpm3.1-NG recruitment is now slower than Lifeact-RFP. This coincides with increased actin polymerisation directed towards the scaffold interior which appears to be devoid of Tpm3.1. Peak Tpm3.1-NG recruitment occurs at approximately 32 s, 10 s after the peak of Lifeact-RFP at approximately 22 s. Fluorescence signal from Lifeact-RFP declines after 30 s while Tpm3.1-NG signal declines after 40 s as scaffold constriction progresses and filaments are disassembled. The simultaneous initial recruitment rates and subsequent delayed Tpm3.1-NG peak fluorescence indicates that multiple actin populations are present on the actin scaffold and that Tpm3.1 is recruited/co-polymerises on a subset of filaments. Inset: Zoom of the first 8 s of scaffold formation showing recruitment of Lifeact-RFP and Tpm3.1 at 6 s. n = 18 events from 5 animals, error bars are S.E.M.

Our next objective was to compare the recruitment kinetics of Tpm3.1 relative to Tpm4.2 to determine if Tpm4.2 exhibits similar behaviour. To this end, rat salivary glands were transfected with Tpm3.1-NG and Tpm4.2-Ruby2 constructs and imaged using intravital microscopy after isoproterenol stimulation as in Materials and Methods. The fluorescence data indicate that both Tpm3.1 and Tpm4.2 appear on fused SGs at the same time point and have similar fluorescence profiles throughout exocytosis (Figure 5.3 A panel 7 s, C). This suggests that Tpm4.2 is also being recruited to a subset of filaments however it is unclear at this point whether both Tpm3.1 and Tpm4.2 are being recruited to the same filaments, or that a separate population of Tpm4.2 enriched filaments exist that is nucleated at similar time points. Inspection of the kymographs indicates that Tpm4.2, similar to Tpm3.1, is primarily enriched on the outer edges of the scaffold, as shown by the lack of Tpm4.2 enrichment at the scaffold interior (Figure 5.3 B). This indicates that Tpm3.1 and Tpm4.2 might be conferring similar functions to the actin population involved in forming and maintaining the actin scaffold, which supports membrane compression at the scaffold interior.

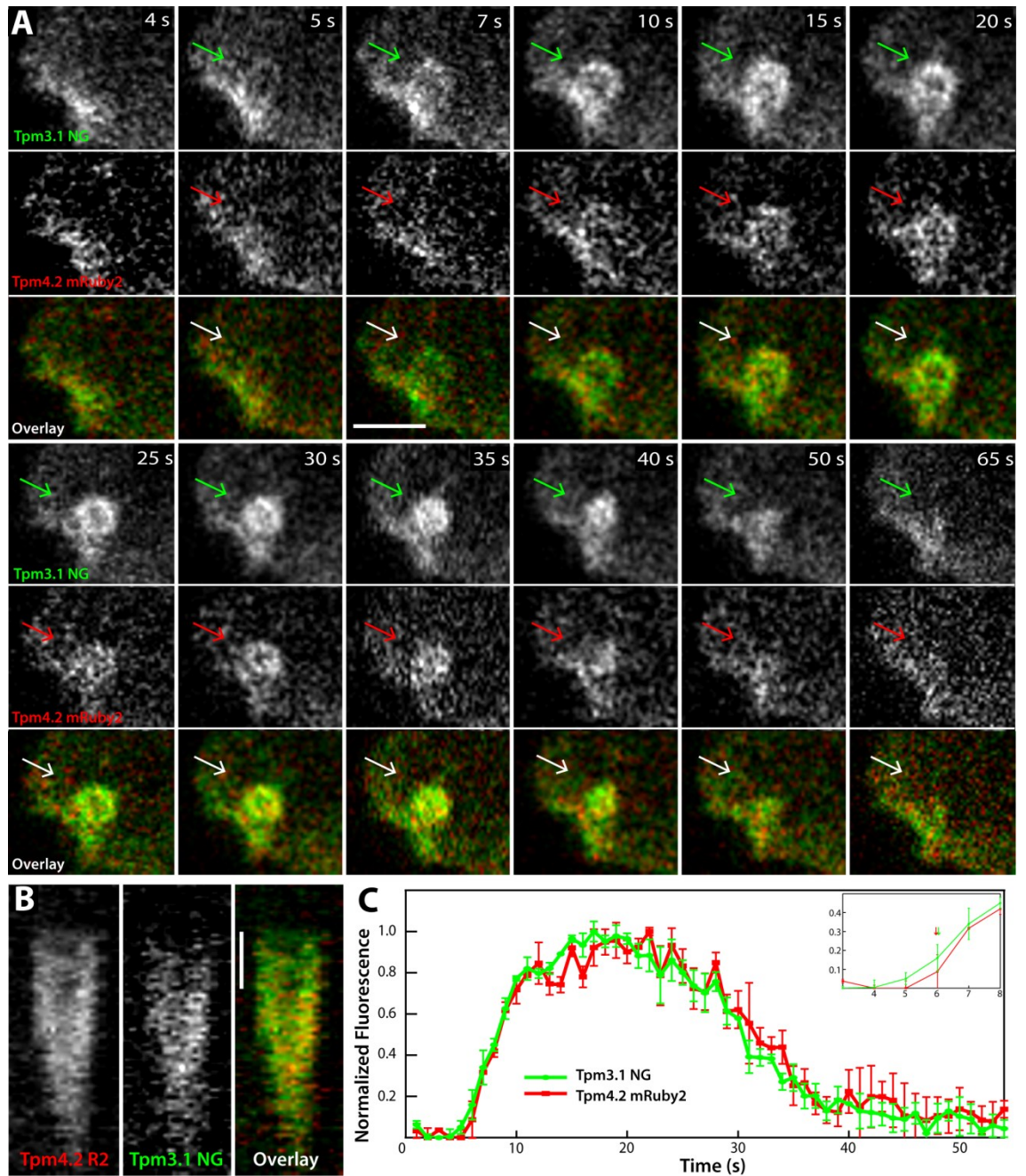


**Figure 5.3 Tpm3.1 and Tpm4.2 are simultaneously recruited onto the actin scaffold.** Wistar rats were co-transfected with Tpm4.2-mRuby2 and Tpm3.1-NG, stimulated with subcutaneous injection of isoproterenol and intravital microscopy was performed as described in Materials and Methods. (A) Time-lapse imaging of a SG fusion and exocytosis event. Both Tpm3.1 and Tpm4.2 are simultaneously recruited to the actin scaffold (panel 7 s) and have similar enrichment patterns throughout the exocytosis event. Numbers denote time in s. (B) Kymographs showing the exocytosis event in separate channels. No enrichment of either Tpm was detected at the scaffold interior.

Scale bar = 20 s. (C) Normalised mean fluorescence intensity of Tpm4.2-mRuby2 and Tpm3.1-NG. Inset: Zoom of the first 8 s of exocytosis showing simultaneous recruitment of Tpm4.2-mRuby2 and Tpm3.1-NG at 6 s. Both Tpm's are recruited simultaneously at 6 s and have similar fluorescence profiles throughout the event, indicating that they are either co-recruited to the same filaments or that they are recruited to separate filaments with identical assembly/disassembly kinetics. n = 5 events from 2 animals, error bars are S.E.M.

The results from Tpm3.1/4.2 recruitment indicate that at least two actin populations exist and work in concert to drive SG exocytosis *in vivo* and that a mechanism of co-assembly likely drives the formation of the Tpm-actin co-polymer (Figures 5.2, 5.3). In addition, the Tpm3.1/4.2 enriched filament population is primarily involved with the outer edges of the scaffold structure while a distinct population acts at the scaffold interior driving membrane compression. What is the mechanism underlying scaffold constriction and disassembly as well as membrane compression within the scaffold and what provides the forces necessary to complete these processes? It is likely that AAPs such as myosins and actin crosslinkers are involved and recruited during scaffold assembly to facilitate exocytosis. Our next objective therefore was to determine the recruitment kinetics of these proteins to the assembling actin scaffold.

### **Myosin IIA is involved in the scaffold constriction and disassembly phase of exocytosis**

Having made observations that indicate multiple actin populations drive two distinct phases during SG exocytosis, we then elected to investigate molecular players that are providing the force necessary to drive these processes. Myosins have been established to be among the major 'workhorses' in cells driving actin filament contraction as well as providing crosslinking support (Blanchoin et al., 2014). In light of our discovery which appears to uncouple the membrane compression/cargo delivery phase from the scaffold constriction and disassembly phase (Figure 5.1), we sought to determine whether myosin IIA is involved in these phases by investigating the kinetics of SG fusion (as marked by dextran filling of the SG) versus myosin IIA recruitment as well as its enrichment pattern during exocytosis.

To this end, mice expressing myosin IIA-GFP were cannulated, infused with Texas Red dextran and stimulated with isoproterenol during intravital imaging to acquire fusion events as in Materials and Methods. Upon fusion of the SG to the APM, the dextran (cargo) in the canaliculi immediately fills the SG and reaches peak fluorescence in 1-2 s (Figure 5.4 A, panels 5-7; C, inset), while myosin IIA recruitment begins at approximately 7 s, 3 s after fusion at approximately 4 s (Figure 5.4 C, inset).

Intriguingly, the majority of dextran/cargo is expunged from the SG into the APM/canaliculi within the first approximately 20 s, 10 s prior to peak myosin IIA-GFP enrichment at approximately 30 s (Figure 5.4 A, C). This indicates that myosin IIA is likely not involved in the membrane compression phase, which is especially evident upon inspection of the kymograph where myosin IIA-GFP is only sparsely recruited by the time dextran is completely delivered from the SG (Figure 5.4 B). One may argue that upon fusion of the SG to the APM, the dextran that fills the SG is drawn out by fluid flow in the canaliculi. However, upon close inspection of the time-lapse images it is clear that dextran is still present in the canaliculi at 35 s (Figure 5.4 A, arrowheads); whereas, dextran in the SG has already been expunged at 20 s (Figure 5.4 A, panels 20 s). This confirms that fluid flow in the canaliculi is not responsible for depleting the dextran present in the fused SG, rather the delivery mechanism exists within the actin scaffold itself. Myosin IIA-GFP does not appear to enrich the scaffold interior at the SG membrane interface during exocytosis (Figure 5.4 A, B), unlike Lifeact-GFP (Figure 5.1 A, B); however, it is highly enriched on the outer edges of the scaffold structure (Figure 5.4 A, B) similar to enrichment of Tpms3.1/4.2 (Figures 5.2, 5.3). This observation, coupled with the recruitment data showing peak enrichment of myosin IIA-GFP occurring when dextran/SG cargo has already been delivered, indicates myosin IIA (and perhaps myosins in general), is likely not involved in the membrane compression phase but functions to support constriction and disassembly of the scaffold after the membrane compression phase. In addition, myosin IIA-GFP enrichment occurs at approximately 7 s, 1-2 s after recruitment of Tpms and actin (Figures 5.2, 5.3) in line with previous studies demonstrating that Tpms regulate the recruitment and activity of myosins (Bryce 2003, Barua 2012, Hundt-Manstein 2016).

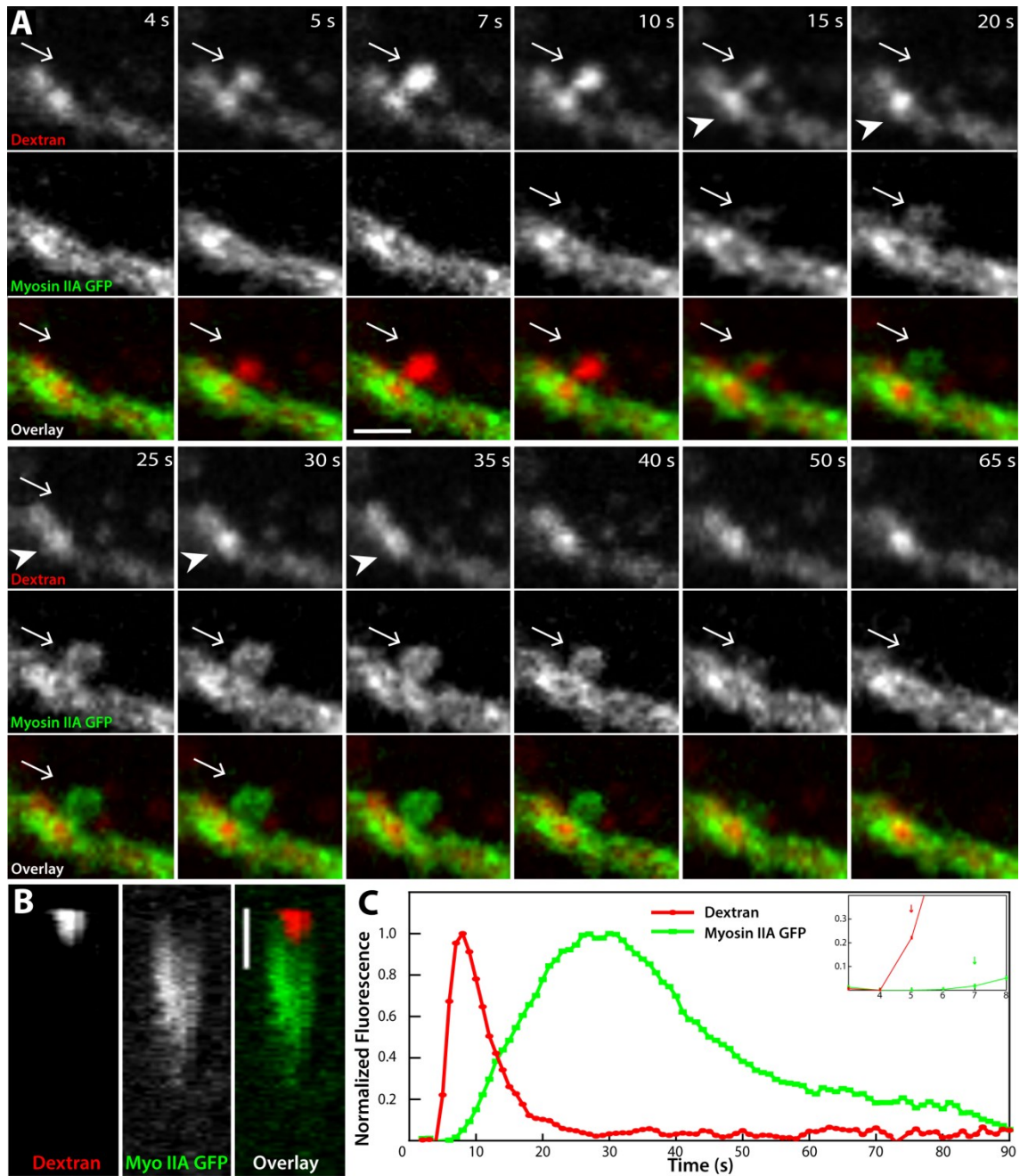


**Figure 5.4 Myosin IIA is enriched at the later phase of SG exocytosis.** A mouse expressing myosin IIA-GFP was cannulated, perfused with Texas Red dextran, stimulated with subcutaneous injection of isoproterenol and intravital microscopy was performed as described in Materials and Methods. (A) Time-lapse imaging of a SG fusion and exocytosis event. The time of fusion is identified by the dextran entering the fused SG and marking the cargo volume (panel 5 s). The majority of dextran labelled cargo is delivered into the canaliculi by approximately 20 s post-fusion, prior to full myosin IIA-GFP recruitment (panel 20). Dextran is present in the canaliculi

(arrowhead, panels 20-35 s) after the membrane compression phase indicating active delivery mechanism. Myosin IIA-GFP commences recruitment onto the fused SG approximately 3 s post-fusion/Dextran filling (panel 10 s) and reaches peak enrichment at approximately 30 s (panel 30 s), indicating that it is primarily involved at the later phase of exocytosis. From time 30-60 s the actin scaffold gradually completes constriction and disassembly in the presence of myosin IIA-GFP. Numbers denote time in s. Scale bar = 2  $\mu$ m. (B) Kymographs showing the exocytosis event in separate channels. Myosin IIA-GFP is enriched at the outer edges of the scaffold and absent from the interior. Scale bar = 20 s. (C) Normalised mean fluorescence intensity of myosin IIA-GFP and Texas Red Dextran. Inset: Zoom of the first 8 s of exocytosis showing SG fusion/Dextran filling (at 4 s) occurs approximately 3 s before the appearance of myosin IIA-GFP (7 s). This time sequence suggests that myosin is recruited 1-2 s after actin polymerisation commences. n = 18 events from 1 animal, error bars are S.E.M, but not visible through the data markers.

This posed yet more intriguing questions about the mechanism of actin-driven regulated exocytosis. We have shown that two distinct phases occur, which uncouples membrane compression/cargo delivery from actin scaffold constriction and disassembly. Myosin IIA (and perhaps myosins in general) appears to only enrich the outer edges of the scaffold along with Tpm3.1/4.2 and likely functions to facilitate scaffold constriction after the membrane compression phase. What therefore provides the force necessary to drive membrane compression within the actin scaffold?

### **Alpha-actinin 4 is recruited onto filaments both on the outer and inner parts of the actin scaffold**

It has been shown that actin polarisation and crosslinking that is independent of myosin motor activity is sufficient to generate contractile forces (Miklavc et al., 2015; Pinto et al., 2013; Sun et al., 2010). In addition, a recent study demonstrated that  $\alpha$ -actinin 4 (hereafter referred to as  $\alpha$ -actinin) is recruited to the actin scaffold together with the initial actin filaments during lamellar body exocytosis and that filament crosslinking is essential for scaffold constriction (Miklavc et al., 2015). We reasoned therefore that actin crosslinkers would be involved during SG exocytosis and hence elected to investigate the recruitment kinetics and localisation of  $\alpha$ -actinin during actin scaffold assembly *in vivo*.

To this end, Wistar rats were co-transfected with Lifeact-RFP and  $\alpha$ -actinin-NG, injected with 0.025 mg/kg isoproterenol to stimulate SG exocytosis and imaged using intravital microscopy as in Materials and Methods. The results show that  $\alpha$ -actinin-NG is recruited to the actin scaffold simultaneously with Lifeact-RFP (Figure 5.5 A, panel 7 s) indicating that  $\alpha$ -actinin is enriched on the filament population comprising the scaffold. The fluorescence profiles of both  $\alpha$ -actinin and Lifeact-RFP appear to be generally similar and peak at approximately 31 s. Interestingly,  $\alpha$ -actinin enrichment approaching the peak lags slightly behind Lifeact-RFP (Figure 5.5 C); however, it appears to be highly enriched on SGs from 25-65 s (Figure 5.5 A). This indicates that  $\alpha$ -actinin is associated with the bulk of actin filaments and is required in larger abundance during the scaffold constriction and disassembly phase. Remarkably,  $\alpha$ -

actinin appears to associate with the actin population driving membrane compression, as shown by  $\alpha$ -actinin-NG being co-enriched with Lifeact-RFP within the scaffold in the kymographs (Figure 5.5 B). This is antagonistic to myosin IIA enrichment which primarily occurs on filaments comprising the outer edges of the scaffold during the scaffold constriction phase (Figure 5.4 A, B). In summary, the data indicates that bundling and crosslinking action by  $\alpha$ -actinin might indeed contribute to a motor-independent force generation mechanism that acts on the actin populations both at the scaffold interior and at its outer edges, previously suggested by other groups (Miklavc et al., 2015; Pinto et al., 2013; Sun et al., 2010).

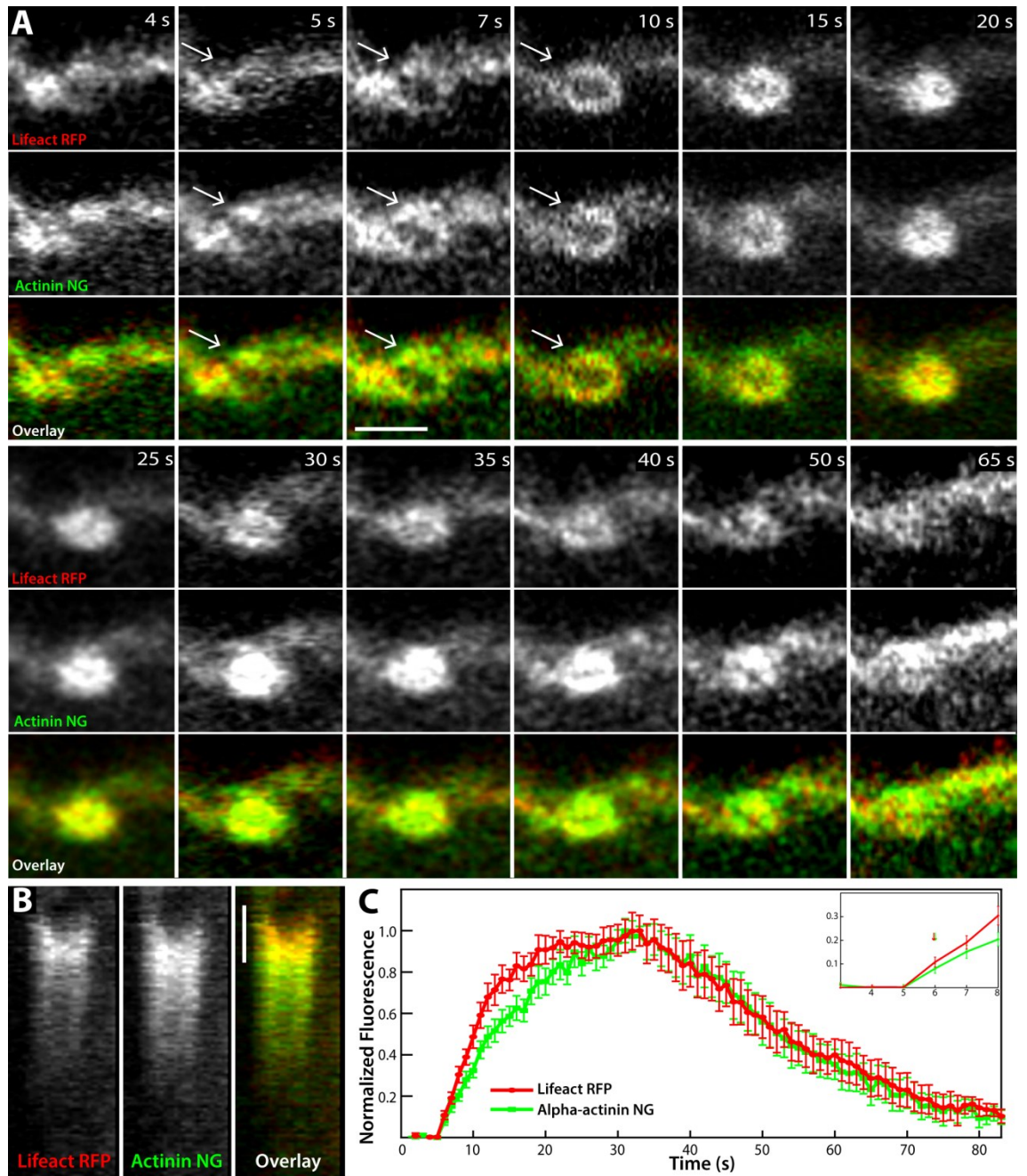


**Figure 5.5  $\alpha$ -Actinin is enriched on filaments both on the actin scaffold and at the scaffold interior driving membrane compression.** Wistar rats were co-transfected with Lifact-RFP and  $\alpha$ -actinin-NG, stimulated with subcutaneous injection of isoproterenol and intravital microscopy was performed as described in Materials and Methods. (A) Time-lapse imaging of a SG fusion and exocytosis event in separate channels.  $\alpha$ -Actinin-NG is recruited with the initial actin filaments that make up the scaffold (panel 7 s) and appears to enrich filaments on both the outer and inner parts of the actin scaffold throughout exocytosis. Numbers denote time in s. Scale bar = 2  $\mu$ m. (B)

Kymographs showing the exocytosis event in separate channels.  $\alpha$ -Actinin-NG is recruited to filaments on the scaffold as well as at the scaffold interior driving membrane compression, with interior enrichment slightly delayed behind Lifeact-RFP at the SG membrane interface. Scale bar = 20 s. (C) Normalised mean fluorescence intensity of Lifeact-RFP and  $\alpha$ -actinin-NG. Inset: Zoom of the first 8 s of exocytosis.  $\alpha$ -Actinin-NG and Lifeact-RFP are simultaneously recruited at approximately 6 s.  $\alpha$ -Actinin-NG enrichment lags slightly behind Lifeact-RFP, however peak recruitment for both constructs occurs at approximately 31 s, indicating that  $\alpha$ -actinin is associated with the bulk of filaments throughout exocytosis. n = 13 events from 4 animals, error bars are S.E.M.

The data so far indicates that multiple functionally distinct actin filament populations operate in tandem to drive exocytosis *in vivo*. Tpm3.1,4.2 and myosin IIA are recruited to a subset of these localised on the outer edges, while  $\alpha$ -actinin appears to enrich multiple populations. Therefore, the next question we sought to address was the mechanism of nucleation of these actin populations. Which actin nucleators are involved? Are there linear and branched filaments present and if so, when are they nucleated and how are they organised? These were questions driving our next line of inquiry, which was to determine the recruitment kinetics of the filament nucleators involved in actin scaffold formation during SG exocytosis.

### **Formins nucleate the initial actin filaments during scaffold formation and have dissimilar recruitment kinetics**

It is well established that in eukaryotic cells the diaphanous formins and the Arp2/3 complex nucleate linear and branched filaments respectively in various cell systems (Campellone and Welch, 2010; Pollard, 2016). Miklavc and colleagues have recently demonstrated that formin inhibition, not Arp2/3, prevents actin scaffold formation around fused lamellar bodies in a cell culture based system (Miklavc et al., 2015). That study has been elegantly corroborated by recent work from Tran et al., demonstrating that Arp2/3 appears after F-actin on fused SGs to drive exocytosis, leading them to hypothesise that Arp2/3 nucleates the branched network using pre-existing linear filaments as templates (Tran et al., 2015). Additionally, formins and the Arp2/3 complex have been shown to cooperate when assembling actin structures such as filopodia and lamellipodia, in a process known as convergent evolution (Siton-Mendelson and Bernheim-Groswasser, 2017).

To date however, there is no data on the *de novo* recruitment kinetics of these nucleators working in concert during actin assembly in a living, intact mammal. The *in vivo* rodent SG exocytosis model allows this to be investigated and could provide insights into the mechanism of assembly of the linear and branched actin networks, as well as their respective functions during the phases of exocytosis. To this end, we

elected to investigate the recruitment kinetics of diaphanous formins mDia1, mDia2 and the Arp2/3 complex versus actin using our rat transfection model.

To investigate the recruitment of formin mDia2 during actin scaffold formation, Wistar rats were co-transfected with Lifeact-RFP and mDia2-Emerald, injected with 0.025 mg/kg isoproterenol to stimulate SG exocytosis and imaged using intravital microscopy as in Materials and Methods. As expected, mDia2-Emerald is recruited to fused SGs approximately 2 s prior to the appearance of actin, as shown by the appearance of mDia2-Emerald on the SG before Lifeact-RFP (Figure 5.6 A, panel 5 s; C inset). Peak recruitment occurs at approximately 8 s, 10 s prior to the Lifeact-RFP peak at approximately 18 s (Figure 5.6 C). This is in agreement with formins nucleating the initial actin filaments of the actin scaffold, proposed by Tran and colleagues (Tran et al. 2015). mDia2 disengagement occurs from 10-18 s as Lifeact-RFP reaches peak enrichment. Inspection of the kymographs indicate that mDia2 is involved in nucleating actin only during scaffold assembly and is absent from the scaffold interior, as shown by the lack of enrichment of mDia2 after 10 s (Figure 5.6 B). This suggests that mDia2 is responsible for nucleating an actin population that specifically functions to assemble the initial scaffold after SG fusion.

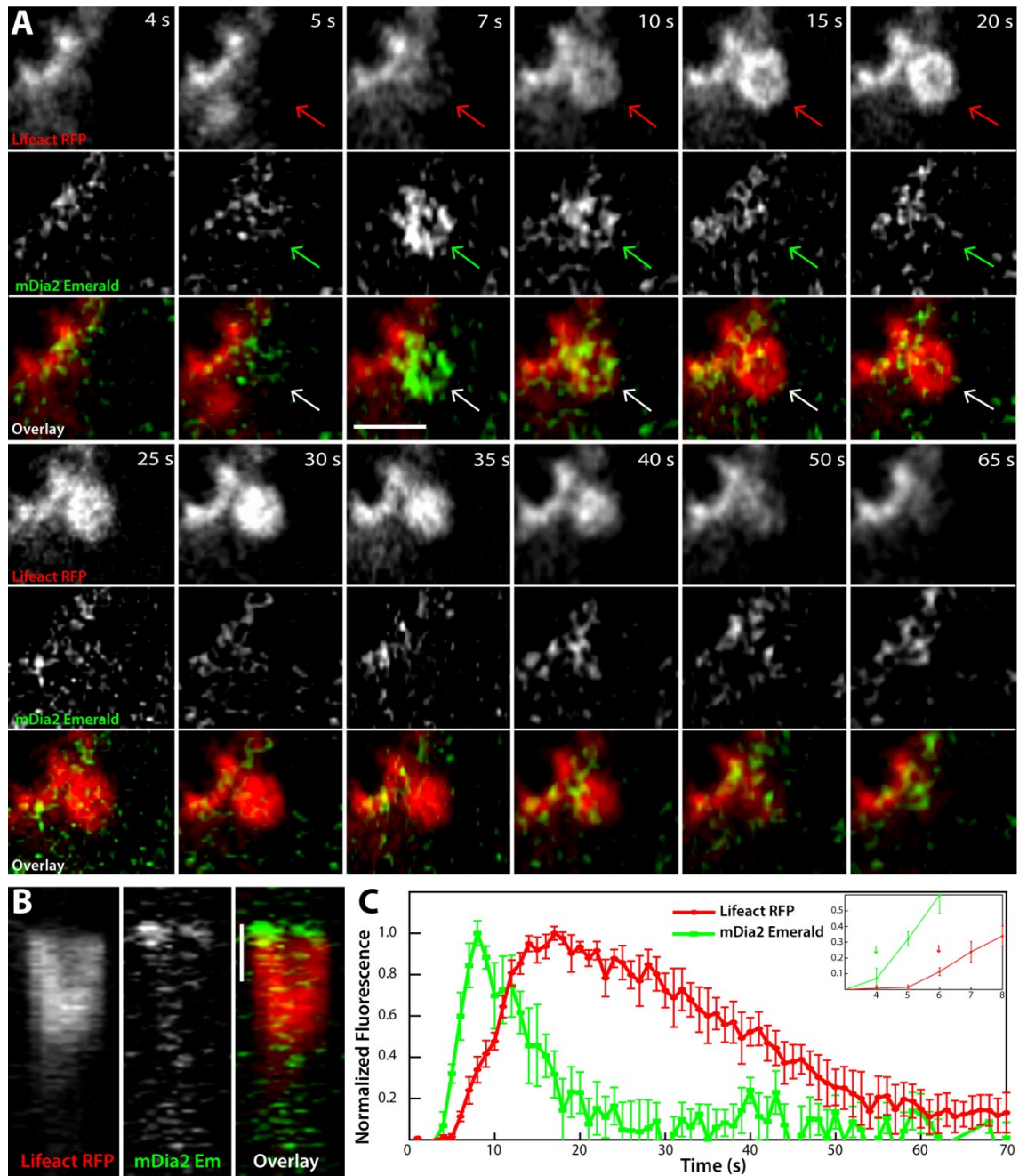


**Figure 5.6 mDia2 is recruited to SGs prior to actin and nucleates the initial actin filaments.** Wistar rats were co-transfected with Lifeact-RFP and mDia2-Emerald stimulated with subcutaneous injection of isoproterenol and intravital microscopy was performed as described in Materials and Methods. (A) Time-lapse imaging of a SG fusion and exocytosis event. mDia2-Emerald is recruited prior to the appearance of actin (panels 5 and 7 s) and is primarily enriched during the first 10 s of the exocytosis event (panels 5-15 s) indicating that mDia2 functions to nucleate the initial linear filaments during scaffold assembly. Numbers denote time in s. (B) Kymographs

showing the exocytosis event in separate channels. mDia2-Emerald is absent from the scaffold interior. Scale bar = 20 s. (C) Normalised mean fluorescence intensity of Lifeact-RFP and mDia2-Emerald. Inset: Zoom of the first 10 s of exocytosis. mDia2-Emerald is recruited at approximately 4 s, 2 s prior to Lifeact-RFP recruitment at 6 s. mDia2-Emerald is present on SGs only during the first 20 s of exocytosis. n = 7 events from 2 animals, error bars are S.E.M.

We next sought to investigate the recruitment kinetics of mDia1 to the actin scaffold. Wistar rats were co-transfected with Lifeact-RFP and mDia1-Emerald, injected with 0.025 mg/kg isoproterenol to stimulate SG exocytosis and imaged using intravital microscopy as in Materials and Methods. mDia1-Emerald fluorescence was detected approximately 2 s prior to Lifeact-RFP and peak fluorescence occurred at approximately 10 s, similar to mDia2 recruitment. Remarkably, the recruitment profile of mDia1 differs from mDia2, where mDia1 has a double peak and is recruited at 2 phases during the event, indicating multiple rounds of nucleation and/or elongation by mDia1. The second recruitment round occurs at approximately 15 s, following partial detachment at 10-15 s (Figure 5.7 C). This is clearly illustrated in the kymograph showing two rounds of enrichment, the first occurring prior to Lifeact-RFP appearance and the second occurring just prior to scaffold interior enrichment by Lifeact-RFP at 15-20 s, with the second recruitment round persisting till the completion of exocytosis (Figure 5.7 B). mDia1-Emerald does not appear to enrich the scaffold interior along with Lifeact-RFP during membrane compression but appears to be involved in completing the scaffold constriction and disassembly phase (Figure 5.7 B). This suggests that actin polymerisation is constantly occurring during this period, with mDia1 possibly nucleating and/or elongating linear filaments.

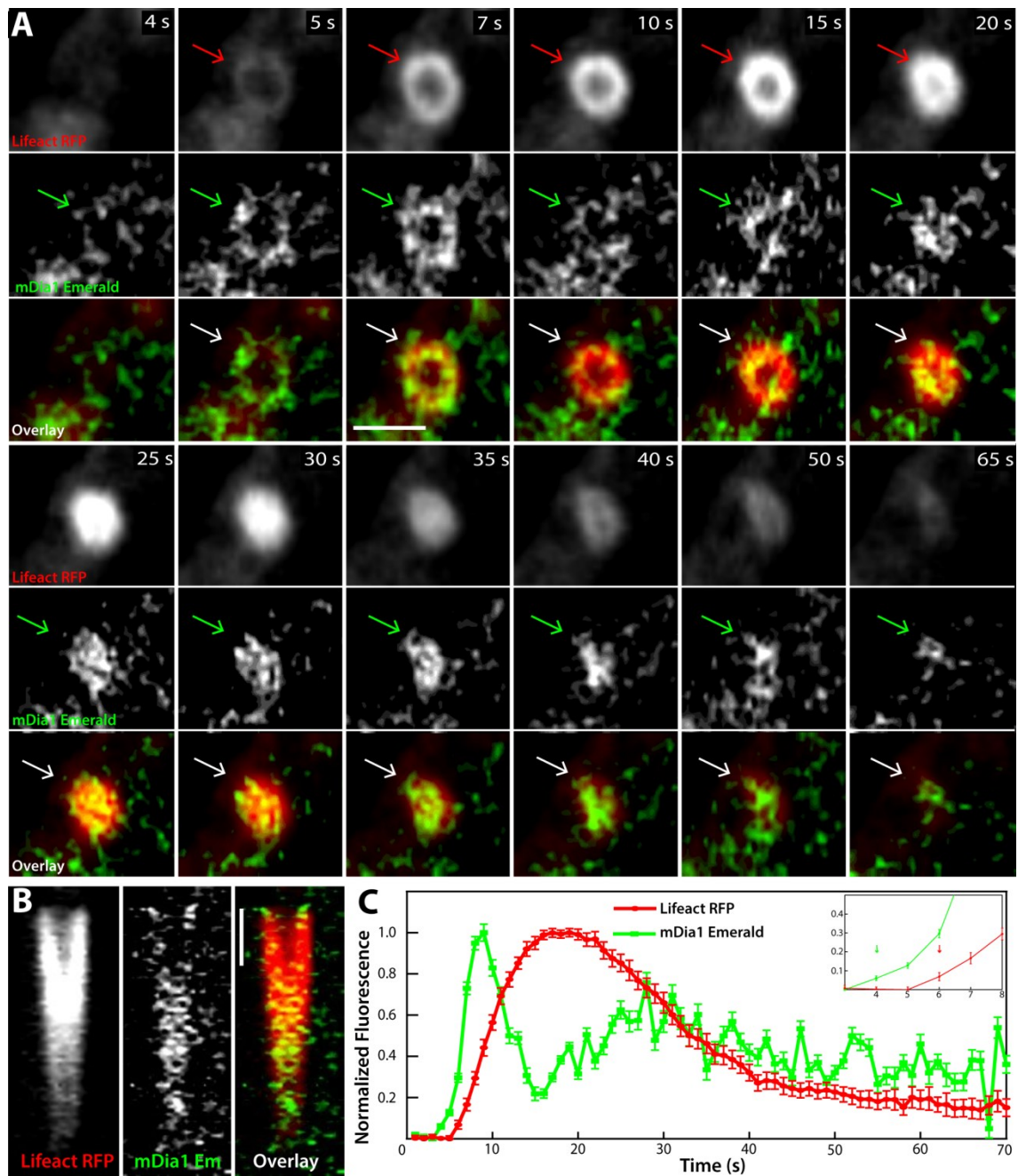


**Figure 5.7 mDia1 is recruited at multiple phases during SG exocytosis.** Wistar rats were co-transfected with Lifact-RFP and mDia1-Emerald, stimulated with subcutaneous injection of isoproterenol and intravital microscopy was performed as described in Materials and Methods. (A) Time-lapse imaging of a SG fusion and exocytosis event. mDia1-Emerald is recruited at two phases during exocytosis. The first phase occurs prior to the appearance of actin (panel 4-5 s) while the second phase occurs at approximately 15 s into the event (panel 15 s) and recruitment continues until completion of exocytosis. Numbers denote time in s. (B) Kymographs showing

the exocytosis event in separate channels. mDia1-Emerald appears to be absent from the scaffold interior during both recruitment phases. Scale bar = 20 s. (C) Normalised mean fluorescence intensity of Lifeact-RFP and mDia1-Emerald. Inset: Zoom of the first 8 s of exocytosis. The first phase of mDia1-Emerald recruitment occurs at approximately 4 s, 2 s prior to the appearance of actin at 6 s. Peak mDia1-Emerald enrichment occurs at approximately 9 s, 10 s prior to the peak of Lifeact-RFP. mDia1-Emerald begins disengagement after 9 s; however, it undergoes a second recruitment phase at approximately 15 s and recruitment continues until completion of exocytosis. The second recruitment phase occurs just prior to peak Lifeact-RFP enrichment at approximately 19 s just as the scaffold diameter starts to decline, suggesting that actin polymerisation is coupled to scaffold constriction and disassembly. n = 17 events from 2 animals, error bars are S.E.M.

The data provides evidence that at least two formins are recruited prior to actin during actin scaffold assembly, nucleating the initial linear filaments that make up the scaffold. This is corroborated by recent work from Miklavc and colleagues who observed that formin inhibition with SMIFH2 prevents actin scaffold formation around fused lamellar bodies whereas Arp2/3 inhibition does not (Miklavc et al., 2012). Interestingly mDia1 and mDia2 have dissimilar recruitment kinetics, which suggests that they are nucleating and/or elongating distinct actin filament populations. The second recruitment round of mDia1 begins after disengagement along with mDia2 (Figures 5.6 C, 5.7 C) indicating that two separate linear filament polymerisation phases occur to maintain the integrity of the scaffold. As there was no apparent enrichment by either formin at the interior of the scaffold with Lifeact-RFP during the membrane compression phase, we hypothesised that perhaps it is the branched actin network that drives membrane compression. The next objective was therefore to determine if the Arp2/3 complex is involved in nucleating and polymerising the actin population driving membrane compression at the scaffold interior.

### **The Arp2/3 complex is involved in driving membrane compression at the scaffold interior using pre-existing formin-generated filaments as nucleation templates**

The Arp2/3 complex has recently been shown to drive exocytosis in an *ex vivo* *Drosophila* model system (Tran et al., 2015) therefore it was reasonable to hypothesise that the branched network would play a major role in mammalian SG exocytosis as well. Having shown that mDia1 and mDia2 are involved in generating the initial filaments of the actin scaffold, we intended to investigate the recruitment kinetics and enrichment pattern of the Arp2/3 complex during SG exocytosis versus actin.

To this end, Wistar rats were co-transfected with Lifeact-RFP and Arp2-Emerald, injected with 0.025 mg/kg isoproterenol to stimulate SG exocytosis and imaged using intravital microscopy as in Materials and Methods. From the fluorescence data, Arp2-Emerald is recruited approximately 2 s after the initial appearance of the scaffold around the fused SG (Figure 5.8 A, panel 10 s; C, inset). This is in agreement with the

study by Tran et al. which demonstrates the recruitment of the Arp2/3 complex after the appearance of F-actin on fused SGs (Tran et al., 2015) and that Arp2/3 generates the branched network using pre-existing linear filaments as templates (Rouiller et al., 2008). The Arp2/3 recruitment profile is generally similar to Lifeact-RFP, although peak Arp2-Emerald enrichment occurs approximately 10 s after peak recruitment of Lifeact-RFP at approximately 23 s (Figure 5.8 C). This greatly contrasts the formin recruitment kinetics (Figure 5.7, 5.7) and suggests that the branched actin population comprises the bulk of filaments during exocytosis. As predicted, Arp2-Emerald appears to enrich the scaffold interior at the SG membrane interface as membrane compression progresses, shown in the time-lapse images (Figure 5.8 A). Arp2-Emerald is clearly observed to be recruited on the outer part of the scaffold during initial recruitment, however its enrichment is subsequently directed towards the scaffold interior from 10-25 s. This is shown by yellow fluorescence (indicating a mixed signal acquired from both Lifeact-RFP and Arp2-Emerald) present at the outer edges of the scaffold which then progressively travels inward to the interior (Figure 5.8 A panels 10-30 s). Inspection of the kymographs also shows that Arp2-Emerald is co-enriched with Lifeact-RFP at the SG membrane interface within the scaffold (Figure 5.8 B), which is in agreement with the view that Arp2/3 generates membrane pushing forces (Borisy and Svitkina, 2000). Arp2-Emerald begins disengagement midway into exocytosis at approximately 31 s, in accordance with completion of the membrane compression phase by this point. Arp2-Emerald remains present until the last approximately 5 s of exocytosis however, suggesting that it is involved in the scaffold constriction and disassembly phase as well, possibly in collaboration with mDia1 (Figure 5.7), also demonstrated in other studies (Isogai et al., 2015; Young et al., 2015).

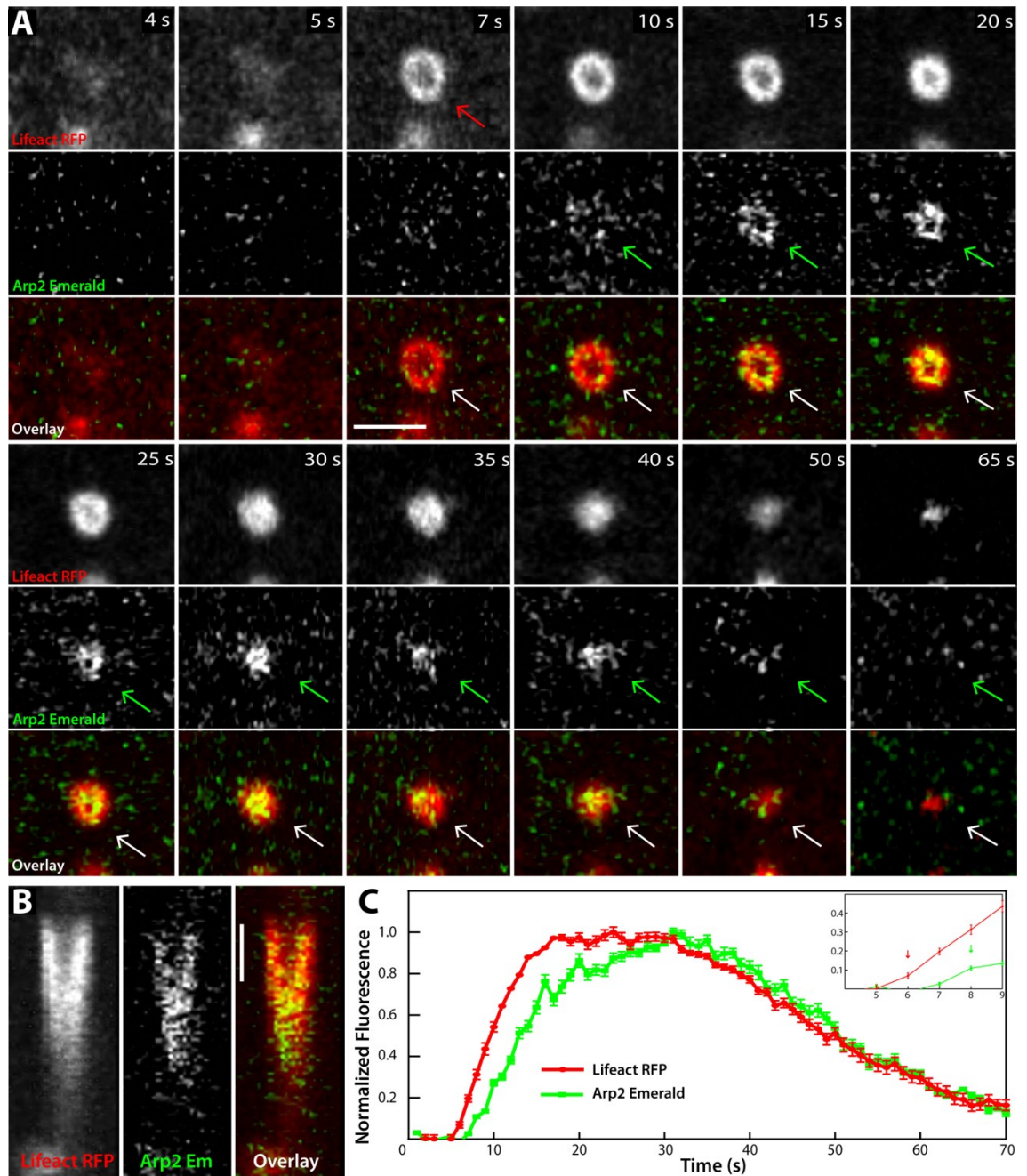


**Figure 5.8 The Arp2/3 complex nucleates branched filaments which drive membrane compression at the scaffold interior.** Wistar rats were co-transfected with Lifact-RFP and mDia1-Emerald, stimulated with subcutaneous injection of isoproterenol and intravital microscopy was performed as described in Materials and Methods. **A:** Time-lapse imaging of a SG fusion and exocytosis event. Arp2-Emerald is recruited approximately 2 s after the appearance of Lifact-RFP on fused SGs (panel 7 s). Arp2-Emerald is present throughout exocytosis and is largely enriched within the interior of the actin scaffold, likely at the SG membrane interface. As membrane compression

progresses and its diameter is reduced (panel 10-25 s Lifeact-RFP), Arp2/3 enrichment is progressively enriched at the scaffold interior, suggesting that Arp2/3 nucleates the branched actin network which drives membrane compression (panel 10-30 s Arp2 Emerald). This is shown by yellow fluorescence (mixed signal acquired from both Lifeact-RFP and Arp2-Emerald) present on the actin scaffold which then progresses inward within the scaffold (panel 10-30 s, overlay). Numbers denote time in s. B: Kymographs showing the exocytosis event in separate channels. Arp2/3-Emerald fluorescence co-localises with Lifeact-RFP enrichment at the scaffold interior. Scale bar = 20 s. C: Normalised mean fluorescence intensity of Lifeact-RFP and Arp2-Emerald. Inset: Zoom of the first 9 s of exocytosis. Arp2-Emerald is recruited approximately 2 s after Lifeact-RFP, demonstrating that Arp2/3 complex is recruited to pre-existing linear filaments nucleated by formins. The fluorescence profiles of Lifeact-RFP and Arp2-Emerald are generally similar, with Arp2-Emerald enrichment being slightly delayed behind Lifeact-RFP, peaking at approximately 31 s. This suggests that Arp2/3 complex nucleates the majority of filaments during exocytosis. n = 14 events from 2 animals, error bars are S.E.M.

## **Discussion**

The results from this chapter have illuminated several interesting new aspects of actin biology *in vivo*. For the first time the stepwise *de novo* recruitment of actin nucleators, Tpms and crosslinkers involved in the construction of a functional actin scaffold was investigated directly inside a living mammal. The data presents evidence indicating that multiple actin filament populations exist and operate collaboratively with one another. Moreover, proteins such as Tpms and myosins are recruited to distinct populations. Additionally, there are multiple phases occurring in regulated SG exocytosis *in vivo* which has not been described before, suggesting clear distinctions exist between the functions of the branched and linear actin networks that work interdependently to facilitate exocytosis.

### **Actin nucleators have unique dynamics and collaborate to drive regulated SG exocytosis *in vivo***

The mDia1, mDia2 and Arp2/3 recruitment profiles indicate that formin-nucleated linear filaments form the initial actin scaffold, providing the templates upon which Arp2/3 nucleates the branched filament population that appears to drive membrane compression (Figures 5.6, 5.7, 5.8). This is in agreement with the observations made by Miklavc and colleagues who demonstrated that formin inhibition by the small molecule inhibitor SMIFH2 prevents actin scaffold formation thereby disrupting exocytosis (Miklavc et al., 2012), as well as the prediction made by Tran and colleagues where ARP2/3 nucleates the branched network using pre-existing linear filaments (Tran et al., 2015).

Interestingly, mDia1 is recruited to the scaffold at multiple stages during exocytosis, unlike mDia2. This indicates that there are at least two linear filament populations operating on the actin scaffold, the mDia2 filament population being only required for scaffold assembly while the mDia1 population is required for the subsequent constriction and disassembly phase as well. Hence, the formins appear to be generating functionally distinct filament populations, also indicated in another study (Kage et al., 2017). mDia1 could be generating new filaments or elongating existing

filaments during the scaffold constriction phase, possibly in collaboration with Arp2/3, which generates branched filaments with free barbed ends capable of binding formins. Two recent studies recently demonstrated using *in vitro* and cell culture models that formins are indeed capable of elongating Arp2/3 generated filaments (Isogai et al., 2015; Young et al., 2015). Moreover, mDia1 is required for efficient branched network formation by Arp2/3 and removal of mDia1 adversely affects lamellipodia and ruffle formation. Interestingly, Arp2/3 is able to generate the branched network in an autocatalytic fashion if mDia1 is present at the initial stages of branched network assembly (Isogai et al., 2015). Applying this to the kinetics and visual observations presented here, it is possible that mDia1 and even mDia2 are generating filaments that are compatible with Arp2/3 autocatalytic branched network generation, which drives the membrane compression phase within the scaffold interior. Furthermore, this provides the first kinetic and mechanistic evidence *in vivo* in mammals supporting the model of extended convergent elongation, where collaboration between multiple linear and branched nucleators drive the formation of actin structures, postulated by Young *et al.* (Young et al., 2015).

The unique kinetics of mDia1 also suggests that formins may have functions that extend beyond filament nucleation and elongation, as suggested previously by other groups. Jegou *et al.* showed that mDia1 can sense mechanical tension and modulate its elongation activities (Jégou et al., 2013) while Bugyi *et al.* demonstrated that mDia1 can change filament conformation and flexibility, thus affecting binding of downstream proteins to filaments (Bugyi et al., 2006). Hence, the second recruitment round of mDia1 could be a response to changes in structural tension during the membrane compression and scaffold constriction phases. mDia1 may be required to generate new filaments or modify the conformation of existing filaments to allow recruitment of AAPs such as Tpms and myosins to increase filament stability (Ujfalusi et al., 2012; Ujfalusi et al., 2009). This view fits with the kinetics data demonstrating that Tpms 3.1, 4.2 and myosin IIA are highly enriched on the actin scaffold towards the end of the constriction and disassembly phase. Moreover, it is in agreement with the hypothesis that formins dictate Tpm isoform recruitment to filaments, hence specifying their function (Johnson et al., 2014). Interestingly, a study showed that the presence of

yeast Tpm lengthens formin filaments by increasing their elongation rates as well as facilitating end-to-end annealing of filaments (Skau et al., 2009). Hence, it is possible that a positive feedback cycle is established between Tpm-formin pairs to generate linear filament populations, which could explain the increased Tpm enrichment as well as second recruitment phase of mDia1 during the scaffold constriction phase.

From the fluorescence profiles Arp2/3 is present throughout the entire event after initial recruitment and appears to coincide with the actin enrichment pattern within the scaffold during the membrane compression phase (Figure 5.8). This suggests that the Arp2/3 branched population likely accounts for the bulk of actin filaments polymerised within the scaffold interior which drives membrane compression. Furthermore, this fits with the established paradigm of the dense branched filament network being rapidly generated to provide the pushing forces necessary to drive membrane protrusions such as lamellipodia (Borisy and Svitkina, 2000). This has not been described in classical models of regulated exocytosis and intriguingly reveals a non-myosin force generation mechanism to drive cargo delivery/membrane compression *in vivo* in mammals.

Remarkably,  $\alpha$ -actinin is recruited together with the initial linear filaments comprising the actin scaffold, however is also enriched on the actin population driving membrane compression at the scaffold interior (Figure 5.5). This indicates a possible association with Arp2/3 and the branched network which drives membrane compression, likely functioning to crosslink/bundle filaments to maintain structural stability of the branched network during this phase (Figure 5.8). These observations are in agreement with a study demonstrating that  $\alpha$ -actinin is a promiscuous crosslinker, able to bind filaments regardless of their geometry (Courson and Rock, 2010). Additionally, the recent discovery of the existence of multiple families of Arp2/3 complexes and hybrids supports this hypothesis (Abella et al., 2016; Pizarro-Cerda et al., 2017). Arp2/3 was shown to form a stable hybrid complex with  $\alpha$ -actinin and is involved in focal adhesions (Chorev et al., 2014). Furthermore, work from another group demonstrated that  $\alpha$ -actinin is essential for Arp2/3 polymerisation of the branched network at apical cell junctions. Interestingly, the authors also show that  $\alpha$ -actinin is recruited to sites directly on membranes containing  $\beta$ -catenin in the absence of actin (Tang and Brieher,

2012) and other groups have shown that  $\alpha$ -actinin is co-immunoprecipitated with cadherin-catenin complexes (Knudsen et al., 1995). Based on the  $\alpha$ -actinin-NG, mTomato and Lifeact recruitment data in this chapter however, it is unlikely that  $\alpha$ -actinin is recruited directly to the SG membrane prior to actin. Further work could confirm this by investigating the kinetics of SG fusion/mTomato versus  $\alpha$ -actinin recruitment using mouse transfection techniques developed in Chapter 3.

### **Tpm recruitment to distinct actin populations**

Tpms3.1, 4.2 and actin are simultaneously recruited to fused SGs however peak enrichment of both Tpms lags behind peak actin enrichment by approximately 10 s. In addition, these Tpms primarily enrich the actin scaffold during exocytosis and appear not to be involved with the actin population driving membrane compression at the scaffold interior (Figures 5.2 and 5.3). This strongly indicates that Tpms 3.1/4.2 are associating with a subset of actin filaments and poses interesting questions such as 1) why are the Tpms enriching these particular actin populations on the actin scaffold and absent from the interior and 2) why do they have a slower and broader recruitment profile compared to total F-actin? (Figure 5.2 C)

Previous studies from our lab and others have shown that formins specify Tpm recruitment to actin filaments (Johnson et al., 2014; Tojkander et al., 2011) and that Tpms3.1/4.2 do not enrich the branched filament population (Blanchoin et al., 2001; DesMarais et al., 2002; Ponti et al., 2004). In addition, Fritzsche and colleagues have demonstrated that formin nucleated filaments are longer, have slower turnover kinetics and are better suited to absorb mechanical stresses (Fritzsche et al., 2016; Fritzsche et al., 2013). It is therefore likely that Tpms3.1/4.2 are sorted to formin nucleated filaments that are required for structural support to increase their stability. As membrane compression progresses and scaffold constriction begins, a higher abundance of more stable filaments would be required to withstand the opposing forces generated from Arp2/3 polymerisation at the interior, which could explain the delayed peak of Tpms 3.1/4.2. In line with this, mDia1 has a second recruitment phase

which begins at approximately 15 s, likely marking the onset of the scaffold constriction and disassembly phase (Figure 5.7).

Towards the end of the membrane compression phase, the actin scaffold begins constriction in addition to disassembly, as shown by the reduction in size of the actin scaffold as well as Lifeact-RFP fluorescence intensity from 30-65 s (Figures 5.1, 5.2,) suggesting that the total amount of filaments are gradually declining during this time. Tpm enriched filaments however peak at 30-40 s and subsequently appear to be more enriched compared to non Tpm-bound filaments towards the end of exocytosis (Figure 5.2 A, B). How is it possible that more Tpm are recruited to the scaffold in this phase when there is apparently less total actin compared to the start of exocytosis? By this point, branched actin abundance within the scaffold has decreased, hence the remaining filaments are likely skewed towards Tpm and myosin-coated linear filaments. Additionally, several groups have previously shown that actin treadmilling/depolymerisation mediated by cofilin severing of filaments can produce substantial contractile forces in the presence of actin crosslinkers (Miklavc et al., 2015; Sun et al., 2010). Complementary to this, Hsiao and colleagues demonstrated that Tpm preferentially bind the pointed ends of filaments severed by cofilin (Hsiao et al., 2015). Therefore, it is possible that cofilin-mediated filament severing on the actin scaffold is providing more available pointed ends for Tpm to bind towards the latter phase of exocytosis, thus contributing to scaffold constriction while simultaneously allowing more Tpm to be recruited. In support of this,  $\alpha$ -actinin is also recruited to the scaffold with the initial filaments and is highly enriched towards the end of exocytosis (Figure 5.5). Future work could therefore investigate the involvement of cofilin during actin scaffold assembly to determine its recruitment kinetics as well as localisation on the scaffold. Furthermore, cofilin inhibition/knockout studies could be performed to determine if Tpm are still enriched at the later phase of exocytosis in cells lacking functional cofilin.

What about the branched actin population driving membrane compression within the scaffold? A recent study in our lab demonstrates that Tpm 1.8/1.9 are recruited to the actin population at the leading edge of cells, suggesting that the 'older' branched filaments could be remodelled to linear filaments behind Arp2/3 polymerisation

activity at the membrane interface (Brayford et al., 2016). Therefore, is it possible that a similar process is occurring during SG exocytosis *in vivo*, where Tpm1.8/1.9 could be insulating the 'older' filaments behind Arp2/3, which drives branched network polymerisation at the membrane interface. Moreover,  $\alpha$ -actinin is also highly enriched on the actin population in the scaffold interior, hence may also be involved in filament remodelling behind Arp2/3. Further work could assess the recruitment kinetics of Tpm1.8/1.9 versus Arp2/3 and F-actin by utilising the mouse transfection techniques developed in Chapter 3 to delivering fluorescently tagged Tpm1.8/1.9 constructs.

### **A new model of actin-driven exocytosis *in vivo***

In conclusion, the findings in this chapter indicate that the actin scaffold is assembled upon SG fusion to the APM by first recruiting formins to nucleate the initial linear filaments enriched with Tpm3.1,4.2 and  $\alpha$ -actinin, followed by myosins. The Arp2/3 complex is subsequently recruited to build the branched network. Additionally, regulated SG exocytosis in the salivary glands of rodents occurs in two distinct phases. The first phase being membrane compression/cargo delivery into the canaliculi by approximately 30 s and the second phase being constriction and disassembly of the actin scaffold from 30-65 s. The membrane compression phase appears to be driven by the Arp2/3 branched actin population within the scaffold, supported by  $\alpha$ -actinin crosslinking, while the subsequent scaffold constriction and disassembly phase involves myosin IIA, at least one formin (mDia1) and increased enrichment of  $\alpha$ -actinin as well as Tpm3.1/4.2 coated filaments.

This new evidence has allowed us to construct a timeline for AAP recruitment in relation to SG and actin scaffold diameter reduction kinetics (Figure 5.9) as well as propose a new and more detailed model of SG exocytosis (Figure 5.10).  $\beta$ -adrenergic stimulation causes the SGs to fuse with the APM of cells at time 0 s and recruits the initial nucleators, formins mDia1 and mDia2 (Figure 5.9/5.10 A). The formins build the initial actin scaffold by nucleating linear and presumably more stable filaments decorated with Tpm3.1/4.2 and  $\alpha$ -actinin, which are detected approximately 2 s after formin recruitment (Figure 5.9/5.10 B). Myosin IIA and Arp2/3 complex are recruited

approximately 1 and 2 s, respectively, after scaffold appearance (Figure 5.9/5.10 C). Arp2/3 branched network polymerisation is then directed towards the SG membrane interface at the scaffold interior, thus driving the membrane compression phase, supported by  $\alpha$ -actinin crosslinking closely behind Arp2/3 (Figure 5.9/5.10 D). During this time myosin IIA and  $\alpha$ -actinin enrichment is simultaneously increased on the outer part of the scaffold, hence providing crosslinking support to withstand forces generated by membrane compression at the scaffold interior. The second phase of mDia1 recruitment peaks at approximately 30 s, coinciding with the beginning of the scaffold constriction and disassembly phase and the end of membrane compression. Myosin IIA reaches peak recruitment at this time point. From 30-65 s the scaffold constriction and disassembly phase gradually completes, with actin polymerisation occurring with mDia1 and Tpm-coated filaments, supported by myosin IIA and  $\alpha$ -actinin crosslinking (Figure 5.9/5.10 E-F).

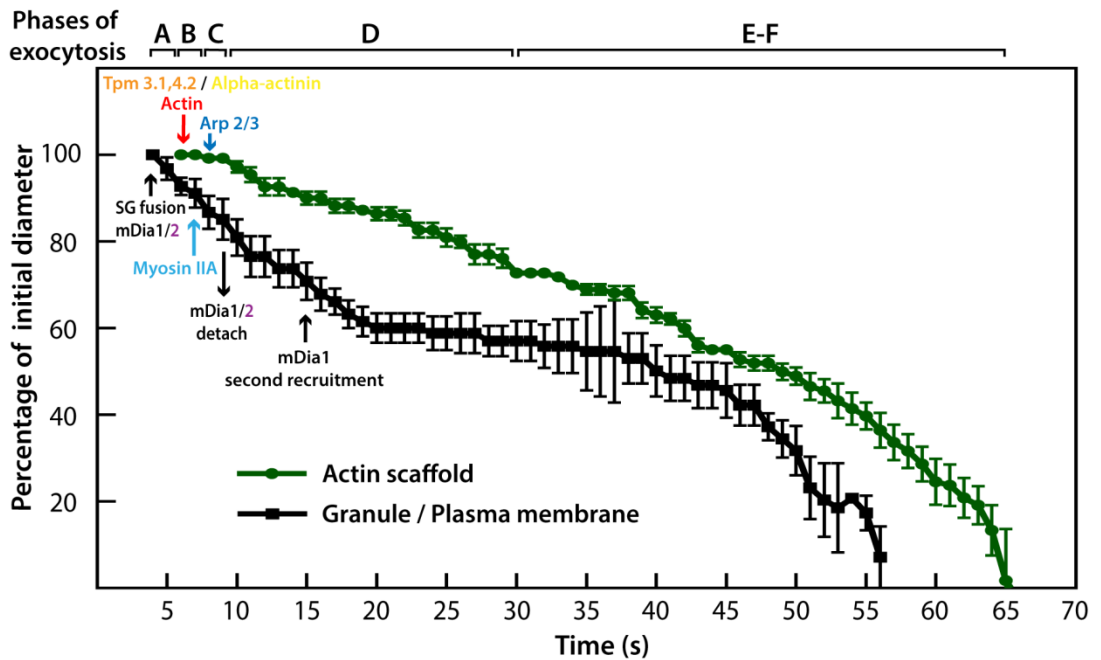


**Figure 5.9 SG membrane and actin scaffold outer diameter kinetics during exocytosis and AAP recruitment timeline.** Wistar rats were transfected with Farnesyl-TdTomato (SG/PM marker) or Lifeact-RFP (F-actin marker), stimulated with subcutaneous injection of isoproterenol and intravital microscopy was performed as described in Materials and Methods. The outer diameter of the granule membranes and actin scaffolds were measured. Phases of exocytosis (described in Figure 5.10): (A 4-6 s): SG fusion to the APM and formin recruitment. (B 6-8 s): Actin scaffold assembly. (C 8-9 s): Arp2/3 branched network generation. (D 9-30 s): Membrane compression. (E-F 30-65 s): Scaffold constriction and disassembly until completion of exocytosis. Arrows denote point of recruitment or detachment of AAPs. SG fusion and formin recruitment occurs at 4 s, linear actin filament scaffold assembly with Tpm<sub>s</sub> and  $\alpha$ -actinin at 6 s, myosin IIA recruitment at 7 s, Arp2/3 recruitment and branched actin generation within the scaffold at 8 s, formin detachment at 9 s and mDia1 second recruitment phase at 15 s. n = 4-7 events from 2-3 animals, error bars are S.E.M.

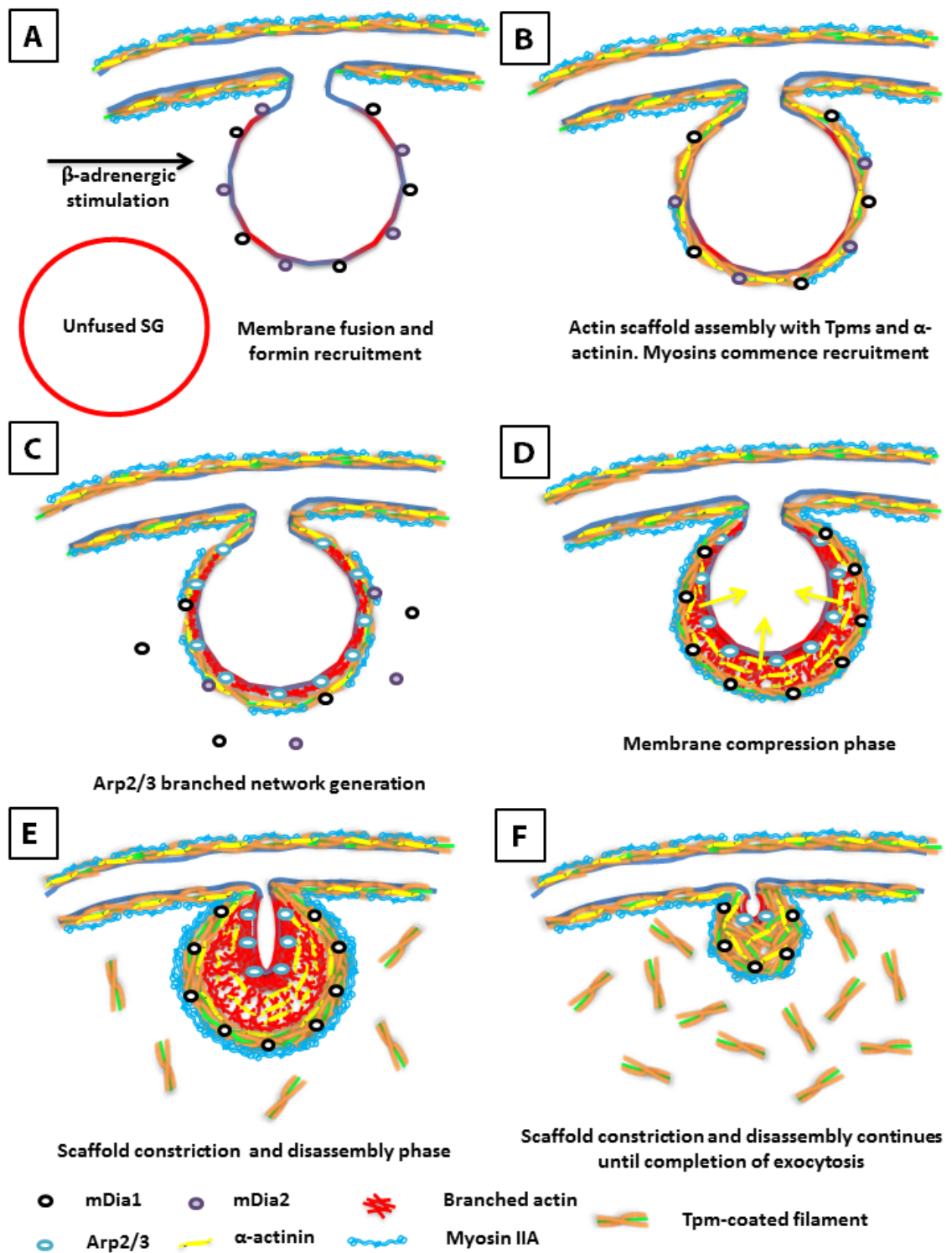


**Figure 5.10 Proposed model for regulated SG exocytosis in rodent salivary glands.** (A)  $\beta$ -Adrenergic (isoproterenol) stimulation initiates SG fusion with the APM, causing a mixing of apical and SG membranes and recruitment of formins mDia1 and mDia2. (B) The actin scaffold is assembled around the fused SG, nucleated by formins and decorated with Tpm 3.1,4.2 as well as  $\alpha$ -actinin. Myosin IIA begins its recruitment. (C)

Arp2/3 complex is recruited to the scaffold and commences generation of the branched actin network directed towards SG membrane. Formins begin disengaging, while myosin IIA enrichment progresses. (D) Rapid Arp2/3 branched network polymerisation at the SG membrane interface drives membrane compression within the scaffold interior, supported by  $\alpha$ -actinin crosslinking. Formin mDia1 is recruited to the scaffold for a second phase. (E) Membrane compression progresses at the scaffold interior while scaffold constriction and disassembly begins. Myosin IIA and Tpm3.1/4.2-coated filaments are increasingly enriched on the scaffold. (F) After membrane compression is complete, a sliver of the SG membrane remains within the scaffold interior which is gradually integrated into the APM, while the actin scaffold continues to be constricted and disassembled, thus completing exocytosis.

## Chapter 6. General Discussion

### Overview of findings

This thesis investigated the relative dynamics of cytoskeletal Tpm-actin co-polymers in cells and the recruitment kinetics of AAPs during *de novo* actin scaffold assembly in living mammals. Furthermore, techniques for viral and non-viral gene delivery into the salivary acini of living mice were developed and refined.

The primary outcome of this work was the mechanistic insights gained by observing the *de novo* assembly and operation of actin structures in living mammals. Actin scaffold assembly around fused SGs occurs in a clockwork-style mechanism which requires collaboration between Arp2/3 and formins, with individual formins having distinct recruitment kinetics. Tpm recruitment data indicate these proteins are recruited to a subset of filaments, suggesting that multiple distinct actin populations co-exist and are functionally specified by Tpm. Hence, individual actin nucleators likely generate distinct filament populations that recruit specific Tpm to modulate filaments, as well as the recruitment and activity of other AAPs. Remarkably, post-SG fusion and scaffold assembly, actin drives exocytosis via two distinct phases, membrane compression followed by scaffold constriction. This suggests that the branched network has a novel function, where rapid polymerisation by Arp2/3 and crosslinking by  $\alpha$ -actinin drives SG membrane compression and cargo delivery, supported by the linear Tpm and myosin decorated filaments of the actin scaffold.

A secondary finding demonstrated for the first time *in vivo* that cytoskeletal Tpm polymer dynamics are independent of actin filament dynamics. Tpm3.1 was observed to rapidly cycle on and off actin filaments in stress fibres in MEFs as well as filament bundles *in vivo* in rodents. This revealed novel insights into filament regulation by Tpm in mammalian cells in culture and *in vivo*.

The third outcome of this thesis was the development of an *in vivo* plasmid DNA transfection method for acinar cells in mouse salivary glands using commercially available reagents. This provides an efficient, reproducible and relatively inexpensive

means to manipulate the different components of the filaments in salivary acini. As well it expands the scope of experimentation when used in combination with the large number of genetically manipulated cytoskeletal mouse models.

### **Interdependence between linear and branched actin networks**

The observations in Chapter 5 demonstrate that the linear and branched actin networks, despite co-existing in time and space, are actually independent entities that collaborate to perform cellular functions. This further supports the collaboration-based mechanism for filament diversification described by Gunning and Hardeman (2017, Figure 1). In SGs *in vivo*, actomyosin-driven exocytosis post-fusion occurs in two distinct phases mediated by the linear and branched actin networks that each perform a specific function. Membrane compression appears to occur independently of scaffold constriction which suggests that Arp2/3 is able to respond to local stimuli. This supports the hypothesis of linear and branched networks behaving as independent entities and would allow for efficient membrane compression/cargo delivery once the scaffold is assembled. In agreement with this, Fritzsche *et al.* recently demonstrated that the linear and branched filament networks can be regulated independently of each other and independently of actin turnover, indicating that cells are able to modulate the activity of the branched and linear networks downstream of signalling events in order to have a faster local response (Fritzsche *et al.*, 2016).

Arp2/3 is recruited approximately 2 seconds after the initial appearance of (linear) actin filaments which supports the view that formin filaments are required in order to generate the branched network (Tran *et al.*, 2015). Hence, the linear formin filament network is the primary determinant of cytoskeletal function, while the Arp2/3 branched network relies on the linear network to direct its activities and likely plays a secondary or support role during cytoskeletal processes. Various studies support this view, the foremost being that Arp2/3 ablation only perturbs certain aspects of cell migration (Wu *et al.*, 2012). This suggests that Arp2/3 has a secondary function involving remodelling activities (Anderson *et al.*, 2017) and that leading edge advancement depends on the linear lamella network (Ponti *et al.*, 2004). Furthermore, Fritzsche and colleagues have shown that the formin nucleated linear filaments

represent <10% of cortical actin filaments in a cell culture model. Although this is a small portion of the overall cortical actin population, the formin nucleated linear filaments play a pivotal role in maintaining the elasticity of the overall network, as they are longer and are able to dissipate mechanical stress much more effectively than the shorter filaments in the branched network (Fritzsche et al., 2016). Additionally, Kage *et al.* demonstrated that ablation of FMNL formins affects fibroblast migration through a polymer matrix, indicating that the lack of FMNL formin filaments affects the cell's ability to cope with counteracting forces during migration (Kage et al., 2017). These studies are in agreement with work in Chapter 5 showing that the initial formin filaments on the scaffold, stabilised by Tpm's, myosins and to a lesser extent  $\alpha$ -actinin, are likely high tensile and highly elastic. These properties would be ideal to resist forces generated by branched actin polymerisation driving SG membrane compression and remodelling.

Arp2/3 has a unique ability to utilise its rapid polymerisation activity to drive force production at the membrane interface during a variety of cellular processes (Rotty et al., 2013). Work in Chapter 5 demonstrates that Arp2/3 polymerisation activity, in conjunction with  $\alpha$ -actinin crosslinking and bundling, mediates membrane compression and remodelling post-SG fusion *in vivo*. Functionally, this is in agreement with other studies demonstrating that crosslinkers must be recruited to stiffen actin networks for successful remodelling of the lamellipodial envelope (Vinzenz et al., 2012) and that the rate of network assembly affects their stabilising action (Falzone et al., 2012). Collectively, this suggests that the branched network is structurally more 'brittle' compared to the linear network which is more elastic (Fritzsche et al., 2016). Hence, rapid branched network polymerisation would be functionally suited for generating an evenly distributed force on a large surface area such as the membrane interface. This is ideal for membrane compression within the scaffold as the scaffold structure completely encompasses fused SGs, thus directing and supporting Arp2/3 polymerisation at the SG membrane interface. These observations provide *in vivo* confirmation supporting recent study showing a similar mechanism in cell culture, where linear myosin-coated formin filaments at the rear of cells are critical to

withstand forces generated by Arp2/3 branched network which drives bleb formation at the leading edge, thus contributing to cell migration (Ramalingam et al., 2015).

### **Multiple linear actin populations co-exist in time and space and are functionally specified by Tpms**

Recruitment kinetics data in Chapter 5 provides the first *in vivo* evidence indicating that formins are generating distinct filament populations. Hence, the linear actin network is comprised of multiple sub-populations of filaments, in agreement with a recent study demonstrating similar observations *in vitro* and in cell culture (Kage et al., 2017). Furthermore, recruitment data demonstrating that Tpms 3.1 and 4.2 sort to a subset of actin filaments at the initiation of scaffold assembly implies that Tpm insulation allows segregation of these populations. This is supported by studies showing that formins specify the Tpm isoform recruited to actin filaments (Johnson et al., 2014; Tojkander et al., 2011) and the recent discovery showing that Tpm1.8/1.9 define a subset of filaments in lamellipodia (Brayford et al., 2016). Hence, a major contribution of this study is kinetic evidence *in vivo* demonstrating that assembly of cytoskeletal structures is likely controlled by specific formin-Tpm pairs, which allow multiple functionally distinct filament populations to co-exist in time and space.

Intriguingly in Chapter 4, Tpm3.1 turnover kinetics was observed to be highly dynamic and independent of actin turnover kinetics, demonstrating that Tpms on filaments are able to exchange with free Tpms in the cytosol. This discovery revealed how Tpms, with <40 isoforms existing in mammals (Gunning et al., 2008), regulate actin filaments. Specific Tpms could be initially co-assembled or recruited to filaments by a formin, but subsequently may undergo exchange with an alternative isoform which mediates other regulatory functions. This agrees with a model proposed by Manstein and Mulvihill (Manstein and Mulvihill, 2016b). Taken together with data in Chapter 5 and other studies demonstrating that multiple linear actin populations co-exist (Kage et al., 2017) and are likely generated by specific formin-Tpm pairs (Johnson et al., 2014; Tojkander et al., 2011), this indicates that an individual actin filament may play multiple functional roles during its lifetime. This strongly agrees with the view that

eukaryotic actin forms a single universal pool that is modulated by AAPs for diverse functions (Gunning et al., 2015a), with Tpm's being the foremost regulatory factor (Gunning et al., 2015b).

### **Specific actin populations can be targeted to manipulate biological processes**

A final insight from this work is that multiple distinct filament populations collaborate to function as a single unified network. This implies that each population likely contributes a specific function, which has implications for the manipulation of cellular processes. It should be noted however that these functions may also overlap, thus conferring robustness to the system. The recruitment data indicates that multiple AAPs are specifically recruited to each population, suggesting that their collective action defines its function. Furthermore, each filament population is likely assembled and regulated by specific formin-Tpm pairs, which dictates the binding of other AAPs. Hence, in order to perturb specific cytoskeletal processes, it is imperative that the entire corresponding filament population is targeted by focusing on key components at the assembly and regulatory stage, such as formins and Tpm's. Downstream or non-regulatory AAPs such as myosin or  $\alpha$ -actinin, respectively, likely contribute supportive roles involving multiple filament populations, hence may not be suitable candidates for targeting. Viewed in this context, this could explain the observations that myosin II inhibition does not completely disrupt large granule exocytosis in other models, but merely delays it (Masedunskas et al., 2011a; Miklavc et al., 2015). With this understanding of filament specification it should be possible to develop more effective therapeutics since it may be possible to target specific filaments and their respective functions. This approach has proven successful for developing a novel anti-Tpm cancer drug (Stehn et al., 2013a).

Future work could determine the relationship between formin and Tpm isoforms by specifically ablating the expression of formins and subsequently assessing the recruitment kinetics of Tpm's. Likewise, Tpm isoforms could be manipulated to investigate their downstream effects on AAPs and cytoskeletal function. This approach

would allow for rigorous investigation not only into the functions and relationships between individual formins, Tpm's and downstream AAPs, but also provide insights into the functional relevance of that particular filament population in the context of biological processes. This could be performed using viral and non-viral gene delivery techniques developed and refined in Chapter 3 in combination with gene-editing techniques such as CRISPR (Long et al., 2016). Furthermore, this could also be extended to targeting individual subunits and binding partners of the Arp2/3 complex, since recent discoveries indicate that multiple families of Arp2/3 complexes exist (Abella et al., 2016; Pizarro-Cerda et al., 2017) that may very well be generating multiple distinct branched populations.

## References

- Abella, J.V., C. Galloni, J. Pernier, D.J. Barry, S. Kjaer, M.F. Carlier, and M. Way. 2016. Isoform diversity in the Arp2/3 complex determines actin filament dynamics. *Nature cell Biology*. 18:76-86.
- Abràmoff, M.D., P.J. Magalhães, and S.J. Ram. 2004. Image processing with ImageJ. *Biophotonics International*. 11:36-42.
- Anderson, K.L., C. Page, M.F. Swift, P. Suraneni, M.E. Janssen, T.D. Pollard, R. Li, N. Volkmann, and D. Hanein. 2017. Nano-scale actin-network characterization of fibroblast cells lacking functional Arp2/3 complex. *Journal of Structural Biology*. 197:312-321.
- Aoyagi, K., T. Sugaya, M. Umeda, S. Yamamoto, S. Terakawa, and M. Takahashi. 2005. The activation of exocytotic sites by the formation of phosphatidylinositol 4, 5-bisphosphate microdomains at syntaxin clusters. *Journal of Biological Chemistry*. 280:17346-17352.
- Appaduray, M.A., A. Masedunskas, N.S. Bryce, C.A. Lucas, S.C. Warren, P. Timpson, J.H. Stear, P.W. Gunning, and E.C. Hardeman. 2016. Recruitment Kinetics of Tropomyosin Tpm3. 1 to Actin Filament Bundles in the Cytoskeleton Is Independent of Actin Filament Kinetics. *PloS One*. 11:e0168203.
- Aunis, D., and M.-F. Bader. 1988. The cytoskeleton as a barrier to exocytosis in secretory cells. *Journal of Experimental Biology*. 139:253-266.
- Bach, C.T., S. Creed, J. Zhong, M. Mahmassani, G. Schevzov, J. Stehn, L.N. Cowell, P. Naumanen, P. Lappalainen, and P.W. Gunning. 2009. Tropomyosin isoform expression regulates the transition of adhesions to determine cell speed and direction. *Molecular and Cellular Biology*. 29:1506-1514.
- Bader, M.-F., F. Doussau, S. Chasserot-Golaz, N. Vitale, and S. Gasman. 2004. Coupling actin and membrane dynamics during calcium-regulated exocytosis: a role for Rho and ARF GTPases. *Biochimica et Biophysica Acta (BBA)-Molecular Cell Research*. 1742:37-49.
- Barua, B., D.A. Winkelmann, H.D. White, and S.E. Hitchcock-DeGregori. 2012. Regulation of actin-myosin interaction by conserved periodic sites of tropomyosin. *Proceedings of the National Academy of Sciences of the United States of America*. 109:18425-18430.
- Baum, B.J., I. Alevizos, J.A. Chiorini, A.P. Cotrim, and C. Zheng. 2015. Advances in salivary gland gene therapy - oral and systemic implications. *Expert Opinion on Biological Therapy*. 15:1443-1454.
- Benihoud, K., P. Yeh, and M. Perricaudet. 1999. Adenovirus vectors for gene delivery. *Current Opinion in Biotechnology*. 10:440-447.
- Bessis, N., F. GarciaCozar, and M. Boissier. 2004. Immune responses to gene therapy vectors: influence on vector function and effector mechanisms. *Gene Therapy*. 11:S10-S17.
- Bett, A., L. Prevec, and F. Graham. 1993. Packaging capacity and stability of human adenovirus type 5 vectors. *Journal of Virology*. 67:5911-5921.
- Blanchoin, L., K.J. Amann, H.N. Higgs, J.B. Marchand, D.A. Kaiser, and T.D. Pollard. 2000. Direct observation of dendritic actin filament networks nucleated by Arp2/3 complex and WASP/Scar proteins. *Nature*. 404:1007-1011.
- Blanchoin, L., R. Boujemaa-Paterski, C. Sykes, and J. Plastino. 2014. Actin dynamics, architecture, and mechanics in cell motility. *Physiological Reviews*. 94:235-263.
- Blanchoin, L., T.D. Pollard, and S.E. Hitchcock-DeGregori. 2001. Inhibition of the Arp2/3 complex-nucleated actin polymerization and branch formation by tropomyosin. *Current Biology*. 11:1300-1304.

- Block, J., D. Breitsprecher, S. Kuhn, M. Winterhoff, F. Kage, R. Geffers, P. Duwe, J.L. Rohn, B. Baum, C. Brakebusch, M. Geyer, T.E. Stradal, J. Faix, and K. Rottner. 2012. FMNL2 drives actin-based protrusion and migration downstream of Cdc42. *Current Biology*. 22:1005-1012.
- Boerner, K., E. Kienle, A. Sacher, L.-Y. Huang, M. Bechtle, E. Wiedtke, P. Bayer, H.-G. Kräusslich, M. Agbandje-McKenna, and D. Grimm. 2015. 307. Rational Development of 12 Different AAV Serotypes as Scaffolds for Peptide Display. *Molecular Therapy*. 23:S124.
- Borgonovo, B., J. Ouwendijk, and M. Solimena. 2006. Biogenesis of secretory granules. *Current Opinion in Cell Biology*. 18:365-370.
- Borisy, G.G., and T.M. Svitkina. 2000. Actin machinery: pushing the envelope. *Current opinion in cell biology*. 12:104-112.
- Bouard, D., N. Alazard-Dany, and F.L. Cosset. 2009. Viral vectors: from virology to transgene expression. *British Journal of Pharmacology*. 157:153-165.
- Boussif, O., F. Lezoualc'h, M.A. Zanta, M.D. Mergny, D. Scherman, B. Demeneix, and J.-P. Behr. 1995. A versatile vector for gene and oligonucleotide transfer into cells in culture and in vivo: polyethylenimine. *Proceedings of the National Academy of Sciences*. 92:7297-7301.
- Bovellan, M., Y. Romeo, M. Biro, A. Boden, P. Chugh, A. Yonis, M. Vaghela, M. Fritzsche, D. Moulding, and R. Thorogate. 2014. Cellular control of cortical actin nucleation. *Current Biology*. 24:1628-1635.
- Brayford, S., N.S. Bryce, G. Schevzov, E.M. Haynes, J.E. Bear, E.C. Hardeman, and P.W. Gunning. 2016. Tropomyosin promotes lamellipodial persistence by collaborating with Arp2/3 at the leading edge. *Current Biology*. 26:1312-1318.
- Brooker, H.R., M.A. Geeves, and D.P. Mulvihill. 2016. Analysis of biophysical and functional consequences of tropomyosin-fluorescent protein fusions. *FEBS Letters*. 590:3111-3121.
- Brown, A.M., A.J. O'Sullivan, and B.D. Gomperts. 1998. Induction of exocytosis from permeabilized mast cells by the guanosine triphosphatases Rac and Cdc42. *Molecular Biology of the Cell*. 9:1053-1063.
- Brunner, S., T. Sauer, S. Carotta, M. Cotten, M. Saltik, and E. Wagner. 2000. Cell cycle dependence of gene transfer by lipoplex, polyplex and recombinant adenovirus. *Gene Therapy*. 7:401-407.
- Bryce, N.S., G. Schevzov, V. Ferguson, J.M. Percival, J.J. Lin, F. Matsumura, J.R. Bamburg, P.L. Jeffrey, E.C. Hardeman, P. Gunning, and R.P. Weinberger. 2003. Specification of actin filament function and molecular composition by tropomyosin isoforms. *Molecular Biology of the Cell*. 14:1002-1016.
- Bubb, M.R., I. Spector, B.B. Beyer, and K.M. Fosen. 2000. Effects of Jasplakinolide on the Kinetics of Actin Polymerization: AN EXPLANATION FOR CERTAIN IN VIVO OBSERVATIONS. *Journal of Biological Chemistry*. 275:5163-5170.
- Bugyi, B., and M.-F. Carlier. 2010. Control of actin filament treadmilling in cell motility. *Annual Review of Biophysics*. 39:449-470.
- Bugyi, B., G. Papp, G. Hild, D. Lőrinczy, E.M. Nevalainen, P. Lappalainen, B. Somogyi, and M. Nyitrai. 2006. Formins regulate actin filament flexibility through long range allosteric interactions. *Journal of Biological Chemistry*. 281:10727-10736.
- Burgoyne, R.D., and A. Morgan. 2003. Secretory granule exocytosis. *Physiological Reviews*. 83:581-632.
- Campellone, K.G., and M.D. Welch. 2010. A nucleator arms race: cellular control of actin assembly. *Nature reviews Molecular Cell Biology*. 11:237-251.

- Carlsson, L., L.-E. Nyström, I. Sundkvist, F. Markey, and U. Lindberg. 1977. Actin polymerizability is influenced by profilin, a low molecular weight protein in non-muscle cells. *Journal of Molecular Biology*. 115:465-483.
- Chalovich, J.M., P.B. Chock, and E. Eisenberg. 1981. Mechanism of action of troponin. tropomyosin. Inhibition of actomyosin ATPase activity without inhibition of myosin binding to actin. *Journal of Biological Chemistry*. 256:575-578.
- Chang, F. 1999. Movement of a cytokinesis factor cdc12p to the site of cell division. *Current Biology*. 9:849-852.
- Cheek, T.R. 1991. Calcium signalling and the triggering of secretion in adrenal chromaffin cells. *Pharmacology & Therapeutics*. 52:173-189.
- Cheek, T.R., and R.D. Burgoyne. 1986. Nicotine-evoked disassembly of cortical actin filaments in adrenal chromaffin cells. *FEBS Letters*. 207:110-114.
- Chirmule, N., K. Propert, S. Magosin, Y. Qian, R. Qian, and J. Wilson. 1999. Immune responses to adenovirus and adeno-associated virus in humans. *Gene therapy*. 6.
- Cho, Y.J., J. Liu, and S.E. Hitchcock-DeGregori. 1990. The amino terminus of muscle tropomyosin is a major determinant for function. *The Journal of Biological Chemistry*. 265:538-545.
- Choi, C.K., M. Vicente-Manzanares, J. Zareno, L.A. Whitmore, A. Mogilner, and A.R. Horwitz. 2008. Actin and  $\alpha$ -actinin orchestrate the assembly and maturation of nascent adhesions in a myosin II motor-independent manner. *Nature Cell Biology*. 10:1039-1050.
- Chorev, D.S., O. Moscovitz, B. Geiger, and M. Sharon. 2014. Regulation of focal adhesion formation by a vinculin-Arp2/3 hybrid complex. *Nature Communications*. 5:3758.
- Cockrell, A.S., and T. Kafri. 2007. Gene delivery by lentivirus vectors. *Molecular Biotechnology*. 36:184-204.
- Coscoy, S., F. Waharte, A. Gautreau, M. Martin, D. Louvard, P. Mangeat, M. Arpin, and F. Amblard. 2002. Molecular analysis of microscopic ezrin dynamics by two-photon FRAP. *Proceedings of the National Academy of Sciences*. 99:12813-12818.
- Courson, D.S., and R.S. Rock. 2010. Actin cross-link assembly and disassembly mechanics for  $\alpha$ -actinin and fascin. *Journal of Biological Chemistry*. 285:26350-26357.
- Dai, Y., E.M. Schwarz, D. Gu, W.-W. Zhang, N. Sarvetnick, and I.M. Verma. 1995. Cellular and humoral immune responses to adenoviral vectors containing factor IX gene: tolerization of factor IX and vector antigens allows for long-term expression. *Proceedings of the National Academy of Sciences*. 92:1401-1405.
- DeMali, K.A., C.A. Barlow, and K. Burridge. 2002. Recruitment of the Arp2/3 complex to vinculin. *The Journal of Cell Biology*. 159:881-891.
- DesMarais, V., I. Ichetovkin, J. Condeelis, and S.E. Hitchcock-DeGregori. 2002. Spatial regulation of actin dynamics: a tropomyosin-free, actin-rich compartment at the leading edge. *Journal of Cell Science*. 115:4649-4660.
- Di Paolo, G., and P. De Camilli. 2006. Phosphoinositides in cell regulation and membrane dynamics. *Nature*. 443:651-657.
- Dominguez, R., and K.C. Holmes. 2011. Actin structure and function. *Annual Review of Biophysics*. 40:169-186.
- Erami, Z., D. Herrmann, S.C. Warren, M. Nobis, E.J. McGhee, M.C. Lucas, W. Leung, N. Reischmann, A. Mrowinska, and J.P. Schwarz. 2016. Intravital FRAP imaging using an E-cadherin-GFP mouse reveals disease- and drug-dependent dynamic regulation of cell-cell junctions in live tissue. *Cell Reports*. 14:152-167.
- Eskelinen, E.-L. 2005. Maturation of autophagic vacuoles in mammalian cells. *Autophagy*. 1:1-10.

- Evangelista, M., K. Blundell, M.S. Longtine, C.J. Chow, N. Adames, J.R. Pringle, M. Peter, and C. Boone. 1997. Bni1p, a yeast formin linking cdc42p and the actin cytoskeleton during polarized morphogenesis. *Science*. 276:118-122.
- Evangelista, M., D. Pruyne, D.C. Amberg, C. Boone, and A. Bretscher. 2002. Formins direct Arp2/3-independent actin filament assembly to polarize cell growth in yeast. *Nature Cell Biology*. 4:32-41.
- Falzone, T.T., M. Lenz, D.R. Kovar, and M.L. Gardel. 2012. Assembly kinetics determine the architecture of  $\alpha$ -actinin crosslinked F-actin networks. *Nature Communications*. 3:861.
- Fleming, J., S.L. Ginn, R.P. Weinberger, T.N. Trahair, J.A. Smythe, and I.E. Alexander. 2001. Adeno-associated virus and lentivirus vectors mediate efficient and sustained transduction of cultured mouse and human dorsal root ganglia sensory neurons. *Human Gene Therapy*. 12:77-86.
- Fritzsche, M., C. Erenkämper, E. Moendarbary, G. Charras, and K. Kruse. 2016. Actin kinetics shapes cortical network structure and mechanics. *Science Advances*. 2:e1501337.
- Fritzsche, M., A. Lewalle, T. Duke, K. Kruse, and G. Charras. 2013. Analysis of turnover dynamics of the submembranous actin cortex. *Molecular Biology of the Cell*. 24:757-767.
- Ganguly, A., Y. Tang, L. Wang, K. Ladit, J. Loi, B. Dargent, C. Leterrier, and S. Roy. 2015. A dynamic formin-dependent deep F-actin network in axons. *The Journal of Cell Biology*. 210:401-417.
- Gao, X., and L. Huang. 1991. A novel cationic liposome reagent for efficient transfection of mammalian cells. *Biochemical and Biophysical Research Communications*. 179:280-285.
- Gasman, S., S. Chasserot-Golaz, M. Malacombe, M. Way, and M.-F. Bader. 2004. Regulated exocytosis in neuroendocrine cells: a role for subplasmalemmal Cdc42/N-WASP-induced actin filaments. *Molecular Biology of the Cell*. 15:520-531.
- Gasman, S., S. Chasserot-Golaz, M.R. Popoff, D. Aunis, and M.-F. Bader. 1999. Involvement of Rho GTPases in calcium-regulated exocytosis from adrenal chromaffin cells. *Journal of Cell Science*. 112:4763-4771.
- Gateva, G., E. Kremneva, T. Reindl, T. Kotila, K. Kogan, L. Gressin, P.W. Gunning, D.J. Manstein, A. Michelot, and P. Lappalainen. 2017. Tropomyosin isoforms specify functionally distinct actin filament populations in vitro. *Current Biology*. 27:705-713.
- Gauthier, N.C., T.A. Masters, and M.P. Sheetz. 2012. Mechanical feedback between membrane tension and dynamics. *Trends in Cell Biology*. 22:527-535.
- Geeves, M.A., S.E. Hitchcock-DeGregori, and P.W. Gunning. 2015. A systematic nomenclature for mammalian tropomyosin isoforms. *Journal of Muscle Research and Cell Motility*. 36:147-153.
- Geiger, B., K. Tokuyasu, A.H. Dutton, and S. Singer. 1980. Vinculin, an intracellular protein localized at specialized sites where microfilament bundles terminate at cell membranes. *Proceedings of the National Academy of Sciences*. 77:4127-4131.
- Giner, D., I. Lopez, J. Villanueva, V. Torres, S. Viniestra, and L. Gutierrez. 2007. Vesicle movements are governed by the size and dynamics of F-actin cytoskeletal structures in bovine chromaffin cells. *Neuroscience*. 146:659-669.
- Giner, D., P. Neco, M. del Mar Francés, I. López, S. Viniestra, and L.M. Gutiérrez. 2005. Real-time dynamics of the F-actin cytoskeleton during secretion from chromaffin cells. *Journal of Cell Science*. 118:2871-2880.
- Gleich, G.J., and C.R. Adolphson. 1986. The eosinophilic leukocyte: structure and function. *Advances in Immunology*. 39:177-253.

- Goley, E.D., and M.D. Welch. 2006. The ARP2/3 complex: an actin nucleator comes of age. *Nature reviews Molecular Cell Biology*. 7:713-726.
- Goode, B.L., and M.J. Eck. 2007. Mechanism and function of formins in the control of actin assembly. *Annual Review of Biochemistry*. 76:593-627.
- Greenfield, N.J., G.V. Swapna, Y. Huang, T. Palm, S. Graboski, G.T. Montelione, and S.E. Hitchcock-DeGregori. 2003. The structure of the carboxyl terminus of striated alpha-tropomyosin in solution reveals an unusual parallel arrangement of interacting alpha-helices. *Biochemistry*. 42:614-619.
- Gunning, P., G. O'Neill, and E. Hardeman. 2008. Tropomyosin-based regulation of the actin cytoskeleton in time and space. *Physiological Reviews*. 88:1-35.
- Gunning, P.W., U. Ghoshdastider, S. Whitaker, D. Popp, and R.C. Robinson. 2015a. The evolution of compositionally and functionally distinct actin filaments. *Journal of Cell Science*. 128:2009-2019.
- Gunning, P.W., E.C. Hardeman, P. Lappalainen, and D.P. Mulvihill. 2015b. Tropomyosin - master regulator of actin filament function in the cytoskeleton. *Journal of Cell Science*. 128:2965-2974.
- Harrach, B., M. Benko, G. Both, M. Brown, A. Davison, M. Echavarría, M. Hess, M. Jones, A. Kajon, and H. Lehmkuhl. 2011. Family adenoviridae. Elsevier: San Diego, CA, USA. 95-111.
- Harris, E.S., T.J. Gauvin, E.G. Heimsath, and H.N. Higgs. 2010. Assembly of filopodia by the formin FRL2 (FMNL3). *Cytoskeleton*. 67:755-772.
- Harris, E.S., I. Rouiller, D. Hanein, and H.N. Higgs. 2006. Mechanistic differences in actin bundling activity of two mammalian formins, FRL1 and mDia2. *Journal of Biological Chemistry*. 281:14383-14392.
- He, T.-C., S. Zhou, L.T. Da Costa, J. Yu, K.W. Kinzler, and B. Vogelstein. 1998. A simplified system for generating recombinant adenoviruses. *Proceedings of the National Academy of Sciences*. 95:2509-2514.
- Heald, R.W., and S.E. Hitchcock-DeGregori. 1988. The structure of the amino terminus of tropomyosin is critical for binding to actin in the absence and presence of troponin. *The Journal of Biological Chemistry*. 263:5254-5259.
- Heimsath, E.G., and H.N. Higgs. 2012. The C terminus of formin FMNL3 accelerates actin polymerization and contains a WH2 domain-like sequence that binds both monomers and filament barbed ends. *Journal of Biological Chemistry*. 287:3087-3098.
- Helfman, D.M., J.R. Feramisco, W.M. Ricci, and S.H. Hughes. 1984. Isolation and sequence of a cDNA clone that contains the entire coding region for chicken smooth-muscle alpha-tropomyosin. *The Journal of Biological Chemistry*. 259:14136-14143.
- Hermens, W.T., and J. Verhaagen. 1998. Suppression of inflammation by dexamethasone prolongs adenoviral vector-mediated transgene expression in the facial nucleus of the rat. *Brain Research Bulletin*. 47:133-140.
- Higashida, C., T. Miyoshi, A. Fujita, F. Oceguera-Yanez, J. Monypenny, Y. Andou, S. Narumiya, and N. Watanabe. 2004. Actin polymerization-driven molecular movement of mDia1 in living cells. *Science*. 303:2007-2010.
- Higgs, H.N. 2005. Formin proteins: a domain-based approach. *Trends in Biochemical Sciences*. 30:342-353.
- Higgs, H.N., and T.D. Pollard. 2000. Activation by Cdc42 and PIP 2 of Wiskott-Aldrich syndrome protein (WASp) stimulates actin nucleation by Arp2/3 complex. *The Journal of Cell Biology*. 150:1311-1320.
- Hoi-Ying, E.Y., and W.M. Bement. 2007. Multiple myosins are required to coordinate actin assembly with coat compression during compensatory endocytosis. *Molecular Biology of the Cell*. 18:4096-4105.

- Holmes, K.C., and W. Lehman. 2008. Gestalt-binding of tropomyosin to actin filaments. *Journal of Muscle Research and Cell Motility*. 29:213-219.
- Holzinger, A. 2010. Jasplakinolide: an actin-specific reagent that promotes actin polymerization. *Cytoskeleton Methods and Protocols*:71-87.
- Honigsmann, A., G. Van Den Bogaart, E. Iraheta, H.J. Risselada, D. Milovanovic, V. Mueller, S. Müllar, U. Diederichsen, D. Fasshauer, and H. Grubmüller. 2013. Phosphatidylinositol 4, 5-bisphosphate clusters act as molecular beacons for vesicle recruitment. *Nature Structural & Molecular Biology*. 20:679-686.
- Hotulainen, P., and P. Lappalainen. 2006. Stress fibers are generated by two distinct actin assembly mechanisms in motile cells. *The Journal of cell biology*. 173:383-394.
- Hsiao, J.Y., L.M. Goins, N.A. Petek, and R.D. Mullins. 2015. Arp2/3 complex and cofilin modulate binding of tropomyosin to branched actin networks. *Current Biology : CB*. 25:1573-1582.
- Hundt, N., W. Steffen, S. Pathan-Chhatbar, M.H. Taft, and D.J. Manstein. 2016. Load-dependent modulation of non-muscle myosin-2A function by tropomyosin 4.2. *Scientific Reports*. 6:20554.
- Isogai, T., R. van der Kammen, D. Leyton-Puig, K.M. Kedziora, K. Jalink, and M. Innocenti. 2015. Initiation of lamellipodia and ruffles involves cooperation between mDia1 and the Arp2/3 complex. *Journal of Cell Science*. 128:3796-3810.
- Jaiswal, R., D. Breitsprecher, A. Collins, I.R. Corrêa, M.-Q. Xu, and B.L. Goode. 2013. The formin Daam1 and fascin directly collaborate to promote filopodia formation. *Current Biology*. 23:1373-1379.
- Jégou, A., M.-F. Carlier, and G. Romet-Lemonne. 2013. Formin mDia1 senses and generates mechanical forces on actin filaments. *Nature communications*. 4:1883.
- Johns, L.M., E.S. Levitan, E.A. Shelden, R.W. Holz, and D. Axelrod. 2001. Restriction of secretory granule motion near the plasma membrane of chromaffin cells. *The Journal of Cell Biology*. 153:177-190.
- Johnson, M., D.A. East, and D.P. Mulvihill. 2014. Formins determine the functional properties of actin filaments in yeast. *Current Biology : CB*. 24:1525-1530.
- Kage, F., M. Winterhoff, V. Dimchev, J. Mueller, T. Thalheim, A. Freise, S. Bruhmann, J. Kollasser, J. Block, G. Dimchev, M. Geyer, H.J. Schnittler, C. Brakebusch, T.E. Stradal, M.F. Carlier, M. Sixt, J. Kas, J. Faix, and K. Rottner. 2017. FMNL formins boost lamellipodial force generation. *Nature communications*. 8:14832.
- Katano, H., M.R. Kok, A.P. Cotrim, S. Yamano, M. Schmidt, S. Afione, B.J. Baum, and J.A. Chiorini. 2006. Enhanced transduction of mouse salivary glands with AAV5-based vectors. *Gene therapy*. 13:594-601.
- Kay, M.A., J.C. Glorioso, and L. Naldini. 2001. Viral vectors for gene therapy: the art of turning infectious agents into vehicles of therapeutics. *Nature medicine*. 7:33-40.
- Knudsen, K.A., A.P. Soler, K.R. Johnson, and M.J. Wheelock. 1995. Interaction of alpha-actinin with the cadherin/catenin cell-cell adhesion complex via alpha-catenin. *The Journal of cell biology*. 130:67-77.
- Korn, E.D. 1982. Actin polymerization and its regulation by proteins from nonmuscle cells. *Physiological reviews*. 62:672-737.
- Kovar, D.R. 2006. Molecular details of formin-mediated actin assembly. *Current opinion in cell biology*. 18:11-17.
- Kovar, D.R., E.S. Harris, R. Mahaffy, H.N. Higgs, and T.D. Pollard. 2006. Control of the assembly of ATP- and ADP-actin by formins and profilin. *Cell*. 124:423-435.
- Kowluru, A., G. Li, M.E. Rabaglia, V.B. Segu, F. Hofmann, K. Aktories, and S.A. Metz. 1997. Evidence for differential roles of the Rho subfamily of GTP-binding proteins in glucose- and calcium-induced insulin secretion from pancreatic  $\beta$  cells. *Biochemical pharmacology*. 54:1097-1108.

- Krause, M., and A. Gautreau. 2014. Steering cell migration: lamellipodium dynamics and the regulation of directional persistence. *Nature reviews Molecular cell biology*. 15:577-590.
- Kuhn, J.R., and T.D. Pollard. 2005. Real-time measurements of actin filament polymerization by total internal reflection fluorescence microscopy. *Biophysical journal*. 88:1387-1402.
- Lam, A.J., F. St-Pierre, Y. Gong, J.D. Marshall, P.J. Cranfill, M.A. Baird, M.R. McKeown, J. Wiedenmann, M.W. Davidson, M.J. Schnitzer, R.Y. Tsien, and M.Z. Lin. 2012. Improving FRET dynamic range with bright green and red fluorescent proteins. *Nature methods*. 9:1005-1012.
- Lazarides, E. 1976. Actin, alpha-actinin, and tropomyosin interaction in the structural organization of actin filaments in nonmuscle cells. *The Journal of cell biology*. 68:202-219.
- Lee, R., and J. Trifaró. 1981. Characterization of anti-actin antibodies and their use in immunocytochemical studies on the localization of actin in adrenal chromaffin cells in culture. *Neuroscience*. 6:2087-2108.
- Li, F., and H.N. Higgs. 2003. The mouse Formin mDia1 is a potent actin nucleation factor regulated by autoinhibition. *Current biology*. 13:1335-1340.
- Li, F., and H.N. Higgs. 2005. Dissecting requirements for auto-inhibition of actin nucleation by the formin, mDia1. *Journal of Biological Chemistry*. 280:6986-6992.
- Li, S., M. Rizzo, S. Bhattacharya, and L. Huang. 1998. Characterization of cationic lipid-protamine-DNA (LPD) complexes for intravenous gene delivery. *Gene therapy*. 5.
- Li, Y., S. Mui, J.H. Brown, J. Strand, L. Reshetnikova, L.S. Tobacman, and C. Cohen. 2002. The crystal structure of the C-terminal fragment of striated-muscle alpha-tropomyosin reveals a key troponin T recognition site. *Proceedings of the National Academy of Sciences of the United States of America*. 99:7378-7383.
- Liou, W., H.J. Geuze, M.J. Geelen, and J.W. Slot. 1997. The autophagic and endocytic pathways converge at the nascent autophagic vacuoles. *The Journal of cell biology*. 136:61-70.
- Long, C., L. Amoasii, A.A. Mireault, J.R. McAnally, H. Li, E. Sanchez-Ortiz, S. Bhattacharyya, J.M. Shelton, R. Bassel-Duby, and E.N. Olson. 2016. Postnatal genome editing partially restores dystrophin expression in a mouse model of muscular dystrophy. *Science*. 351:400-403.
- Longtine, M.S., D.J. DeMarini, M.L. Valencik, O.S. Al-Awar, H. Fares, C. De Virgilio, and J.R. Pringle. 1996. The septins: roles in cytokinesis and other processes. *Current opinion in cell biology*. 8:106-119.
- Lv, H., S. Zhang, B. Wang, S. Cui, and J. Yan. 2006. Toxicity of cationic lipids and cationic polymers in gene delivery. *Journal of Controlled Release*. 114:100-109.
- Machesky, L.M., R.D. Mullins, H.N. Higgs, D.A. Kaiser, L. Blanchoin, R.C. May, M.E. Hall, and T.D. Pollard. 1999. Scar, a WASp-related protein, activates nucleation of actin filaments by the Arp2/3 complex. *Proceedings of the National Academy of Sciences of the United States of America*. 96:3739-3744.
- Machesky, L.M., E. Reeves, F. Wientjes, F.J. Mattheyse, A. Grogan, N.F. Totty, A.L. Burlingame, J.J. Hsuan, and A.W. Segal. 1997. Mammalian actin-related protein 2/3 complex localizes to regions of lamellipodial protrusion and is composed of evolutionarily conserved proteins. *The Biochemical journal*. 328 ( Pt 1):105-112.
- Maiti, S., A. Michelot, C. Gould, L. Blanchoin, O. Sokolova, and B.L. Goode. 2012. Structure and activity of full-length formin mDia1. *Cytoskeleton*. 69:393-405.
- Manstein, D.J., and D.P. Mulvihill. 2016a. Tropomyosin-Mediated Regulation of Cytoplasmic Myosins. *Traffic*. 17:872-877.

- Manstein, D.J., and D.P. Mulvihill. 2016b. Tropomyosin-Mediated Regulation of Cytoplasmic Myosins. *Traffic*. 17:872-877.
- Martin, C., G. Schevzov, and P. Gunning. 2010. Alternatively spliced N-terminal exons in tropomyosin isoforms do not act as autonomous targeting signals. *Journal of structural biology*. 170:286-293.
- Masedunskas, A., M. Appaduray, E.C. Hardeman, and P.W. Gunning. 2013a. What makes a model system great? A case for intravital microscopy for studying the actin cytoskeleton. *IntraVital*. 2:e26287.
- Masedunskas, A., O. Milberg, N. Porat-Shliom, M. Sramkova, T. Wigand, P. Amornphimoltham, and R. Weigert. 2012a. Intravital microscopy: a practical guide on imaging intracellular structures in live animals. *Bioarchitecture*. 2:143-157.
- Masedunskas, A., N. Porat-Shliom, and R. Weigert. 2012b. Regulated exocytosis: novel insights from intravital microscopy. *Traffic*. 13:627-634.
- Masedunskas, A., M. Sramkova, L. Parente, K.U. Sales, P. Amornphimoltham, T.H. Bugge, and R. Weigert. 2011a. Role for the actomyosin complex in regulated exocytosis revealed by intravital microscopy. *Proceedings of the National Academy of Sciences of the United States of America*. 108:13552-13557.
- Masedunskas, A., M. Sramkova, L. Parente, and R. Weigert. 2013b. Intravital microscopy to image membrane trafficking in live rats. *Methods in molecular biology*. 931:153-167.
- Masedunskas, A., M. Sramkova, and R. Weigert. 2011b. Homeostasis of the apical plasma membrane during regulated exocytosis in the salivary glands of live rodents. *Bioarchitecture*. 1:225-229.
- Masedunskas, A., and R. Weigert. 2008. Intravital two-photon microscopy for studying the uptake and trafficking of fluorescently conjugated molecules in live rodents. *Traffic*. 9:1801-1810.
- Maucort, G., R. Kasula, A. Papadopulos, T.A. Nieminen, H. Rubinsztein-Dunlop, and F.A. Meunier. 2014. Mapping organelle motion reveals a vesicular conveyor belt spatially replenishing secretory vesicles in stimulated chromaffin cells. *PloS one*. 9:e87242.
- Meunier, F.A., and L.M. Gutiérrez. 2016. Captivating new roles of F-actin cortex in exocytosis and bulk endocytosis in neurosecretory cells. *Trends in neurosciences*. 39:605-613.
- Miklavc, P., K. Ehinger, A. Sultan, T. Felder, P. Paul, K.E. Gottschalk, and M. Frick. 2015. Actin depolymerisation and crosslinking join forces with myosin II to contract actin coats on fused secretory vesicles. *Journal of cell science*. 128:1193-1203.
- Miklavc, P., E. Hecht, N. Hobi, O.H. Wittekindt, P. Dietl, C. Kranz, and M. Frick. 2012. Actin coating and compression of fused secretory vesicles are essential for surfactant secretion--a role for Rho, formins and myosin II. *Journal of cell science*. 125:2765-2774.
- Miller, F., E. de Harven, and G.E. Palade. 1966. The structure of eosinophil leukocyte granules in rodents and in man. *The Journal of cell biology*. 31:349-362.
- Milosevic, I., J.B. Sørensen, T. Lang, M. Krauss, G. Nagy, V. Haucke, R. Jahn, and E. Neher. 2005. Plasmalemmal phosphatidylinositol-4, 5-bisphosphate level regulates the releasable vesicle pool size in chromaffin cells. *Journal of Neuroscience*. 25:2557-2565.
- Mullins, R.D., and S.D. Hansen. 2013. In vitro studies of actin filament and network dynamics. *Current opinion in cell biology*. 25:6-13.
- Mullins, R.D., J.A. Heuser, and T.D. Pollard. 1998. The interaction of Arp2/3 complex with actin: nucleation, high affinity pointed end capping, and formation of branching networks of filaments. *Proceedings of the National Academy of Sciences of the United States of America*. 95:6181-6186.

- Murakoshi, H., S.-J. Lee, and R. Yasuda. 2008. Highly sensitive and quantitative FRET–FLIM imaging in single dendritic spines using improved non-radiative YFP. *Brain cell biology*. 36:31-42.
- Muruve, D.A. 2004. The innate immune response to adenovirus vectors. *Human gene therapy*. 15:1157-1166.
- Muzumdar, M.D., B. Tasic, K. Miyamichi, L. Li, and L. Luo. 2007. A global double-fluorescent Cre reporter mouse. *Genesis*. 45:593-605.
- Naldini, L., U. Blomer, P. Gallay, D. Ory, R. Mulligan, F.H. Gage, I.M. Verma, and D. Trono. 1996. In vivo gene delivery and stable transduction of nondividing cells by a lentiviral vector. *Science*. 272:263-267.
- Nayak, S., and R.W. Herzog. 2010. Progress and prospects: immune responses to viral vectors. *Gene therapy*. 17:295-304.
- Ñeco, P., C. Fernández-Peruchena, S. Navas, L.M. Gutiérrez, G.Á. de Toledo, and E. Alés. 2008. Myosin II contributes to fusion pore expansion during exocytosis. *Journal of Biological Chemistry*. 283:10949-10957.
- Ñeco, P., D. Giner, S. Viniestra, R. Borges, A. Villarreal, and L.M. Gutiérrez. 2004. New roles of myosin II during vesicle transport and fusion in chromaffin cells. *Journal of Biological Chemistry*. 279:27450-27457.
- Nightingale, T.D., I.J. White, E.L. Doyle, M. Turmaine, K.J. Harrison-Lavoie, K.F. Webb, L.P. Cramer, and D.F. Cutler. 2011. Actomyosin II contractility expels von Willebrand factor from Weibel–Palade bodies during exocytosis. *The Journal of cell biology:jcb*. 201011119.
- Novy, R.E., J.R. Sellers, L.F. Liu, and J.J.C. Lin. 1993. In vitro functional characterization of bacterially expressed human fibroblast tropomyosin isoforms and their chimeric mutants. *Cytoskeleton*. 26:248-261.
- O’Connell, M.R., B.L. Oakes, S.H. Sternberg, A. East-Seletsky, M. Kaplan, and J.A. Doudna. 2014. Programmable RNA recognition and cleavage by CRISPR/Cas9. *Nature*. 516:263-266.
- Oheim, M., D. Loerke, W. Stühmer, and R.H. Chow. 1998. The last few milliseconds in the life of a secretory granule. *European biophysics journal*. 27:83-98.
- Orci, L., K. Gabbay, and W. Malaisse. 1972. Pancreatic beta-cell web: its possible role in insulin secretion. *Science*. 175:1128-1130.
- Otomo, T., C. Otomo, D.R. Tomchick, M. Machius, and M.K. Rosen. 2005a. Structural basis of Rho GTPase-mediated activation of the formin mDia1. *Molecular cell*. 18:273-281.
- Otomo, T., D.R. Tomchick, C. Otomo, S.C. Panchal, M. Machius, and M.K. Rosen. 2005b. Structural basis of actin filament nucleation and processive capping by a formin homology 2 domain. *Nature*. 433:488-494.
- Paavilainen, V.O., E. Bertling, S. Falck, and P. Lappalainen. 2004. Regulation of cytoskeletal dynamics by actin-monomer-binding proteins. *Trends in cell biology*. 14:386-394.
- Palm, T., N.J. Greenfield, and S.E. Hitchcock-DeGregori. 2003. Tropomyosin ends determine the stability and functionality of overlap and troponin T complexes. *Biophysical journal*. 84:3181-3189.
- Papadopoulos, A., G.A. Gomez, S. Martin, J. Jackson, R.S. Gormal, D.J. Keating, and F.A. Meunier. 2015. Activity-driven relaxation of the cortical actomyosin II network synchronizes Munc18-1-dependent neurosecretory vesicle docking. *Nature communications*. 6.
- Paul, A.S., and T.D. Pollard. 2009. Review of the mechanism of processive actin filament elongation by formins. *Cytoskeleton*. 66:606-617.
- Pelham Jr, R.J., and F. Chang. 2002. Actin dynamics in the contractile ring during cytokinesis in fission yeast. *Nature*. 419:82.

- Pellegrin, S., and H. Mellor. 2005a. The Rho family GTPase Rif induces filopodia through mDia2. *Current biology : CB*. 15:129-133.
- Pellegrin, S., and H. Mellor. 2005b. The Rho family GTPase Rif induces filopodia through mDia2. *Current Biology*. 15:129-133.
- Perrin, B.J., and J.M. Ervasti. 2010. The actin gene family: function follows isoform. *Cytoskeleton*. 67:630-634.
- Pfender, S., V. Kuznetsov, S. Pleiser, E. Kerkhoff, and M. Schuh. 2011. Spire-type actin nucleators cooperate with Formin-2 to drive asymmetric oocyte division. *Current biology : CB*. 21:955-960.
- Pinto, I.M., B. Rubinstein, and R. Li. 2013. Force to divide: structural and mechanical requirements for actomyosin ring contraction. *Biophysical journal*. 105:547-554.
- Piras, B.A., D.M. O'Connor, and B.A. French. 2013. Systemic delivery of shRNA by AAV9 provides highly efficient knockdown of ubiquitously expressed GFP in mouse heart, but not liver. *PloS one*. 8:e75894.
- Pires, P., S. Simões, S. Nir, R. Gaspar, N. Düzgünes, and M.C.P. de Lima. 1999. Interaction of cationic liposomes and their DNA complexes with monocytic leukemia cells. *Biochimica et Biophysica Acta (BBA)-Biomembranes*. 1418:71-84.
- Pittenger, M.F., and D.M. Helfman. 1992. In vitro and in vivo characterization of four fibroblast tropomyosins produced in bacteria: TM-2, TM-3, TM-5a, and TM-5b are co-localized in interphase fibroblasts. *The Journal of cell biology*. 118:841-858.
- Pizarro-Cerda, J., D.S. Chorev, B. Geiger, and P. Cossart. 2017. The Diverse Family of Arp2/3 Complexes. *Trends in cell biology*. 27:93-100.
- Pollard, T.D. 1986. Rate constants for the reactions of ATP- and ADP-actin with the ends of actin filaments. *The Journal of cell biology*. 103:2747-2754.
- Pollard, T.D. 2016. Actin and Actin-Binding Proteins. *Cold Spring Harbor perspectives in biology*. 8.
- Pollard, T.D., L. Blanchoin, and R.D. Mullins. 2000. Molecular mechanisms controlling actin filament dynamics in nonmuscle cells. *Annual review of biophysics and biomolecular structure*. 29:545-576.
- Pollard, T.D., and G.G. Borisy. 2003. Cellular motility driven by assembly and disassembly of actin filaments. *Cell*. 112:453-465.
- Pollard, T.D., and J.-Q. Wu. 2010. Understanding cytokinesis: lessons from fission yeast. *Nature reviews. Molecular cell biology*. 11:149.
- Ponti, A., M. Machacek, S.L. Gupton, C.M. Waterman-Storer, and G. Danuser. 2004. Two distinct actin networks drive the protrusion of migrating cells. *Science*. 305:1782-1786.
- Porat-Shliom, N., O. Milberg, A. Masedunskas, and R. Weigert. 2013. Multiple roles for the actin cytoskeleton during regulated exocytosis. *Cellular and molecular life sciences : CMLS*. 70:2099-2121.
- Pring, M., M. Evangelista, C. Boone, C. Yang, and S.H. Zigmond. 2003. Mechanism of formin-induced nucleation of actin filaments. *Biochemistry*. 42:486-496.
- Ramalingam, N., C. Franke, E. Jaschinski, M. Winterhoff, Y. Lu, S. Brühmann, A. Junemann, H. Meier, A.A. Noegel, and I. Weber. 2015. A resilient formin-derived cortical actin meshwork in the rear drives actomyosin-based motility in 2D confinement. *Nature communications*. 6.
- Ramalingam, N., H. Zhao, D. Breitsprecher, P. Lappalainen, J. Faix, and M. Schleicher. 2010. Phospholipids regulate localization and activity of mDia1 formin. *European journal of cell biology*. 89:723-732.
- Reits, E.A., and J.J. Neefjes. 2001. From fixed to FRAP: measuring protein mobility and activity in living cells. *Nature cell biology*. 3:E145-147.

- Ridley, A.J. 2015. Rho GTPase signalling in cell migration. *Current opinion in cell biology*. 36:103-112.
- Riedl, J., A.H. Crevenna, K. Kessenbrock, J.H. Yu, D. Neukirchen, M. Bista, F. Bradke, D. Jenne, T.A. Holak, Z. Werb, M. Sixt, and R. Wedlich-Soldner. 2008. Lifeact: a versatile marker to visualize F-actin. *Nature methods*. 5:605-607.
- Riedl, J., K.C. Flynn, A. Raducanu, F. Gärtner, G. Beck, M. Bösl, F. Bradke, S. Massberg, A. Aszodi, and M. Sixt. 2010. Lifeact mice for studying F-actin dynamics. *Nature methods*. 7:168-169.
- Robinson, R.C., K. Turbedsky, D.A. Kaiser, J.-B. Marchand, H.N. Higgs, S. Choe, and T.D. Pollard. 2001. Crystal structure of Arp2/3 complex. *Science*. 294:1679-1684.
- Rohatgi, R., L. Ma, H. Miki, M. Lopez, T. Kirchhausen, T. Takenawa, and M.W. Kirschner. 1999. The interaction between N-WASP and the Arp2/3 complex links Cdc42-dependent signals to actin assembly. *Cell*. 97:221-231.
- Rose, R., M. Weyand, M. Lammers, T. Ishizaki, M.R. Ahmadian, and A. Wittinghofer. 2005. Structural and mechanistic insights into the interaction between Rho and mammalian Dia. *Nature*. 435:513-518.
- Rottner, K., J. Hänisch, and K.G. Campellone. 2010. WASH, WHAMM and JMY: regulation of Arp2/3 complex and beyond. *Trends in cell biology*. 20:650-661.
- Rotty, J.D., C. Wu, and J.E. Bear. 2013. New insights into the regulation and cellular functions of the ARP2/3 complex. *Nature reviews. Molecular cell biology*. 14:7-12.
- Rouiller, I., X.-P. Xu, K.J. Amann, C. Egile, S. Nickell, D. Nicastro, R. Li, T.D. Pollard, N. Volkmann, and D. Hanein. 2008. The structural basis of actin filament branching by the Arp2/3 complex. *The Journal of cell biology*. 180:887-895.
- Rubin, R. 1970. The role of calcium in the release of neurotransmitter substances and hormones. *Pharmacological Reviews*. 22:389-428.
- Rudolf, R., T. Kögel, S.A. Kuznetsov, T. Salm, O. Schlicker, A. Hellwig, J.A. Hammer, and H.-H. Gerdes. 2003. Myosin Va facilitates the distribution of secretory granules in the F-actin rich cortex of PC12 cells. *Journal of cell science*. 116:1339-1348.
- Rudolf, R., T. Salm, A. Rustom, and H.-H. Gerdes. 2001. Dynamics of immature secretory granules: role of cytoskeletal elements during transport, cortical restriction, and F-actin-dependent tethering. *Molecular biology of the cell*. 12:1353-1365.
- Sanders, C., and L.B. Smillie. 1985. Amino acid sequence of chicken gizzard beta-tropomyosin. Comparison of the chicken gizzard, rabbit skeletal, and equine platelet tropomyosins. *The Journal of biological chemistry*. 260:7264-7275.
- Sarmiento, C., W. Wang, A. Dovas, H. Yamaguchi, M. Sidani, M. El-Sibai, V. Desmarais, H.A. Holman, S. Kitchen, J.M. Backer, A. Alberts, and J. Condeelis. 2008. WASP family members and formin proteins coordinate regulation of cell protrusions in carcinoma cells. *The Journal of cell biology*. 180:1245-1260.
- Schevzov, G., T. Fath, B. Vrhovski, N. Vlahovich, S. Rajan, J. Hook, J.E. Joya, F. Lemckert, F. Puttur, J.J. Lin, E.C. Hardeman, D.F. Wiczorek, G.M. O'Neill, and P.W. Gunning. 2008. Divergent regulation of the sarcomere and the cytoskeleton. *The Journal of biological chemistry*. 283:275-283.
- Schevzov, G., B. Vrhovski, N.S. Bryce, S. Elmir, M.R. Qiu, M. O'Neill G, N. Yang, N.M. Verrills, M. Kavallaris, and P.W. Gunning. 2005. Tissue-specific tropomyosin isoform composition. *The journal of histochemistry and cytochemistry : official journal of the Histochemistry Society*. 53:557-570.
- Schevzov, G., S.P. Whittaker, T. Fath, J.J. Lin, and P.W. Gunning. 2011. Tropomyosin isoforms and reagents. *Bioarchitecture*. 1:135-164.
- Schindelin, J., I. Arganda-Carreras, E. Frise, V. Kaynig, M. Longair, T. Pietzsch, S. Preibisch, C. Rueden, S. Saalfeld, and B. Schmid. 2012. Fiji: an open-source platform for biological-image analysis. *Nature methods*. 9:676-682.

- Schirenbeck, A., T. Bretschneider, R. Arasada, M. Schleicher, and J. Faix. 2005. The Diaphanous-related formin dDia2 is required for the formation and maintenance of filopodia. *Nature cell biology*. 7:619-625.
- Schuh, M. 2011. An actin-dependent mechanism for long-range vesicle transport. *Nature cell biology*. 13:1431-1436.
- Shaner, N.C., G.G. Lambert, A. Chammas, Y. Ni, P.J. Cranfill, M.A. Baird, B.R. Sell, J.R. Allen, R.N. Day, M. Israelsson, M.W. Davidson, and J. Wang. 2013. A bright monomeric green fluorescent protein derived from *Branchiostoma lanceolatum*. *Nature methods*. 10:407-409.
- Simoës, S., V. Slepishkin, P. Pires, R. Gaspar, M. De Lima, and N. Düzgüneş. 1999. Mechanisms of gene transfer mediated by lipoplexes associated with targeting ligands or pH-sensitive peptides. *Gene therapy*. 6.
- Siton-Mendelson, O., and A. Bernheim-Groswasser. 2017. Functional Actin Networks under Construction: The Cooperative Action of Actin Nucleation and Elongation Factors. *Trends in Biochemical Sciences*.
- Skau, C.T., E.M. Neidt, and D.R. Kovar. 2009. Role of tropomyosin in formin-mediated contractile ring assembly in fission yeast. *Molecular biology of the cell*. 20:2160-2173.
- Sobieszek, A., and J. Small. 1977. Regulation of the actin-myosin interaction in vertebrate smooth muscle: activation via a myosin light-chain kinase and the effect of tropomyosin. *Journal of molecular biology*. 112:559-576.
- Sramkova, M., L. Parente, T. Wigand, M.P. Aye, A. Shitara, and R. Weigert. 2014. Polyethylenimine-mediated expression of transgenes in the acinar cells of rats salivary glands in vivo. *Frontiers in cell and developmental biology*. 2:74.
- Stehn, J.R., N.K. Haass, T. Bonello, M. Desouza, G. Kottyan, H. Treutlein, J. Zeng, P.R. Nascimento, V.B. Sequeira, and T.L. Butler. 2013a. A novel class of anticancer compounds targets the actin cytoskeleton in tumor cells. *Cancer research*. 73:5169-5182.
- Stehn, J.R., N.K. Haass, T. Bonello, M. Desouza, G. Kottyan, H. Treutlein, J. Zeng, P.R.B.B. Nascimento, V.B. Sequeira, T.L. Butler, M. Allanson, T. Fath, T.A. Hill, A. McCluskey, G. Schevzov, S.J. Palmer, E.C. Hardeman, D. Winlaw, V.E. Reeve, I. Dixon, W. Weninger, T.P. Cripe, and P.W. Gunning. 2013b. A Novel Class of Anticancer Compounds Targets the Actin Cytoskeleton in Tumor Cells. *Cancer research*. 73:5169-5182.
- Südhof, T.C., and J.E. Rothman. 2009. Membrane fusion: grappling with SNARE and SM proteins. *Science*. 323:474-477.
- Sun, S.X., S. Walcott, and C.W. Wolgemuth. 2010. Cytoskeletal cross-linking and bundling in motor-independent contraction. *Current Biology*. 20:R649-R654.
- Suraneni, P., B. Fogelson, B. Rubinstein, P. Noguera, N. Volkmann, D. Hanein, A. Mogilner, and R. Li. 2015. A mechanism of leading-edge protrusion in the absence of Arp2/3 complex. *Molecular biology of the cell*. 26:901-912.
- Suraneni, P., B. Rubinstein, J.R. Unruh, M. Durnin, D. Hanein, and R. Li. 2012. The Arp2/3 complex is required for lamellipodia extension and directional fibroblast cell migration. *The Journal of cell biology:jcb*. 201112113.
- Svitkina, T.M., and G.G. Borisy. 1999. Arp2/3 complex and actin depolymerizing factor/cofilin in dendritic organization and treadmilling of actin filament array in lamellipodia. *The Journal of cell biology*. 145:1009-1026.
- Takenawa, T., and S. Suetsugu. 2007. The WASP-WAVE protein network: connecting the membrane to the cytoskeleton. *Nature reviews Molecular cell biology*. 8:37-48.

- Takeya, R., K. Taniguchi, S. Narumiya, and H. Sumimoto. 2008. The mammalian formin FHOD1 is activated through phosphorylation by ROCK and mediates thrombin-induced stress fibre formation in endothelial cells. *The EMBO journal*. 27:618-628.
- Tang, V.W., and W.M. Brieher. 2012.  $\alpha$ -Actinin-4/FSGS1 is required for Arp2/3-dependent actin assembly at the adherens junction. *The Journal of cell biology*. 196:115-130.
- Tchakarov, L.E., L. Zhang, S.D. Rosé, R. Tang, and J.-M. Trifaró. 1998. Light and electron microscopic study of changes in the organization of the cortical actin cytoskeleton during chromaffin cell secretion. *Journal of Histochemistry & Cytochemistry*. 46:193-203.
- Thaci, B., I.V. Ulasov, D.A. Wainwright, and M.S. Lesniak. 2011. The challenge for gene therapy: innate immune response to adenoviruses. *Oncotarget*. 2:113-121.
- Theriot, J.A., and T.J. Mitchison. 1991. Actin microfilament dynamics in locomoting cells. *Nature*. 352:126.
- Timiri Shanmugam, P.S., R.D. Dayton, S. Palaniyandi, F. Abreo, G. Caldito, R.L. Klein, and G. Sunavala-Dossabhoy. 2013. Recombinant AAV9-TLK1B administration ameliorates fractionated radiation-induced xerostomia. *Human gene therapy*. 24:604-612.
- Tobacman, L.S. 2008. Cooperative binding of tropomyosin to actin. *Tropomyosin*:85-94.
- Tojkander, S., G. Gateva, G. Schevzov, P. Hotulainen, P. Naumanen, C. Martin, P.W. Gunning, and P. Lappalainen. 2011. A molecular pathway for myosin II recruitment to stress fibers. *Current biology : CB*. 21:539-550.
- Tooze, S.A., and W.B. Huttner. 1990. Cell-free protein sorting to the regulated and constitutive secretory pathways. *Cell*. 60:837-847.
- Torregrosa-Hetland, C.J., J. Villanueva, D. Giner, I. Lopez-Font, A. Nadal, I. Quesada, S. Viniegra, G. Expósito-Romero, A. Gil, and V. Gonzalez-Velez. 2011. The F-actin cortical network is a major factor influencing the organization of the secretory machinery in chromaffin cells. *Journal of cell science*. 124:727-734.
- Tran, D.T., A. Masedunskas, R. Weigert, and K.G. Ten Hagen. 2015. Arp2/3-mediated F-actin formation controls regulated exocytosis in vivo. *Nature communications*. 6:10098.
- Tran, D.T., and K.G. Ten Hagen. 2017. Real-time insights into regulated exocytosis. *Journal of cell science*. 130:1355-1363.
- Trifaró, J.-M., M.-F. Bader, and J.-P. Doucet. 1985. Chromaffin cell cytoskeleton: its possible role in secretion. *Canadian journal of biochemistry and cell biology*. 63:661-679.
- Trifaró, J.-M., and R. Lee. 1980. Morphological characteristics and stimulus-secretion coupling in bovine adrenal chromaffin cell cultures. *Neuroscience*. 5:1533-1546.
- Trifaró, J.-M., M. Vitale, and A.R. Del Castillo. 1992. Cytoskeleton and molecular mechanisms in neurotransmitter release by neurosecretory cells. *European Journal of Pharmacology: Molecular Pharmacology*. 225:83-104.
- Trono, D. 2000. Lentiviral vectors: turning a deadly foe into a therapeutic agent. *Gene therapy*. 7:20-23.
- Ujfalusi, Z., M. Kovacs, N.T. Nagy, S. Barko, G. Hild, A. Lukacs, M. Nyitrai, and B. Bugyi. 2012. Myosin and tropomyosin stabilize the conformation of formin-nucleated actin filaments. *The Journal of biological chemistry*. 287:31894-31904.
- Ujfalusi, Z., A. Vig, G. Hild, and M. Nyitrai. 2009. Effect of tropomyosin on formin-bound actin filaments. *Biophysical journal*. 96:162-168.
- Uruno, T., J. Liu, P. Zhang, Y.-x. Fan, C. Egile, R. Li, S.C. Mueller, and X. Zhan. 2001. Activation of Arp2/3 complex-mediated actin polymerization by cortactin. *Nature cell biology*. 3:259-266.
- Vaillant, D.C., S.J. Copeland, C. Davis, S.F. Thurston, N. Abdennur, and J.W. Copeland. 2008. Interaction of the N-and C-terminal autoregulatory domains of FRL2 does not inhibit FRL2 activity. *Journal of Biological Chemistry*. 283:33750-33762.

- Vavylonis, D., J.-Q. Wu, S. Hao, B. O'shaughnessy, and T.D. Pollard. 2008. Assembly mechanism of the contractile ring for cytokinesis by fission yeast. *Science*. 319:97-100.
- Vinzenz, M., M. Nemethova, F. Schur, J. Mueller, A. Narita, E. Urban, C. Winkler, C. Schmeiser, S.A. Koestler, and K. Rottner. 2012. Actin branching in the initiation and maintenance of lamellipodia. *Journal of cell science*. 125:2775-2785.
- Vitale, M., A.R. Del Castillo, L. Tchakarov, and J. Trifaro. 1991. Cortical filamentous actin disassembly and scinderin redistribution during chromaffin cell stimulation precede exocytosis, a phenomenon not exhibited by gelsolin. *The Journal of cell biology*. 113:1057-1067.
- Vitale, M., E. Seward, and J.-M. Trifaro. 1995. Chromaffin cell cortical actin network dynamics control the size of the release-ready vesicle pool and the initial rate of exocytosis. *Neuron*. 14:353-363.
- Vlahovich, N., A.J. Kee, C. Van der Poel, E. Kettle, D. Hernandez-Deviez, C. Lucas, G.S. Lynch, R.G. Parton, P.W. Gunning, and E.C. Hardeman. 2009. Cytoskeletal tropomyosin Tm5NM1 is required for normal excitation-contraction coupling in skeletal muscle. *Molecular biology of the cell*. 20:400-409.
- von der Ecken, J., M. Muller, W. Lehman, D.J. Manstein, P.A. Penczek, and S. Raunser. 2015. Structure of the F-actin-tropomyosin complex. *Nature*. 519:114-117.
- Walther, W., and U. Stein. 2000. Viral vectors for gene transfer: a review of their use in the treatment of human diseases. *Drugs*. 60:249-271.
- Wang, J., Y. Fan, D.K. Dube, J.M. Sanger, and J.W. Sanger. 2014. Jasplakinolide reduces actin and tropomyosin dynamics during myofibrillogenesis. *Cytoskeleton*. 71:513-529.
- Weaver, A.M., A.V. Karginov, A.W. Kinley, S.A. Weed, Y. Li, J.T. Parsons, and J.A. Cooper. 2001. Cortactin promotes and stabilizes Arp2/3-induced actin filament network formation. *Current Biology*. 11:370-374.
- Wegner, A. 1979. Equilibrium of the actin-tropomyosin interaction. *Journal of molecular biology*. 131:839-853.
- Welch, M.D., A.H. DePace, S. Verma, A. Iwamatsu, and T.J. Mitchison. 1997. The human Arp2/3 complex is composed of evolutionarily conserved subunits and is localized to cellular regions of dynamic actin filament assembly. *The Journal of cell biology*. 138:375-384.
- Wen, P.J., S.L. Osborne, M. Zanin, P.C. Low, H.-T.A. Wang, S.M. Schoenwaelder, S.P. Jackson, R. Wedlich-Söldner, B. Vanhaesebroeck, and D.J. Keating. 2011. Phosphatidylinositol (4, 5) bisphosphate coordinates actin-mediated mobilization and translocation of secretory vesicles to the plasma membrane of chromaffin cells. *Nature communications*. 2:491.
- Westerink, R., and A. Ewing. 2008. The PC12 cell as model for neurosecretion. *Acta Physiologica*. 192:273-285.
- Williamson, J.R., and J.W. Grisham. 1961. Electron microscopy of leukocytic margination and emigration in acute inflammation in dog pancreas. *The American journal of pathology*. 39:239.
- Wu, C., S.B. Asokan, M.E. Berginski, E.M. Haynes, N.E. Sharpless, J.D. Griffith, S.M. Gomez, and J.E. Bear. 2012. Arp2/3 is critical for lamellipodia and response to extracellular matrix cues but is dispensable for chemotaxis. *Cell*. 148:973-987.
- Yang, C., L. Czech, S. Gerboth, S. Kojima, G. Scita, and T. Svitkina. 2007. Novel roles of formin mDia2 in lamellipodia and filopodia formation in motile cells. *PLoS biology*. 5:e317.
- Young, L.E., E.G. Heimsath, and H.N. Higgs. 2015. Cell type-dependent mechanisms for formin-mediated assembly of filopodia. *Molecular biology of the cell*. 26:4646-4659.

- Zeece, M.G., R.M. Robson, and P.J. Bechtel. 1979. Interaction of  $\alpha$ -actinin, filamin and tropomyosin with F-actin. *Biochimica et Biophysica Acta (BBA)-Protein Structure*. 581:365-370.
- Zhang, Y., M.A. Conti, D. Malide, F. Dong, A. Wang, Y.A. Shmist, C. Liu, P. Zerfas, M.P. Daniels, and C.-C. Chan. 2012. Mouse models of MYH9-related disease: mutations in nonmuscle myosin II-A. *Blood*. 119:238-250.
- Zigmond, S.H., M. Evangelista, C. Boone, C. Yang, A.C. Dar, F. Sicheri, J. Forkey, and M. Pring. 2003. Formin leaky cap allows elongation in the presence of tight capping proteins. *Current Biology*. 13:1820-1823.
- Zincarelli, C., S. Soltys, G. Rengo, and J.E. Rabinowitz. 2008. Analysis of AAV serotypes 1–9 mediated gene expression and tropism in mice after systemic injection. *Molecular therapy*. 16:1073-1080.



